

November 2014

Sedimentological, Geochemical and Isotopic Evidence for the Establishment of Modern Circulation through the Bering Strait and Depositional Environment History of the Bering and Chukchi Seas during the Last Deglaciation

Ben M. Pelto
University of Massachusetts Amherst

Follow this and additional works at: https://scholarworks.umass.edu/masters_theses_2



Part of the [Biogeochemistry Commons](#), [Climate Commons](#), [Geochemistry Commons](#), [Oceanography Commons](#), and the [Sedimentology Commons](#)

Recommended Citation

Pelto, Ben M., "Sedimentological, Geochemical and Isotopic Evidence for the Establishment of Modern Circulation through the Bering Strait and Depositional Environment History of the Bering and Chukchi Seas during the Last Deglaciation" (2014). *Masters Theses*. 108.
https://scholarworks.umass.edu/masters_theses_2/108

This Open Access Thesis is brought to you for free and open access by the Dissertations and Theses at ScholarWorks@UMass Amherst. It has been accepted for inclusion in Masters Theses by an authorized administrator of ScholarWorks@UMass Amherst. For more information, please contact scholarworks@library.umass.edu.

SEDIMENTOLOGICAL, GEOCHEMICAL AND ISOTOPIC EVIDENCE FOR THE
ESTABLISHMENT OF MODERN CIRCULATION THROUGH THE BERING STRAIT AND
DEPOSITIONAL ENVIRONMENT HISTORY OF THE BERING AND CHUKCHI SEAS
DURING THE LAST DEGLACIATION

A Thesis Presented

By

BEN M. PELTO

Submitted to the Graduate School of the
University of Massachusetts Amherst in partial fulfillment
of the requirements for the degree of

MASTER OF SCIENCE

September 2014

Department of Geosciences

© Copyright by Ben M. Pelto 2014

All Rights Reserved

SEDIMENTOLOGICAL, GEOCHEMICAL AND ISOTOPIC EVIDENCE FOR THE
ESTABLISHMENT OF MODERN CIRCULATION THROUGH THE BERING STRAIT AND
DEPOSITIONAL ENVIRONMENT HISTORY OF THE BERING AND CHUKCHI SEAS
DURING THE LAST DEGLACIATION

A Thesis Presented

By

BEN M. PELTO

Approved as to style and content by:

Julie Brigham-Grette, Chair

Steven Petsch, Member

Jonathan D. Woodruff, Member

Julie Brigham-Grette, Department Head
Department of Geosciences

ACKNOWLEDGEMENTS

The Department of Geosciences at the University of Massachusetts Amherst offered me an opportunity to grow as a scientist over the past two years. The guidance and support of the faculty, staff, and fellow graduate students has made my experience at UMass productive, fun, and rewarding.

I would most like to thank my advisor Dr. Julie Brigham-Grette. She provided me with the chance to pursue my desire to become an expert in climate science. Her belief in me and unwavering support made my time here truly great, and gave me the confidence to complete this project.

I thank Steven Petsch for always being an enthusiastic audience for my various ideas and questions, allowing me to test and pursue hypotheses that got me excited about my research. His feedback was particularly valuable on my various abstracts, which gave me a better idea of how one should write scientific documents. Jon Woodruff was always willing to field any question from statistics to how to format radiocarbon dates in a paper. Jon provided me with the introduction to PCA that enabled me to dig into my data statistically, which I feel greatly added to my final product.

My time at UMass helped me grow tremendously as a scientist and furthered my understanding of the global climate system. For that knowledge in particular, I would like to thank the faculty of the department, who happily share their wealth of knowledge. I, and many of my fellow climate science graduate students, feel this is perhaps the most valuable aspect our department. In particular I enjoyed Robert DeConto's excellent courses that taught me so much about physical oceanography, climate modeling, and how the global climate system functions. Other excellent courses taught by Steven Petsch, Stephen Burns, and Ray Bradley expanded my

knowledge of sediment geochemistry, isotopes and paleoclimate, giving me the level of knowledge necessary to be able to critically read climate science publications and to best interpret my data.

Thank you to Beth Caissie, Mea Cook, and Leonid Polyak for providing an external source of knowledge, and allowing me to bounce ideas off them and receive valuable feedback on various questions and problems that arose. Their willingness to share their expertise was greatly appreciated. Beth was an excellent host when I visited her Marine Sediments Lab at Iowa State University to run grain size analysis.

I would like to acknowledge Jim Kocis for being a helpful resource, conference companion, and a motivator, as we both worked on parallel but unique projects with the same cores. Mark Leckie helped me with preparing samples from 24JPC to analyze under a microscope, and his methods and knowledge proved to be an invaluable resource that I should have drawn upon far more. I would like to thank Pete Dawson for his help operating the ITRAX, Nick Balascio and Greg DeWet for their assistance with the GEOTEK, and Anthony Coletti for helping me as a novice MATLAB user. I would also like to thank Jenn Nikonczyk, Laura Bishop, Linda Moore, Lorna Stinchfield, and Marsha Howe of the front office, who were always super helpful, kind and cheerful; they often made my day.

The work I present in this thesis is entirely lab-based. Prior to attending UMass my experience was primarily in fieldwork, and thus UMass afforded me an opportunity to delve into paleoclimate research and lab-based science, using state-of-the-art equipment. I enjoyed diversifying my expertise by working with various types of sophisticated equipment, and gaining an understanding of the lab. I am also very grateful for the opportunities that Julie and Steve provided and allowed me to pursue outside of UMass. The cores used in this study were

collected by a team led by Julie Brigham Grette in 2002 aboard the USCGC Healy, and thanks to Julie, I had the opportunity to participate in a three-week research cruise aboard the USCGC Healy. I worked as a coring technician, allowing me to take part in every step of the core collection process, and better understand the split cores that I had previously only known in our lab. A trip to Mt. Kilimanjaro with Dr. Doug Hardy to service an automatic weather station and collect ablation measurements, and a two-week field season with the North Cascades Glacier Climate project, were not directly related to my thesis project, but nonetheless were very valuable to my continued growth as a climate scientist.

The Department of Geosciences gave me the opportunity to attend a number of conferences and meetings including the Arctic Workshops at UMass and CU Boulder, a Chukchi Sea drilling meeting at Ohio State, and the AGU annual meeting in San Francisco, where I was able to secure a PhD position. These conferences were an excellent opportunity to learn what is going on in my field, hear about ongoing research, and use feedback from my presentations at those conferences to refine and add to my study.

I would also like to thank my family for their constant support and love. My mom's editing and support was invaluable. My dad helped me find this opportunity at UMass, and I credit him with putting me in a position to be where I am today.

I believe that I am walking away from UMass with valuable new tools in my scientific arsenal, and am ready to continue to a PhD where I will design, execute, and publish my own glacier change project in British Columbia. The knowledge, confidence and skill I have gained at UMass will allow me to succeed at UNBC and in my future endeavors as a scientist.

ABSTRACT

SEDIMENTOLOGICAL, GEOCHEMICAL AND ISOTOPIC EVIDENCE FOR THE ESTABLISHMENT OF MODERN CIRCULATION THROUGH THE BERING STRAIT AND DEPOSITIONAL ENVIRONMENT HISTORY OF THE BERING AND CHUKCHI SEAS DURING THE LAST DEGLACIATION

SEPTEMBER 2014

BEN M. PELTO, B.A., ALFRED UNIVERSITY

M.S., UNIVERSITY OF MASSACHUSETTS AMHERST

Directed by: Professor Julie Brigham-Grette

Sea level regression during the Last Glacial Maximum exposed the Bering Land Bridge, and cut off the connection between the North Pacific and Arctic Ocean, ending the exchange of North Pacific Water through the Bering Strait. Exchange of North Pacific Water comprises a major portion of fresh water input to the Arctic Ocean, and is of vital importance to North Atlantic Deep Water formation, a vital component of Atlantic Meridional Overturning Circulation. Bering Strait throughflow thus plays an integral role in global climate stability. A suite of four cores was selected, three in the Bering Sea and one in the Chukchi Sea, to bracket the Bering Strait in order to elucidate changes in sediment delivery, productivity and regional oceanography as the Bering Land Bridge flooded and modern ocean circulation was established during the last deglaciation. The arrival of nutrient rich North Pacific Water in the Chukchi Sea is recorded around 8 ka by organic carbon isotope depletion and an increase in total organic carbon and organic nitrogen, reflecting an increasingly marine isotopic signal and increased productivity. In the Bering Sea, the early deglaciation is marked by depleted organic carbon

isotopes that indicate increasing terrestrial input, and increased total organic carbon. Principal component analysis of sedimentologic, geochemical and isotopic data clearly captures discrete sediment populations that correspond to key climatic intervals, representing changes in sediment delivery, productivity and circulation during the last deglaciation. In the Bering Sea we observe that deglaciation began in earnest around 18–17 ka, but lack of confidence in our age control does not allow for a precise date. Our results suggest that modern circulation through the Bering Strait, and thus for the Bering and Chukchi Seas, was established ~8 ka. Prior to 8 ka there is an interval of sediment that appears record a possible reversal of flow through the Bering Strait corresponding to the 8.2 ka event.

Preface

This thesis is being submitted to fulfill the requirements of a Master of Science degree in Geoscience at the University of Massachusetts, Amherst. The thesis presents results and conclusions drawn from a suite of sediment cores collected during two legs (HLY02-02 and HLY02-04) of the Arctic West Summer 2002 cruise of the USCGC Healy in the Bering and Chukchi Seas. The two cruise legs were funded by a National Science Foundation (NSF) grant to Julie Brigham-Grette (University of Massachusetts, Amherst), Neil Driscoll (Scripps Oceanographic Institution), and Llyod Keigwin (Woods Hole Oceanographic Institution) entitled "Marine Climate and Relative Sea Level Across Central Beringia".

My research was directly funded by an NSF grant awarded to Julie Brigham-Grette and Steven Petsch (University of Massachusetts, Amherst) entitled "Late Quaternary Sea Ice History of the Beringian Arctic Gateway".

This thesis presents the findings obtained through analyses of three Bering Sea and one Chukchi Sea sediment cores, building on the work of Beth Caissie, Mea Cook, and Zach Lundeen. The focus of this study is to describe the sediment deposition history of the Bering and Chukchi Sea during the last deglaciation, and to better constrain the establishment of modern circulation through the Bering Strait following the flooding of the Bering Land Bridge.

Our work adds to a growing body of Arctic paleoclimate data, in a region which still suffers from a paucity of paleoclimate data despite the sensitivity of the Arctic to climatic change. A better understanding of the recent climatic and oceanographic transitions, recorded in sediments from the Bering and Chukchi Seas, can aid our ability to predict and adjust to a rapidly changing Arctic.

Three chapters comprise this thesis, followed by an appendix. Chapter One is a general introduction to the geography of Beringia and the physical oceanography of the surround seas where the general climatic history of the last deglaciation and the primary research questions of this study are covered. Chapter Two is the backbone of this thesis, and covers the data collected during this study as well as the hypotheses tested and conclusions drawn from our data. Statistical analyses and plots display all of the relevant data that allowed us to draw conclusions regarding the history of sediment delivery and paleoceanographic changes as recorded in the sediment. Chapter Three is a brief discussion regarding avenues of research that would be valuable to pursue, based primarily upon implications of our data that require better evidence or more detailed investigation. The Appendix features a series of auxiliary figures.

All data from this study presented here will be archived with the Advanced Cooperative Arctic Data and Information Service (ACADIS, <https://www.aoncadis.org/home.htm>), and with ScholarWorks here at UMass. ACADIS is a joint effort between the National Snow and Ice Data Center (NSIDC), the University Corporation for Atmospheric Research (UCAR), UNIDATA, and the National Center for Atmospheric Research (NCAR) to provide data archival, preservation and access for all projects funded by NSF's Arctic Science Program (ARC).

TABLE OF CONTENTS

	Page
ACKNOWLEDGEMENTS	iv
ABSTRACT	vii
PREFACE	ix
LIST OF TABLES	xv
LIST OF FIGURES	xvi
CHAPTER	
1. OVERVIEW OF THE PHYSICAL GEOGRAPHY AND OCEANOGRAPHY OF BERINGIA AND THE SURROUNDING SEAS, AND LAST DEGLACIATION CLIMATIC HISTORY	1
1.1 Introduction	1
1.2. Regional Geography and Paleoceanography	4
1.2.1. Bering Land Bridge	4
1.2.2. Bering Strait Role in Global Circulation	5
1.2.3. Arctic Ocean	7
1.2.4. Bering Sea	9
1.2.5. Chukchi Sea	10
1.2.6. River Routing	12
1.3. Regional Paleoclimate and Productivity History	14
1.3.1. Reservoir Age	14
1.3.2. Last Glacial Maximum	16
1.3.3. Early Deglacial Period (18 to 15 ka)	17

1.3.4. Bølling-Allerød (15 to 13 ka)	18
1.3.5. Younger Dryas (12.9 to 11.7 ka)	21
1.3.6. Pre-Boreal (11.7 to 10.5 ka)	22
1.3.7. Holocene (10.5 ka to present)	22
1.4. Primary Research Questions	23
2. SEDIMENTOLOGIC, GEOCHEMICAL AND ISOTOPIC EVIDENCE FOR THE ESTABLISHMENT OF MODERN CIRCULATION THROUGH THE BERING STRAIT AND DEPOSITIONAL ENVIRONMENT HISTORY OF THE BERING AND CHUKCHI SEAS DURING THE LAST DEGLACIATION	26
2.1. Introduction	27
2.2. Background	31
2.2.1. Bering Sea	32
2.2.2. Bering Strait	33
2.2.3. Chukchi Sea	35
2.2.4. Laminations	36
2.3. Methods	37
2.3.1. Age Models	38
2.3.2. Non-Destructive Analyses	41
2.3.2.1. Elemental XRF	41
2.3.2.2. MSCL Data	42
2.3.3. Destructive Analyses	43
2.3.3.1. Elemental Isotopic Analyses	43
2.3.3.2. Carbon Isotope Mixing Models	44
2.3.3.3. C/N Ratios and %N _{org}	45

2.3.3.4. Grain Size Analysis	45
2.3.3.5. Sediment Compositional Analysis	47
2.3.4. Principal Component Analysis	47
2.4. Results	48
2.4.1. Western Bering Sea Shelf Slope, 3JPC	48
2.4.2. Northwest Chukchi Shelf, 24JPC	56
2.4.3. Southwest Bering Sea, Bowers Ridge, 17JPC	62
2.4.4. Southeast Bering Sea, Umnak Plateau, 51JPC	67
2.5. Discussion	72
2.5.1. Principal Component Analysis End-Member Selection	72
2.5.2. Last Glacial Maximum (27 to 18 ka)	75
2.5.2.1. Western Bering Sea Shelf Slope, 3JPC	75
2.5.2.2. Southwestern Bering Sea, Bowers Ridge, 17JPC	76
2.5.2.3. Umnak Plateau, Southeastern Bering Sea, 51JPC	77
2.5.3. Early Deglaciation (18 to 15 ka)	78
2.5.3.1. Increased Terrestrial Influx, Bering Sea	78
2.5.3.2. Organic Carbon Isotopes and Terrestrial Carbon Input	78
2.5.3.3. Elemental XRF data and PCA Analysis	79
2.5.3.4. Nitrogen Isotopes of the Early Deglacial	80
2.5.3.5. Early Deglacial River Drainage Networks	81
2.5.4. Bølling-Allerød (15 to 13 ka)	84
2.5.4.1. Bølling-Allerød Laminations	84
2.5.4.2. Increased Bølling-Allerød Productivity	85

2.5.4.3. $\delta^{13}\text{C}_{\text{org}}$ and Alaskan Stream Water	87
2.5.4.4. Bølling-Allerød Nitrogen Isotopes	88
2.5.5. Younger Dryas (12.9 to 11.7 ka)	89
2.5.5.1. Decreased Younger Dryas Productivity	89
2.5.5.2. Northwest Chukchi Shelf, 24 JPC	91
2.5.5.3. Younger Dryas Summary	92
2.5.6. Pre-Boreal Warm Period (11.7 to 10.5 ka)	93
2.5.6.1. Increased Pre-Boreal Productivity	94
2.5.7. Holocene (10.5 to 2.5 ka)	96
2.5.7.1. Holocene Changes in the Chukchi Sea, 24JPC	96
2.5.7.2. Bering Sea Sandy Core-top, 3JPC	99
2.6. Conclusions	100
3. FUTURE PESPCTIVES	102
3.1. Reversal of Flow through the Bering Strait?	102
3.2. Reservoir Ages	103
3.3. Bering Strait Flooding and Isostatic Sea Level	105
3.4. Biogenic Silica	106
3.5. PCA in Paleoclimate Studies	106
3.6. Summary	107
APPENDIX: AUXILIARY PRINCIPAL COMPONENT FIGURES	109
REFERENCES.....	114

LIST OF TABLES

Table	Page
2.1. Regional cores referred to in text with primary citations, location and relevant proxies	31
2.2. Uncorrected AMS ^{14}C ages, and corrected, calibrated ages measured on <i>N. pachyderma</i> (s.) in 3, 17, and 51JPC, and shells in 24JPC	38

LIST OF FIGURES

Table	Page
1.1. Bathymetric and topographic map of Beringia, the North Pacific, and the Bering and Chukchi Seas with locations of cores	2
1.2. Map of the Bering Land Bridge	13
2.1. Bathymetric and topographic map of Beringia, the North Pacific, and the Bering and Chukchi Seas with locations of cores	29
2.2. Map of the Bering Land Bridge	30
2.3. Age depth models for 3JPC, 24JPC, 17JPC, and 51JPC	40
2.4. Total organic carbon versus total nitrogen correlation in 3JPC, 24JPC, and 17JPC	46
2.5. 3JPC Bulk $\delta^{13}\text{C}_{\text{org}}$ and $\delta^{15}\text{N}$, %TOC, estimated %OC _{mar} and %OC _{terr} , %N _{org} , and C/N	51
2.6. 3JPC Grain size data, accumulation rate, bulk density, and magnetic susceptibility	52
2.7. 3JPC XRF elemental intensity data	53
2.8. 3JPC PCA biplots	54
2.9. 24JPC %TOC, estimated %OC _{mar} and %OC _{terr} , %N _{org} , $\delta^{13}\text{C}_{\text{org}}$, $\delta^{15}\text{N}$, and C/N	57
2.10. 24JPC grain size data, accumulation rate, bulk density, and magnetic susceptibility	58
2.11. 24JPC XRF elemental intensity data	59
2.12. 24JPC PCA biplots	60
2.13. 17JPC bulk $\delta^{15}\text{N}$, %N _{org} , %TOC, estimated %OC _{terr} and %OC _{mar} , bulk $\delta^{13}\text{C}_{\text{org}}$, C/N, grain size data, and accumulation rate	64
2.14. 17JPC elemental XRF intensity data	65
2.15. 17JPC PCA biplots	66
2.16. 51JPC %TOC, estimated %OC _{mar} and %OC _{terr} , bulk $\delta^{13}\text{C}_{\text{org}}$, grain size data, and accumulation rate	68

2.17. 51JPC elemental XRF intensity data	69
2.18. 51JPC PCA biplots	70
A.19. 3JPC percent variance explained and eigenvalues for each principal component for both full suite and XRF PCAs	110
A.20. 24JPC percent variance explained and eigenvalues for each principal component for both full suite and XRF PCAs	111
A.21. 17JPC percent variance explained and eigenvalues for each principal component for both full suite and XRF PCAs	112
A.22. 51JPC percent variance explained and eigenvalues for each principal component for both full suite and XRF PCAs	113

CHAPTER 1

OVERVIEW OF THE PHYSICAL GEOGRAPHY AND OCEANOGRAPHY OF BERINGIA AND THE SURROUNDING SEAS, AND LAST DEGLACIATION CLIMATIC HISTORY

1.1. Introduction

Rapid climatic change repeatedly punctuated a warming trend during the last deglaciation, as global climate ameliorated following the Last Glacial Maximum (LGM) [e.g. *Thornalley et al.*, 2011; *Shakun et al.*, 2012]. During the LGM, the region between Chukotka and Alaska was subaerially exposed as the vast Bering Land Bridge (BLB) [*Hopkins*, 1959], uniting Beringia from the Kolyma to the Mackenzie Rivers (Figure 1.1). The land bridge occupied what today is the Bering Strait (BS), and isolated the Arctic Ocean from the North Pacific, thereby halting exchange between the North Pacific and North Atlantic via the Arctic Ocean.

Subaerial exposure of the Chukchi and Bering Sea shelves greatly reduced the area covered by the two seas [*Jakobsson*, 2002], exposing nearly all of the Chukchi Sea and essentially restricting the Bering Sea to its deep basin. The modern circulation of the Bering and Chukchi Seas are dominated by Bering Strait throughflow, an overall northward flow that defines the regional circulation pattern [*Coachman et al.*, 1975]. With a closed Bering Strait during the LGM, the circulation regime would have been markedly different, not only in the Bering and Chukchi Seas, but also within the Arctic Ocean [*Polyak et al.*, 2004]. Interpreting sediment cores from the region requires an understanding of the sensitivity of the region's circulation which also affects age-depth model application. Changes in past circulation affect nutrient supply, sediment delivery, and water mass interaction, which changes preservation, the reservoir age and productivity. In order to determine sediment provenance and better explain the

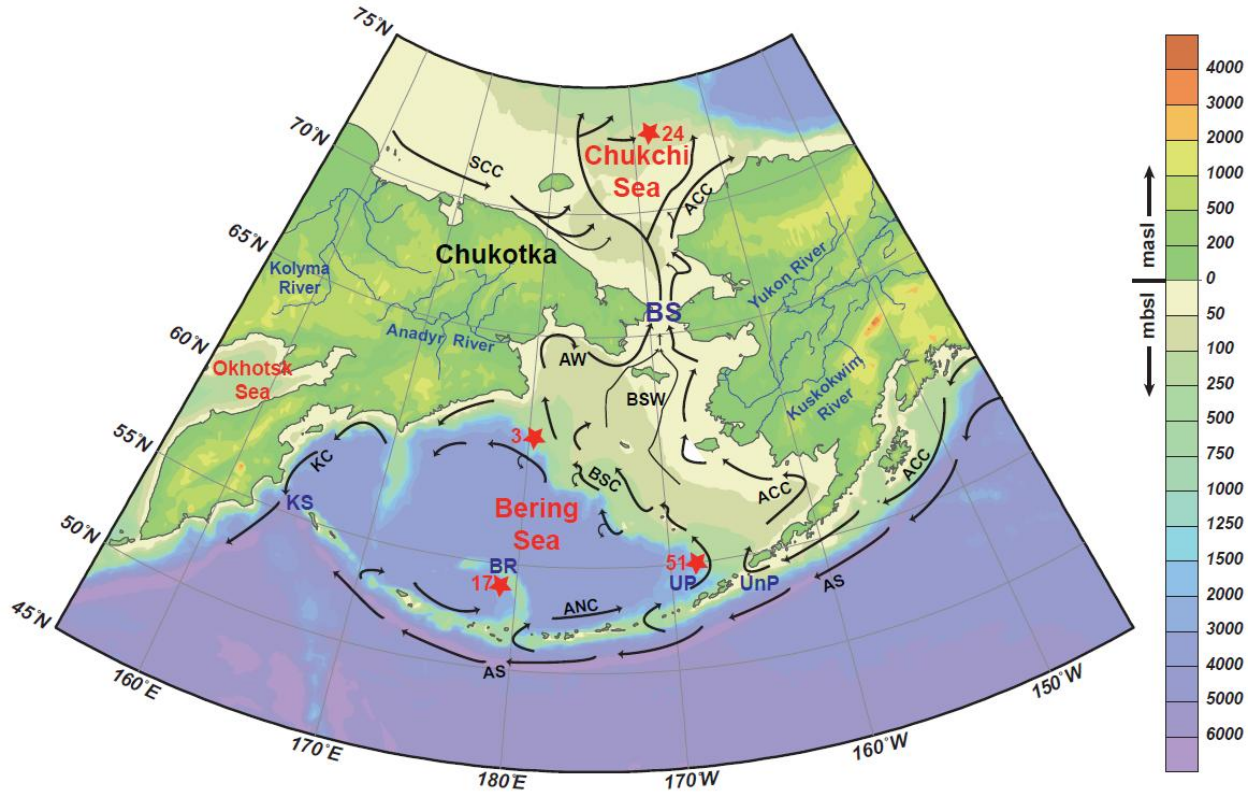


Figure 1.1. Bathymetric and topographic map of Beringia, the North Pacific, and the Bering and Chukchi Seas with locations of cores (numbered red stars). Currents denoted by black arrows and labeled in black: Alaskan Stream (AS), Aleutian North Slope Current (ANC), Alaskan Coastal Current (ACC), Bering Shelf Current (BSC), Bering Shelf Water (BSW), Anadyr Water (AW), and Siberian Coastal Current (SCC). The Bering Strait (BS), Umnak Plateau (UP), Unimak Pass (UnP), Bowers Ridge (BR), and Kamchatka Strait (KS) are labeled in blue.

sensitivity of these marginal seas and Pacific Arctic Gateway to changing conditions, the paleogeography and paleocirculation must be constrained. The North Pacific Ocean experienced large changes in water mass properties and productivity that appear synchronous with those from the Bering Sea to the northwest Mexican coast [Crusius *et al.*, 2004]. Explaining these widespread periods of change has been a focal point of Pacific paleoclimate study and is an area of ongoing debate and research [Davies *et al.*, 2011; Lam *et al.*, 2013]. Sea level, sea ice cover, and the extent of ice sheets are all factors that must be taken into account when interpreting past records. Elucidating the story told by sediments in the Arctic requires using a changing lens, as

it appears that circulation and water mass interactions changed with rising sea level during deglaciation.

The purpose of this thesis is to better describe changes in circulation, productivity, and sediment delivery in the seas that surround Beringia, using five marine sediment cores that span the deglaciation (Figure 1.1). The sediment cores were chosen to bracket the BS, and best represent the diverse water masses that influence the region. The setting and a brief sedimentologic description of each core is as follows:

Jumbo Piston Core 3 (HLY02-02-3JPC) was taken between Navarin and Pervenets Canyons on the Bering Sea shelf slope (60.13°N, 179.44°W) about 230 km southeast of Cape Navarin, Russia, at 1132 m water depth. 3JPC contains the most expanded deglacial sequence of the cores in this study, 14 m long, with an average sediment accumulation rate of 185 cm/kyr from the beginning to the end of the laminated sequences. There are four visibly laminated intervals, which are composed of pairs of dark and light olive laminae ranging in thickness from <1 to 2 mm. The first three laminated intervals occur during the Bølling-Allerød (BA) (901–763 cm, 724–602 cm, 574–533 cm) spanning 14.7–12.9 ka (14.7–14.2 ka, 14–13.45 ka, 13.2–12.9 ka), in excellent correspondence with NGRIP-dated (North Greenland Ice Core Project) BA/Younger Dryas (YD) [*Rasmussen et al.*, 2006], with the final interval deposited during the PB from 11.5–10.8 ka (342–215 cm), though there are three minor laminae groups of 2–5 cm after 10.8 ka. Intervening massive intervals and the deepest 5.4 m of sediment are composed of homogeneous sticky dark olive-gray silty mud, with a slower sedimentation rate (87 cm/kyr).

24JPC (HLY04-02-24JPC) was taken from the northwest Chukchi shelf at 80 m water depth (73.23°N, 167.88°W), and spans much of the Holocene (14.3–2.5 ka) recorded in 7.5 m of dark grey-green silty mud. There is an interval of rapid sedimentation from 9–6 ka (223 cm/kyr),

with slower accumulation before and after this interval (30–40 cm/kyr), although the date from the deepest portion of the core may bias the sedimentation rate in the older section of the core.

17JPC (HLY02–02–17JPC), the southern-most and deepest core (2209 mbsl), was taken from Bowers Ridge (53.93°N, 178.70°W), 270 km north of Amchitka Island near the western end of the Aleutian Islands, and comprises the longest record of the cores in this study, from 27–8 ka, contained in only 3 m of massive diatomaceous olive green-grey silty mud with an average sedimentation rate of 20 cm/kyr.

51JPC (HLY02–02–51JPC) was taken from 1467 m water depth on the Umnak Plateau in the southeast Bering Sea (54.55°N, 168.67°W), about 130 km northwest of Unalaska Island. The background sediment of 51JPC is composed of relatively homogenous diatomaceous dark olive green clay and silt, which is punctuated by two tephra deposits which are each followed by laminated intervals are present. The first laminated interval occurs between 218 and 174 cm (15–13.3 ka) and the second between 138 and 134 cm (11.4–11.1 ka). The laminations are composed of black to dark olive green-grey submillimeter thick laminae. Both are underlain by thick tephra deposits (240–219 cm and 148–139 cm). Sediment accumulation rate is 47 cm/kyr from the LGM until around 16 ka when the rate slows to an average of 23 cm/kyr into the Holocene.

1.2. Regional Geography and Paleoceanography

1.2.1. Bering Land Bridge

The continental shelf between Chukotka and Alaska was exposed during the LGM, forming the Bering Land Bridge [*Hopkins, 1959, 1967*], which connected greater Beringia from the Kolyma River in Russia to the Mackenzie River in Canada. The BLB was exposed when sea

level was around 120 m lower than present day [Fairbanks, 1989], or around 105 m lower with a hydrostatic correction [Guilderson *et al.*, 2000]. As an ephemeral continental land mass, the BLB isolated the Arctic Ocean from the North Pacific, and ended direct exchange between the North Pacific and North Atlantic oceans. The Bering Strait was flooded during deglaciation, between 11–12 ka [Elias *et al.*, 1996; Keigwin *et al.*, 2006], consistent with global eustatic sea level [Fairbanks, 1989], though a precise age of 13.3 cal ky BP has been suggested [England and Furze, 2008]. No sea level or flooding history study of the BLB has ever calculated isostatic rebound, and while thought to be small (<10 m) [Keigwin *et al.*, 2006], given the shallow depth of the BS, the timing of the ~10 m isostatic rebound could have influence the flooding chronology of the BLB. Dating the initial flood of the BLB is important, but of equal value is constraining the time at which the water depth over the BLB allowed for significant volume transport where water mass exchange could occur between the Bering and Chukchi Seas. Initial flooding was likely channelized due to the shallow nature of the Strait, and allowed a relatively small amount of interaction between the Bering and Chukchi Seas. Once the BLB became the BS, an uninterrupted and deeper channel capable of significant water mass exchange would have dramatically changed the nutrient supply to the Chukchi Sea, and the early phases of establishing modern circulation would commence.

1.2.2. Bering Strait Role in Global Circulation

The first order significance of the Bering Strait is its role as the connection between the North Pacific and Atlantic oceans via the Arctic Ocean. This connection fosters water mass exchange, which affects North Atlantic Deep Water formation (NADW). Bering Strait water has an average salinity of 32.5 psu [Roach *et al.*, 1995; Aagaard *et al.*, 2006], making it relatively fresh compared to the North Atlantic (34-37 psu). Today, a net northward flow of 0.8 Sv

[*Wijffels et al.*, 1992; *Aagaard et al.*, 2006] through the Strait represents a major contribution of freshwater to the Arctic Ocean (34.8 psu) [*Aagaard and Carmack*, 1989]. The magnitude of the freshwater component exiting the eastern Arctic gateway influences NADW production in the subpolar North Atlantic [*Broecker et al.*, 1990; *Wijffels et al.*, 1992; *Aagaard and Carmack*, 1994; *Keigwin and Cook*, 2007], and hence NADW is a driving force behind Atlantic Meridional Overturning Circulation (AMOC) or the Thermohaline Circulation (TC) [*Broecker*, 1991]. AMOC advects warm, salty surface water from the south into the North Atlantic where it cools and sinks [*Broecker*, 1991; *Thornalley et al.*, 2011]. This northward transport of warm water pulls heat to the North Atlantic [*Ganachaud and Wunsch*, 2000] and is responsible for the mild climate of Europe [*Broecker et al.*, 1988; *Broecker*, 1991]. Modeling simulations [*Stouffer et al.*, 2006; *Hu et al.*, 2013], and paleoclimate records [*Broecker*, 1994; *Keigwin and Jones*, 1994; *Clark et al.*, 2007] indicate that a slowdown in AMOC could result in cooling of the Northern Hemisphere.

An open Bering Strait is thought to act as an 'exhaust valve' for the North Atlantic [*De Boer and Nof*, 2004], capable of dissipating freshwater anomalies in the North Atlantic at a rate hypothesized to be impossible with the Bering Strait closed [*Hu et al.*, 2014]. The reduced volume of land-based ice present in the Northern Hemisphere today [*Church et al.*, 2001] likely does not store enough freshwater to deliver an adequate volume to the NA to shut down THC, though a reduction in THC is possible [*Stouffer et al.*, 2006]. An open BS is potentially able to disperse freshwater anomalies that threaten AMOC, whereas a closed BS significantly strengthens AMOC [*Wadley and Bigg*, 2002], but perhaps makes it less stable. The combination of smaller NH ice volume and open Bering Strait connection, implies that the North Atlantic is largely protected from freshwater hosing today, but causes of rapid climatic change, like the

Younger Dryas are difficult to unequivocally solve [Bradley and England, 2008]. During deglaciation, AMOC experienced both extremes, from a near shutdown during Heinrich Event 1 (H1), to an overshoot during the BA warm period [Timmermann and Menviel, 2009].

Future changes in sea ice extent and duration are expected to have a large impact on Northern Hemisphere climate, which may already be seen [Francis *et al.*, 2009; Tang *et al.*, 2013]. With summer Arctic sea ice expected to disappear completely before the middle of the 21st century [Comiso *et al.*, 2008; Wang and Overland, 2009; Stroeve *et al.*, 2011], understanding past circulation and productivity is vital to projections of possible future circulation and ecosystem changes. Sediment records that span rapid climatic change of the last deglaciation are an ideal analogue for modern climate change in the Arctic, as the changes of the last deglaciation are the most recent large magnitude, rapid climate transitions.

1.2.3. Arctic Ocean

Bering Strait throughflow delivers ~40% of the freshwater entering the Arctic Ocean [Woodgate, 2005], and is also an important nutrient source to Arctic ecosystems. The water properties of the North Pacific and the Arctic Ocean are very different, and small fluctuations in flow magnitude and direction can greatly alter the salinity, stratification, sea ice formation, and nutrient supply of the Arctic Ocean, especially the Chukchi Sea [Aagaard and Carmack, 1994; Wadley and Bigg, 2002]. The net northward flow results from a sea level difference [Coachman and Aagaard, 1966, 1981; Coachman *et al.*, 1975] of about 70 cm between the Bering and Chukchi Seas [Aagaard *et al.*, 2006].

Pacific water accounts for half to two-thirds of the water of the Arctic halocline over the Canadian Basin [Aagaard and Carmack, 1989; Steele, 2004], making Bering Strait inflow an important component of Arctic stratification and the Arctic Ocean nutrient maximum, located in

the upper halocline [Cooper *et al.*, 1997]. The Arctic halocline fosters sea ice growth and protects sea ice from warm Atlantic water that enters at depth via the Fram Strait [Rudels *et al.*, 1994; Schauer *et al.*, 1997], and determines the ventilation depth of the Arctic [Woodgate *et al.*, 2005]. Closure of the Bering Strait during major glacials would likely raise the salinity of the Arctic Ocean, affecting the Arctic halocline and water column stability [Wadley and Bigg, 2002]. With an emergent BLB, BS inflow would have been cut off, removing a controlling portion of Arctic Ocean nutrient budgets [Codispoti and Richards, 1968], and undermining the stratification of the Arctic Ocean. Stratification promotes a hydrological regime conducive to sea ice formation and its associated climate [Aagaard and Carmack, 1989; Rudels, 1989].

The Arctic Ocean basin is nearly landlocked and relatively small, [Jakobsson, 2002], with only one deep-water connection to the world ocean via the Fram Strait. The Arctic Ocean has the highest proportion of continental shelf, ~53% [Jakobsson, 2002], of the world's oceans, which otherwise range from 9.1 to 17.7% [Menard and Smith, 1966]. Exposure of these extensive continental shelves during glacial episodes effectively cut the area of the Arctic Ocean in half. Arctic Ocean circulation during major glaciations is thought to have been restricted [Polyak *et al.*, 2004; Bradley and England, 2008] due to both lowered sea level that reduced the size and inputs of Atlantic and Pacific water, and to extensive shelf and sea ice [Landvik *et al.*, 1998; Dyke *et al.*, 2002; Jakobsson, 2002; Svendsen *et al.*, 2004; Ingólfsson *et al.*, 2008]. Modeling simulations support a reduction in Arctic circulation when the BS is closed [Hu *et al.*, 2014]. Weakened circulation is consistent with the closure of the Bering Strait [Hopkins, 1982; Elias *et al.*, 1996], blockage of the Barents Sea inflow by the Eurasian ice Sheet [Landvik *et al.*, 1998; Svendsen *et al.*, 2004], cessation of flow through the Canadian Archipelago [Zreda *et al.*, 1999], and exposure of the extensive continental shelves of the peripheral Arctic Seas by

lowered sea level and ice sheets [Jakobsson, 2002]. No other ocean experienced such dramatic changes in geography between interglacial periods.

1.2.4. Bering Sea

The Bering Sea has a broad continental shelf (50–150 m deep), and a deep basin (<4000 m) bracketed by Chukotka and Kamchatka to the northwest, Alaska to the northeast, and the Aleutian Islands to the south. It is characterized by relatively low salinity but is nutrient rich [Cook *et al.*, 2005], particularly across the shelf and slope region where high nutrient waters of North Pacific origin are upwelled [Walsh *et al.*, 1989], making the Bering Sea one of the most productive marine systems in the world [Sambrotto *et al.*, 1984].

Surface circulation over the basin is roughly defined by a cyclonic gyre, whose western boundary current is the southward flowing Kamchatka Current (Figure 1.1). In the west, within the Gulf of Anadyr, deeper Pacific water is upwelled onto the shelf and mixed with relatively high salinity and nutrient-rich Anadyr Water (AW) [Clement *et al.*, 2005]. The Bering Slope Current (BSC) flows in the upper 300 m along the continental shelf break and defines the eastern edge of the gyre [Schumacher and Reed, 1992], originating near 51JPC and flowing over 3JPC. On the shelf, the principal surface flow is northward through the Bering Strait, which is about 85 m wide and averages 50 m water depth [Schumacher and Stabeno, 1998; Stabeno *et al.*, 1999]. Bering Shelf Water (BSW), a nutrient-rich and less saline water mass, occupies the central region of the northern Bering Sea, while a strong gradient defines the warmer (in summer), nutrient-poor, Alaska Coastal Water (ACW) to the east [Coachman, 1986; Grebmeier *et al.*, 1988]. The ACW originates from the Alaskan Stream (AS), which flows northward through gaps in the Aleutian Islands up onto the shelf [Stabeno *et al.*, 1999] through the Unimak Pass

(<80m deep), and has a major influence on the Uminak Plateau [*Caissie et al.*, 2010].

The BSC is known for high productivity and has been referred to as the Green Belt [*Springer et al.*, 1996], a band with high chlorophyll and primary production throughout the summer [*Springer et al.*, 1996; *Hurst et al.*, 2010]. Tidal mixing and transverse circulation along the shelf break keeps stratification at a minimum, bringing nutrients up from 300 to 800 m [*Springer et al.*, 1996]. The elevated biological productivity associated with the BSC [*Kinney et al.*, 2009] is responsible for high organic carbon accumulation along the Bering shelf slope, thus changes in the strength, trajectory, and nutrient content of the BSC should influence the sediment record of Bering shelf slope cores.

1.2.5. Chukchi Sea

The Chukchi Sea lies to the north of the Bering Strait, bounded by Wrangel Island and the Siberian coast to the west, Alaska to the east, and the irregular and indefinite northern boundary of the continental shelf break to the north. The Chukchi is unique among the Arctic shelf seas as it is dominated by Pacific Water advected through the Bering Strait [*Weingartner et al.*, 2005]. The productive Chukchi Shelf is dependent upon the nutrients of the warm, fresh Pacific inflow, which affects ice formation and productivity [*Walsh et al.*, 1989; *Martin and Drucker*, 1997]. A closed BS would have had a profound impact on the Chukchi Sea.

Based upon a sea level 120 m lower than at present [*Fairbanks*, 1989], roughly 90% of the Chukchi Sea as defined by Jakobsson (2002), would have been subaerially exposed during low stand during the LGM [*Jakobsson*, 2002]. The emergent BLB occupied most of what is today the Chukchi Sea during the LGM, cutting off North Pacific nutrient rich, fresh water from reaching the Arctic Ocean. Chukchi Sea sedimentary records are largely limited to the Holocene [*Darby et al.*, 2009; *Ortiz et al.*, 2009] due to the exposure of the BLB, and a subsequent shallow

transgressive sea in which sediment preservation would have been difficult due to ice scouring [Hill and Driscoll, 2010] and sediment resuspension in its shallow depths [Reimnitz *et al.*, 1998].

The four major currents of the Chukchi Sea are the Siberian Coastal Current in the far west, and the three main branches -- western, central and eastern -- that comprise the northward flowing currents across the Chukchi shelf. The western branch is relatively salty, cold Anadyr Water which flows through the Hope and Herald Valleys [Coachman *et al.*, 1975; Woodgate *et al.*, 2005]. Over the north central Chukchi, flow is bounded by the Herald Shoal to the west and Hanna Shoal to the east [Weingartner *et al.*, 1998, 2005]. The flow over the central Chukchi, averaging 0.2 Sv, accounts for 25% of Bering Strait transport [Woodgate *et al.*, 2005]. Due to a dearth of data from the central shelf, its flow is poorly constrained in comparison to the eastern and western branches [Woodgate *et al.*, 2005]. However, there is an eastern flow component, most noticeable around the Hanna Shoal, where flow appears to bifurcate, with the eastern branch flowing along the southern flank of the shoal, suggesting a connection between the north central shelf water and the ACC [Weingartner *et al.*, 2005]. In the east, warm and nutrient-poor ACW and BSW are coastally trapped in summer and fall, exiting the Chukchi into the Arctic Ocean via Barrow Canyon [Paquette and Bourke, 1974; Coachman *et al.*, 1975; Ahlñäs and Garrison, 1984].

With the BS blocked by the BLB, the Chukchi Sea during the last deglaciation would have been smaller, shallower, and nutrient poor. Circulation over the Chukchi Sea would not have had a northern flow component without BS inflow, and thick sea ice, as well as nearby large ice sheets, would have enabled extensive ice scour/gouging. The Chukchi Sea appears to have been poorly suited to record continuous sedimentation during the early deglaciation.

1.2.6. River Routing

With the Bering Land Bridge exposed, the major regional rivers: Yukon, Kuskowim, and Anadyr, would have crossed the exposed continental shelf to reach the ocean [*Kummer and Creager, 1971*]. There is not enough evidence of buried channels to tie present day rivers to submarine canyons at specific times [*Carlson and Karl, 1984*], but it is likely that these three rivers played an important role in creating many of the huge submarine canyons of the Bering Shelf Slope [*Scholl et al., 1968, 1970; Hopkins, 1972; Carlson and Karl, 1984*]. The discovery of the "Paleo-Anadyr" [*Canada. Defence Research Board. Directorate of Scientific Information Services and Kotenev, 1966*] suggests that perhaps the Anadyr River played a role in excavating either the Navarin or Pervenets Canyons (Figure 1.2) during the Pleistocene [*Canada. Defence Research Board. Directorate of Scientific Information Services and Kotenev, 1966; Hopkins, 1972*].

Though not currently known, the drainage network and debouchement location for the major rivers could have a major impact on sediment delivery in the Bering Sea. The Yukon drains about 855,000 km², has a total length of over 3000 km, and with a sediment discharge of ~55 million metric tons per year [*Eberl, 2004*], it accounts for as much as 90% of river-borne sediment entering the Bering Sea [*Lisitsyn, 1966*]. Although the Yukon empties into the Bering, its contribution of sediment is very important to the Chukchi Sea [*Creager and McManus, 1968; Nelson and Creager, 1977*], due to prevailing northward currents (ACC) [*Coachman and Aagaard, 1966*], and the proximity of the mouth of the Yukon to the Chukchi [*McManus et al., 1974*]. The debouchement of the Yukon and/or Kuskowim Rivers during the LGM may have been at Pribilof Canyon (Figure 1.2) [*Scholl et al., 1970; Carlson and Karl, 1984*]. If this were

the case, then sediment delivery along the Bering shelf slope should have recorded Yukon sedimentation.

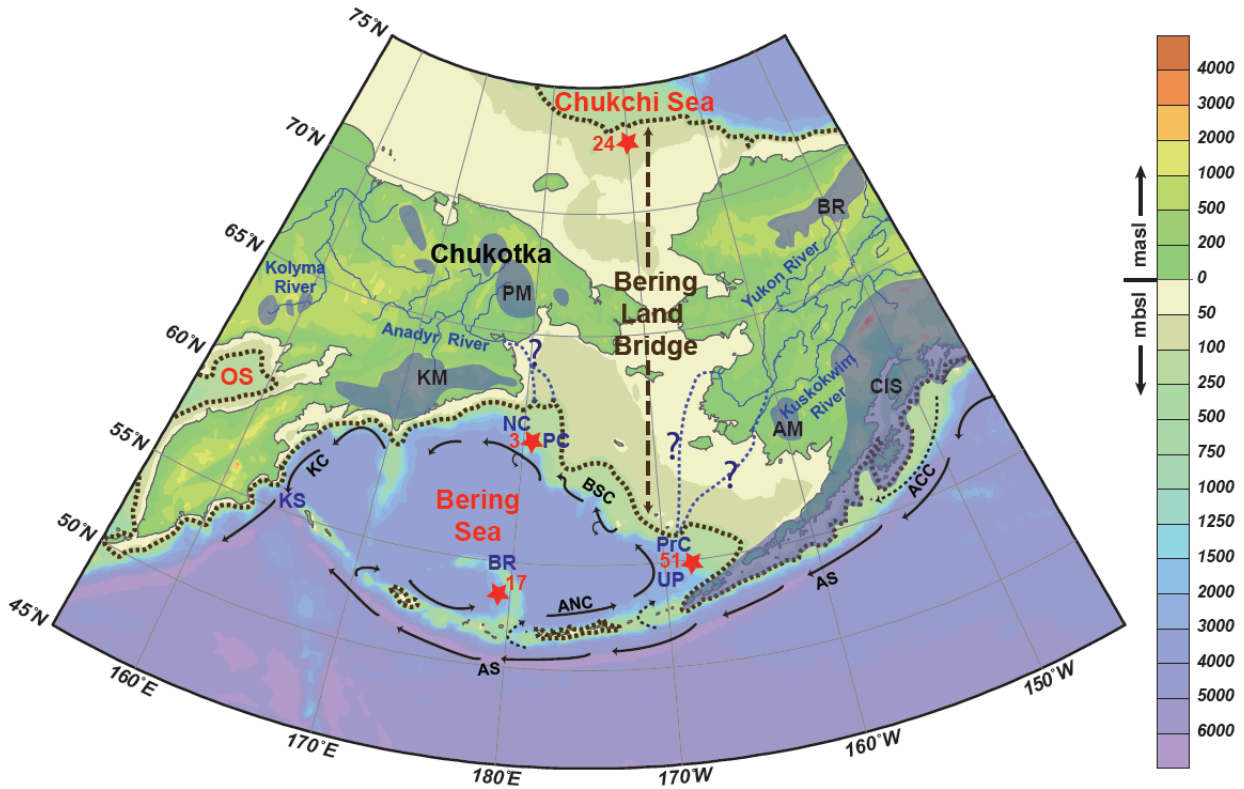


Figure 1.2. Map of the Bering Land Bridge. Brown dashed line indicates the estimated shoreline during the LGM with sea level 120-125 mbp [Peltier and Fairbanks, 2006]. Blue shaded areas on land are estimated glaciation in Alaska [Kaufman and Manley, 2004] and Chukotka [Hughes et al., 1977]: Cordilleran Ice Sheet (CIS), Ahklun Mountains (AM), Brooks Range (BR), Koryak Mountains (KM) and Pekulney Mountains (PM). Modern currents are included along with core locations (numbered red stars). Potential routes of drainage for the Yukon, Kuskokwim and Anadyr Rivers are seen as blue dashed lines based upon Scholl et al. [Scholl et al., 1970] and Carlson and Karl [Carlson and Karl, 1984]. The Anadyr River drains towards Navarin (NC) and Pervenets (PC) Canyons. The Yukon and Kuskokwim Rivers drain towards Pribilof Canyon (PrC).

Where these major rivers drained in the past has implications for sediment delivery at core sites of the Bering and Chukchi Seas, as their nutrients and detrital material are an important part of the ecosystem and sedimentary budget of the region [McManus et al., 1974; Nelson and Creager, 1977; Stein, 2000], and would have been only greater during deglaciation.

1.3. Regional Paleoclimate and Productivity History

1.3.1. Reservoir Age

Before delving into the periods of interest to this study, we must discuss the most important part of sediment core studies: chronology. It is well known that changes in ocean circulation and ventilation can dramatically influence the reservoir age of any water mass over time [Eiriksson *et al.*, 2004].

Paleoclimate reconstructions generally consider that flooding of the Bering Strait took place between 11-12 ka [Elias *et al.*, 1996; Keigwin *et al.*, 2006], a claim which is disputed by ^{14}C dates on *C. kurriana*, a low Arctic bivalve mollusk [England and Furze, 2008], which suggests an age of 13.3 cal yr BP. If correct, the early flooding date of 13.3 ka would change our view of when the BS flooded, and our understanding of conditions at the beginning of the Younger Dryas (YD). If the BS was flooded around 13.3 ka, then the connection of the Arctic and North Pacific could have reestablished circulation in the Arctic Ocean, and led to the break-up and evacuation of ice in the Arctic Ocean as postulated by Bradley and England [2008]. This would seem to require a remarkable establishment of a strong North Pacific inflow to the Arctic Ocean, far quicker than one would imagine given glacio-eustatic sea level information [Fairbanks, 1989]. This example illustrates the integral role of establishing an accurate chronology to determine the timing of the flooding of the BLB.

Accurately applying an age depth model to sediment cores from the Bering and Chukchi Seas spanning the deglaciation period (LGM to late Holocene) is difficult, due to changes in THC, water mass ventilation and interaction, as well as the flooding and opening of the BS. Cores in the Arctic Ocean that date from the YD or older were previously only influenced by old,

long lived, Arctic and Atlantic waters until the Bering Strait flooded, and Pacific water entered the picture, likely with a significant effect on the ^{14}C reservoir.

We chose a reservoir age of 800 years for our Bering Sea cores as a best estimate providing consistency with studies previously published for our cores [Cook *et al.*, 2005; Cook, 2006; Brunelle *et al.*, 2007, 2010; Caissie *et al.*, 2010], and cores proximal to these cores [Itaki *et al.*, 2009; Kim *et al.*, 2011; Schlung *et al.*, 2013]. However, this reservoir correction is relatively poorly constrained with estimates in the Bering Sea and NE and NW Pacific ranging from 460 to 1100 years for total modern reservoir corrections [Kuzmin *et al.*, 2001; Dumond and Griffin, 2002; Kovanen and Easterbrook, 2002; Gorbarenko *et al.*, 2005]. Because the termination of the last glacial stage had pronounced impacts on thermohaline circulation [Keigwin *et al.*, 1991; Weaver, 2003; McManus *et al.*, 2004] as well as during the YD [Keigwin *et al.*, 1991; McManus *et al.*, 2004], the reservoir age for cores in the region may have experienced considerable variation during deglaciation.

We also applied a reservoir age of 800 years in the Chukchi Sea cores consistent with reservoir corrections from the region [Andrews *et al.*, 1993; Polyak *et al.*, 2004]. However, some Arctic studies completely omit a reservoir correction [Polyak *et al.*, 2007; Kaufman *et al.*, 2008] due to high uncertainty in marine Arctic waters, especially during deglaciation [Björck *et al.*, 2003; Eiriksson *et al.*, 2004].

The uncertainty involved with applying reservoir corrections, which may be changing through time, means that absolute dating of events seen in sediment cores is difficult. Changes in water mass interactions associated with global ocean circulation changes, or the location/existence of deepwater formation, like hypothesized for the North Pacific during the early stages of the Last Glacial Termination [Okazaki *et al.*, 2010], makes assigning proper ages

and interpreting changes challenging. The following sections assume that the current accepted reservoir corrections highlighted above are indeed right.

1.3.2. Last Glacial Maximum (~20ka)

Around 20 ka, the Bering and Chukchi Seas were much smaller due to the exposure of the continental shelves (Figure 1.2). With a closed Bering Strait, there was no communication between the Chukchi and Bering Sea. Bering Sea circulation may have been slower with the removal of the incentive for water to enter the Bering Sea and exit through the Chukchi. Given the cold climate of the LGM, there was extensive sea ice cover over the Bering Sea [*Sancetta et al.*, 1985; *Caissie et al.*, 2010], and substantial perennial ice over what little of the Chukchi was not subaerially exposed [*Nørgaard-Pedersen*, 2003].

Sea level reached a low estimated at 125-135 m below present day [*Fairbanks*, 1989] when the ice sheets of the Northern Hemisphere were at a maximum [*Dyke et al.*, 2002]. The Laurentide ice sheet alone held an estimated 40-92 m of sea level equivalent [*Licciardi et al.*, 1998]. The most proximal ice sheet was the Cordilleran Ice Sheet, extending from what is today Washington, Idaho and Montana, northward through British Columbia and along southern Alaska [*Clague et al.*, 1989; *Dyke et al.*, 2002].

Glacier ice extent during the LGM in Chukotka was limited to primarily to valley glaciers and coalescing valley glacier systems [*Glushkova*, 2001] as seen in the Pekulney Mountains [*Brigham-Grette et al.*, 2003] and Koryak Mountains (Figure 1.2), the latter of which likely featured marine terminating glaciers as well [*Gualtieri et al.*, 2000]. Glaciation in Alaska (~730,000 km²) during the LGM was ten times greater than present day [*Kaufman and Manley*, 2004]. The three main glaciated regions of Alaska were the Brooks Range, the Ahklun

Mountains and the northern extension of the Cordilleran Ice Sheet (Figure 1.2) (comprised of the Alaska Range, Aleutian Range and the Coast Mountains) [Kaufman and Manley, 2004].

The cold climate likely limited the input of terrigenous material to the sea, and coupled with light limitation [Caissie *et al.*, 2010] imposed by extensive and thick sea ice cover, this kept productivity relatively low in the Bering Sea [Keigwin *et al.*, 1992; Jaccard, 2005; Okazaki *et al.*, 2005; Tanaka and Takahashi, 2005]. Reduced primary productivity in the Bering Sea and subarctic North Pacific [Nakatsuka *et al.*, 1995; Caissie *et al.*, 2010; Lam *et al.*, 2013] supports the concept that patterns of glacial-interglacial changes include lower biogenic sedimentation during glacial compared to interglacials [Levitan and Stein, 2008].

1.3.3. Early Deglacial Period (18 to 15 ka)

The early deglacial period began with increasing high northern latitude insolation [Berger and Loutre, 1991] and increasing atmospheric carbon dioxide (CO₂) concentration [Marchitto *et al.*, 2007; Shakun *et al.*, 2012]. As ice began to melt, nutrient inputs from melting ice increased [Keigwin *et al.*, 1992], both from glacial runoff, and the subsequent flooding and erosion of continental shelf materials [Davies *et al.*, 2011].

There are few well-dated records of the LGM across Beringia [Briner and Kaufman, 2008]. Intermediate moraines have proven difficult to correlate between Chukotka and Alaska, but the magnitude of glaciation and LGM moraines are relatively comparable [Heiser and Roush, 2001]. Dated terminal and younger end moraines, as well as terraces, indicate that deglaciation in the Koryak Mountains of Chukotka occurred between 24-16 ka [Gualtieri *et al.*, 2000], while glaciers appear to have deposited their younger terminal moraines between 24-10 ka in southern Alaska [Briner and Kaufman, 2008]. This large window of deglaciation makes assigning a

single age for North Pacific deglaciation impossible, assured by the dearth of well-dated records, combined with spatial heterogeneity.

Prior to 17 ka, sea ice over Umnak Plateau of the southeastern Bering Sea, was likely thick and extensive, potentially perennial [Caissie *et al.*, 2010] as was the case during the LGM [Sancetta *et al.*, 1985; Caissie *et al.*, 2010]. At 16.8 ka, there is a transition to seasonal ice conditions on the Umnak Plateau [Caissie *et al.*, 2010]. This shift in sea ice would have relieved light limitation, allowing for an initial small increase in productivity, until increasing meltwater, further sea ice reduction, and nutrient influx spurred a large increase in productivity.

Sediment cores from Bowers Ridge in the southwest Bering Sea were south of the speculated extent of sea ice [Katsuki and Takahashi, 2005], and record no change in productivity proxies, but a 2 ‰ $\delta^{15}\text{N}_{\text{db}}$ decrease [Brunelle *et al.*, 2010] potentially signals a weakening of subarctic North Pacific stratification as hypothesized by Lam *et al.* [2013]. This would be the North Pacific analogue to the increase in vertical exchange thought to have occurred in the Southern Ocean at the time of H1 [Marchitto *et al.*, 2007], when temperature and atmospheric CO_2 began to increase [Monnin, 2001]. Weaker stratification of the North Pacific, in combination with an increase in nutrient supply, is thought to have induced light limitation due to a very deep mixed layer [Lam *et al.*, 2013], dampening other factors that would have encouraged an increase in productivity.

1.3.4. Bølling-Allerød (15 to 13 ka)

The early deglaciation period ended at the onset of the Bølling-Allerød, a warm period associated with rapid Northern Hemisphere warming [Broecker, 1998; Schlung *et al.*, 2013]. AMOC is thought to have collapsed during H1, only to recover and overshoot during the BA [Timmermann and Menviel, 2009], warming the Northern Hemisphere. An abrupt freshening

and/or warming event is recorded in planktonic foraminifer $\delta^{18}\text{O}$ of the Bering shelf-slope at 14.4 ka BP [Cook *et al.*, 2005] and at 15 ka on the Umnak Plateau [Caissie *et al.*, 2010], as well as in the Gulf of Alaska [Davies *et al.*, 2011] and North Pacific [Galbraith *et al.*, 2007], corresponding with the 14.7 ka date of BA onset at NGRIP [Rasmussen *et al.*, 2006]. This freshening may have relieved light limitation by shallowing the depth of the mixed layer [Lam *et al.*, 2013] and fostering elevated productivity as predicted by the critical depth theory [Sverdrup, 1953], which is valid in the western North Pacific [Obata *et al.*, 1996].

The influx of nutrients and increase in upper water column stability due to fresh water input from melting ice [Keigwin *et al.*, 1992], drove an increase in productivity in the Bering Sea [Cook *et al.*, 2005; Brunelle *et al.*, 2010; Caissie *et al.*, 2010; Schlung *et al.*, 2013], that also occurred over the subarctic North Pacific [Keigwin *et al.*, 1992; Crusius *et al.*, 2004; Galbraith *et al.*, 2007; Jaccard *et al.*, 2009]. Ventilation of intermediate waters decreased [Behl and Kennett, 1996; Ikehara *et al.*, 2006; Schlung *et al.*, 2013], supporting weaker ventilation of intermediate waters during interglacials relative to glacial conditions [Keigwin, 1998].

The BA warm period is marked by laminated sediments in the Bering Sea as well as in the Pacific from Mexico north. Generally, these widespread laminations correspond to both the BA and pre-Boreal (PB) warm periods bracketing the bioturbated sediment deposited during the YD from: the northwest coast of Mexico [Ganeshram and Pedersen, 1998], the Gulf of California [Sancetta, 1995; Keigwin, 2002; Barron *et al.*, 2005], the Santa Barbara Basin [Kennett and Ingram, 1995; Hendy and Kennett, 2003], the California margin [Gardner *et al.*, 1997; Mix *et al.*, 1999], to the north western Pacific [Shibahara *et al.*, 2007; Brunelle *et al.*, 2010] (also Keigwin 1992 ILL), the Okhotsk Sea, and into the Bering Sea [Cook *et al.*, 2005;

Brunelle et al., 2007; *Itaki et al.*, 2009; *Caissie et al.*, 2010; *Okazaki et al.*, 2010; *Khim et al.*, 2011; *Kim et al.*, 2011; *Schlung et al.*, 2013].

Laminated sediments are deposited under dysaerobic to anoxic conditions [*Kennett and Ingram*, 1995; *Behl and Kennett*, 1996] with export productivity and ventilation as the accepted primary controls on benthic oxygenation [*Hendy and Pedersen*, 2005]. Deposition of laminated intervals in cores proximal to our Bering Sea sites have been attributed to changes in oxygen content of North Pacific Intermediate Water (NPIW) and increased export production, which fostered dysaerobic conditions [*Cook et al.*, 2005; *Caissie et al.*, 2010; *Davies et al.*, 2011; *Kim et al.*, 2011; *Schlung et al.*, 2013].

Today, mixing of the northward flowing warm and saline Kuroshio Current and the southward flowing cold and fresh Oyashio Current forms NPIW where they meet east of Hokkaido, Japan [*Yasuda*, 1997; *You*, 2003]. NPIW is characterized by low salinity and high oxygen content, and is largely a product of brine rejection during winter sea-ice formation [*Takahashi*, 1998] in the Okhotsk Sea. This water flows out through the Kuril Islands, and mixes with Western Subarctic Gyre (WSAG) water, forming Oyashio Current water.

Extensive sea ice formation during the LGM and cold intervals like the YD had major ramifications for ventilation through the production of well oxygenated intermediate water, and the brine rejection transport of oxygen-rich surface-water toward the seafloor [*Talley*, 1991]. It is estimated that today, with less sea ice cover than the LGM, Okhotsk intermediate water formation is nearly 2 Sv, which has a major effect on NPIW [*Alfultis and Martin*, 1987]. It stands to reason that in a cold climate the production would be higher due to greater sea ice formation [*Gorbarenko et al.*, 2014], enabling benthic life and the bioturbation that produced massive sediments during the LGM and YD. With a weakening of NPIW formation/oxygenation

during the BA, NPIW entering the Bering Sea was less oxygenated, and thus preconditioned to contribute dysoxic conditions under elevated productivity.

1.3.5. Younger Dryas (12.9 to 11.7 ka)

AMOC is thought to have weakened or ceased altogether during the Younger Dryas cold period [Broecker *et al.*, 1988; Timmermann and Menviel, 2009]. The Bering Land Bridge was shrinking in extent, but was still a contiguous east-west landmass with sea level ~65 mbp at the onset of the YD [Fairbanks, 1989]. Alpine glaciers advanced in Alaska during the YD [Briner *et al.*, 2002], illustrating the abrupt change from the warm BA. Sea ice had declined during the BA, but rebounded during the YD (Jim Kocis submitted [Cook *et al.*, 2005]). Such rapid changes in climate had a pronounced effect on the species assemblages of marine organisms and the overall productivity [Cook *et al.*, 2005; Barron *et al.*, 2009].

The YD marked a hiatus in lamina deposition across the range cited in the above BA section [Behl and Kennett, 1996; Cook *et al.*, 2005; Caissie *et al.*, 2010; Schlung *et al.*, 2013]. The increase in oxygenation that curtailed the deposition of laminations was, like before, due to changes in NPIW ventilation [Kennett and Ingram, 1995; Zheng *et al.*, 2000; Max *et al.*, 2014; Okazaki *et al.*, 2014], primary productivity [Mix *et al.*, 1999; Crusius *et al.*, 2004; Schlung *et al.*, 2013], or a combination of both [Hendy and Pedersen, 2005; Ishizaki *et al.*, 2009; Kim *et al.*, 2011; Gorbarenko *et al.*, 2014].

The YD is not a prominent feature in sediment cores from Bower's Ridge, where it is identified as an 11 cm thick massive interval [Schlung *et al.*, 2013], that coincided with a collapse in % biogenic Ba, CaCO₃, and opal [Brunelle *et al.*, 2007], indicative of low productivity. Low sedimentation rates are seen on Bower's Ridge 10 cm/kyr [Schlung *et al.*, 2013], and in the Gulf of Alaska 9 cm/kyr [Davies *et al.*, 2011], consistent with fairly stable cold

and/or saline surface conditions [Davies *et al.*, 2011]. The YD was a stark transition from the preceding BA warm period and the following PB, as glaciers advanced, sea ice spread, productivity declined, and sedimentation rates fell.

1.3.6. Pre-Boreal (11.7 to 10.5 ka)

The pre-Boreal warm period (PB) marked the end of the YD and is the second major laminated interval seen in our Bering Sea cores, as well as the cores cited in the BA section above [Behl and Kennett, 1996; Cook *et al.*, 2005; Caissie *et al.*, 2010; Schlung *et al.*, 2013]. Accompanying these laminations was another increase in productivity [Crusius *et al.*, 2004; Davies *et al.*, 2011; Schlung *et al.*, 2013], and a second abrupt freshening and/or warming event recorded in planktonic foraminifer $\delta^{18}\text{O}$ of the Bering shelf-slope at 11.65 ka BP [Cook *et al.*, 2005]. However, the deposition of laminations in the Gulf of Alaska led the planktonic $\delta^{18}\text{O}$ depletion in the Gulf of Alaska by a few hundred years [Davies *et al.*, 2011].

Around the end of the YD and onset of the early Holocene (PB), the Bering Land Bridge likely ceased to exist as a contiguous landmass connecting Chukotka and Alaska [Elias *et al.*, 1996; Keigwin *et al.*, 2006]. Sea level at the time was at about 50 m below modern [Fairbanks, 1989]. For the first time since ~75ka the BLB connection of Beringia was severed, and the BS began to mediate water interaction between the Bering and Chukchi Seas. The laminated interval of the PB was indicative of an ameliorating climate with elevated productivity in the Bering Sea [Khim *et al.*, 2011].

1.3.7. Holocene (10.5 ka to present)

By ~10 ka, the remainder of the BLB was largely inundated, with sea level at the time at about 20 m below modern [Hopkins, 1979; Fairbanks, 1989]. While the climate has varied

during the Holocene, variability has generally been weaker in magnitude than during the last deglaciation [Mayewski *et al.*, 2004]. NADW production has fluctuated [Oppo *et al.*, 2003] during the Holocene, yet there hasn't been a weakening or shutdown to the extent seen during deglaciation [Keigwin *et al.*, 1991; Thornalley *et al.*, 2011]. Holocene ventilation of the North Pacific has been weak, as NP ventilation is stronger in cold periods [Schlung *et al.*, 2013], whereas NA ventilation increased during the BA and Holocene (warm periods) [Robinson, 2005; Thornalley *et al.*, 2011].

1.4. Primary Research Questions

With our Bering and Chukchi Sea cores, we aim to examine a period of rapid climatic change that was marked by the connection of the Arctic and North Pacific Oceans through the flooding of the BLB and opening of the BS. What can sedimentary archives from across the Bering Sea tell us about oceanographic change during the deglacial period and through the opening of the BS? What story do sediments spanning the BS tell us about productivity, circulation and sediment delivery mechanisms during the deglaciation?

As sea level rose, the Bering Land Bridge shoreline regressed until it was flooded around 11–12 ka [Elias *et al.*, 1996; Keigwin *et al.*, 2006]. The submergence of the Bering Strait was likely a gradual event, punctuated by rapid shifts in the coastline across the flatter portions of the shelf. Modern average depth of the strait is only 50 m, so initial flow would have likely been limited in location and magnitude. Early flooding would have led to a small amount of water mass interaction, but when modern circulation was established remains an open question. Cores from the Chukchi Sea hold the most promise in answering the question of when flow through the Bering Strait approximately reached the magnitude seen today.

Present day flow through the Bering Strait is the result of a pressure gradient driven by a difference in sea surface topography between the Bering and Chukchi Seas [*Coachman and Aagaard, 1966; Woodgate et al., 2005*]. In the past BS flow may have reversed in direction, with a net transport south through the Bering Strait, as supported by modeling simulations [*De Boer and Nof, 2004; Hu and Meehl, 2005; Hu et al., 2007, 2012b, 2013*]. Generally, a reversal of flow is thought to be due to freshwater hosing (strong buoyancy forcing) of the North Atlantic, and subsequent weakening or shutdown of AMOC [*De Boer and Nof, 2004; Hu et al., 2014*]. What was flow like when the Bering Strait initially flooded? Which direction was net Bering Strait throughflow during following land bridge flooding? To date, sediment records from Beringia do not answer the question of flow direction; however, it is important to consider when interpreting both chronology and abrupt shifts in paleorecords from the Chukchi Sea in particular.

How did sediment delivery to the Bering Sea sites change through time? As sea level transgressed, did terrigenous input change in both magnitude and source location? The Yukon and other major rivers would have had to cross the continental shelf to drain into the Bering Sea. Is this recorded in the sediment record on Bering shelf slope and the Umnak Plateau?

Were there distinct sediment units corresponding to separate climate intervals? What properties and characteristics defined these sediment units?

With flow restricted through Unimak Pass, and likely a weaker overall northward flow in the Bering Sea at the time of the LGM, was the Bering Slope Current weaker, and when did it become similar in strength to today? A reduced influx of ACW would have weakened the BSC. At a minimum, it would have been shifted to the south as the coast of the Bering Land Bridge is near its present location. Can we see the BSC increase in strength through productivity data, or a change in material being delivered to the site?

Detailed examination of sedimentologic and geochemical parameters recorded during crucial climatic intervals of deglaciation such as the BA warm period, and YD stadial, are important to elucidate changes in regional oceanography as the Bering Land Bridge flooded, and modern ocean circulation was established. Examining the implications and effects of rapid climatic change seen during deglaciation in the Bering and Chukchi Seas will better aid our understanding of their potential response to modern climate change, be it shifting plankton bloom season, changes in overall primary productivity and species assemblages, or changes in water mass exchange and ventilation. The benthos of the Bering Sea saw major changes during deglaciation, from suboxic intervals when laminations were deposited, to times of bioturbation and plentiful benthic life. The Bering-Chukchi Seas over the shelf are a major sink for CO₂ [Kaltin and Anderson, 2005], and thus understanding how this may change in the near future, as biology, temperature and ice cover control the CO₂ uptake, could have ramifications for the global carbon cycle. Changes in the ventilation and water column stratification are expected in the near future; understanding what these changes can mean for the ecosystems of the Bering Sea via paleoceanographic study can help better prepare us for what is to come. The rapid climatic change of the last deglaciation is the ideal paleoclimatic lens with which to view the potential changes in the near future as the newest climatic interval dawns.

CHAPTER 2

ABSTRACT

SEDIMENTOLOGICAL, GEOCHEMICAL AND ISOTOPIC EVIDENCE FOR THE ESTABLISHMENT OF MODERN CIRCULATION THROUGH THE BERING STRAIT AND DEPOSITIONAL ENVIRONMENT HISTORY OF THE BERING AND CHUKCHI SEAS DURING THE LAST DEGLACIATION

Sea level regression during the Last Glacial Maximum exposed the Bering Land Bridge, and cut off the connection between the North Pacific and Arctic Ocean, ending the exchange of North Pacific Water through the Bering Strait. Exchange of North Pacific Water comprises a major portion of fresh water input to the Arctic Ocean, and is of vital importance to North Atlantic Deep Water formation, a vital component of Atlantic Meridional Overturning Circulation. Bering Strait throughflow thus plays an integral role in global climate stability. A suite of four cores were selected, three in the Bering Sea and one in the Chukchi Sea, to bracket the Bering Strait in order to elucidate changes in sediment delivery, productivity and regional oceanography as the Bering Land Bridge flooded and modern ocean circulation was established during the last deglaciation. The arrival of nutrient rich North Pacific Water in the Chukchi Sea is recorded around 8 ka by organic carbon isotope depletion and increases in total organic carbon and organic nitrogen, reflecting an increasingly marine isotopic signal and increased productivity. In the Bering Sea, the early deglaciation is marked by depleted organic carbon isotopes that indicate increasing terrestrial input, and increased total organic carbon. Principal component analysis of sedimentologic, geochemical and isotopic data clearly captures discrete sediment populations that correspond to key climatic intervals, representing changes in sediment delivery, productivity and circulation during the last deglaciation. In the Bering Sea we observe

that deglaciation is recorded around 18–17 ka, but lack of confidence in our age control does not allow for a more precise date. Our results suggest that modern circulation through the Bering Strait, and thus for the Bering and Chukchi Seas, was established ~8 ka. Prior to 8 ka, the sediment sequence appears to record a possible reversal of flow through the Bering Strait corresponding to the 8.2 ka event.

2.1. Introduction

The transition from the Last Glacial Maximum (LGM) through deglaciation and into the Holocene was a period of rapid climatic change [Keigwin *et al.*, 1991], and though punctuated by cold periods [Broecker *et al.*, 1988; Bradley and England, 2008], featured the most recent significant warming in the Arctic. Today, the Arctic is enduring great impacts of climate change [Grebmeier *et al.*, 2010; Wipf *et al.*, 2013] with rapid warming and decreases in sea ice cover [Overland and Wang, 2007; Comiso *et al.*, 2008; Snape and Forster, 2014] resulting in major changes in energy distribution and atmospheric patterns [Francis *et al.*, 2009; Tang *et al.*, 2013; Peings and Magnusdottir, 2014]. In studying the last intervals of major warming in the Arctic, we hope to better document the Arctic marine response to climatic change, and provide insight into Arctic system dynamics particularly with respect to circulation and productivity, in order to better understand rapid contemporary changes.

While the North Pacific and Arctic Ocean have been the focus of renewed interest in light of climate change [Snape and Forster, 2014], and the potential for economic [Smith and Stephenson, 2013] and scientific activity resulting from the near future projections of an Arctic absent of sea ice [Overland and Wang, 2007; Stroeve *et al.*, 2011; Snape and Forster, 2014], the region still suffers from a paucity of paleodata.

The Bering Strait (BS) serves as the connection between the North Pacific and North Atlantic Oceans via the Arctic Ocean, with the Bering and Chukchi Seas acting as intermediaries (Figure 2.1). During the LGM, the emergent BLB (Figure 2.2) occupied what is today the Chukchi and Bering shelves [Hopkins, 1959]. The subsequent submergence of the BLB and extensive shelf regions [Jakobsson, 2002] put the Bering and Chukchi Seas in a unique position to record postglacial depositional and environmental change.

Previous studies in the Bering Sea (Table 2.1) during the late Quaternary have focused on diatoms as recorders of environmental change and nutrient utilization [Sancetta *et al.*, 1985; Brunelle *et al.*, 2007, 2010; Caissie *et al.*, 2010], sea surface temperature (SST) [Caissie *et al.*, 2010], oxygen isotopes [Cook *et al.*, 2005; Schlung *et al.*, 2013], and radiolarians [Tanaka and Takahashi, 2005]. We aim to complement these studies by providing additional data to better document past changes and thus better constrain hypotheses regarding postglacial sediment delivery and environmental changes.

Our study builds upon a growing body of western Arctic paleoclimate records drawing upon high resolution bulk sediment parameters to produce quantitative and semiquantitative paleoclimate data from cores on either side of the Bering Strait. We apply our bulk biogeochemical and isotopic data to estimate relative productivity, nutrient utilization, and sediment sourcing to more accurately define deglaciation as recorded in the Bering and Chukchi Seas. We use proxy data to define the earliest establishment of modern circulation through the Bering Strait based upon our Chukchi Sea records. Our data document postglacial changes in sediment delivery, productivity, and circulation across greater Beringia.

As the BLB flooded, our selected cores became less proximal to land, and river routing likely changed, with a net result of weakening terrestrial input. The cores selected for this study

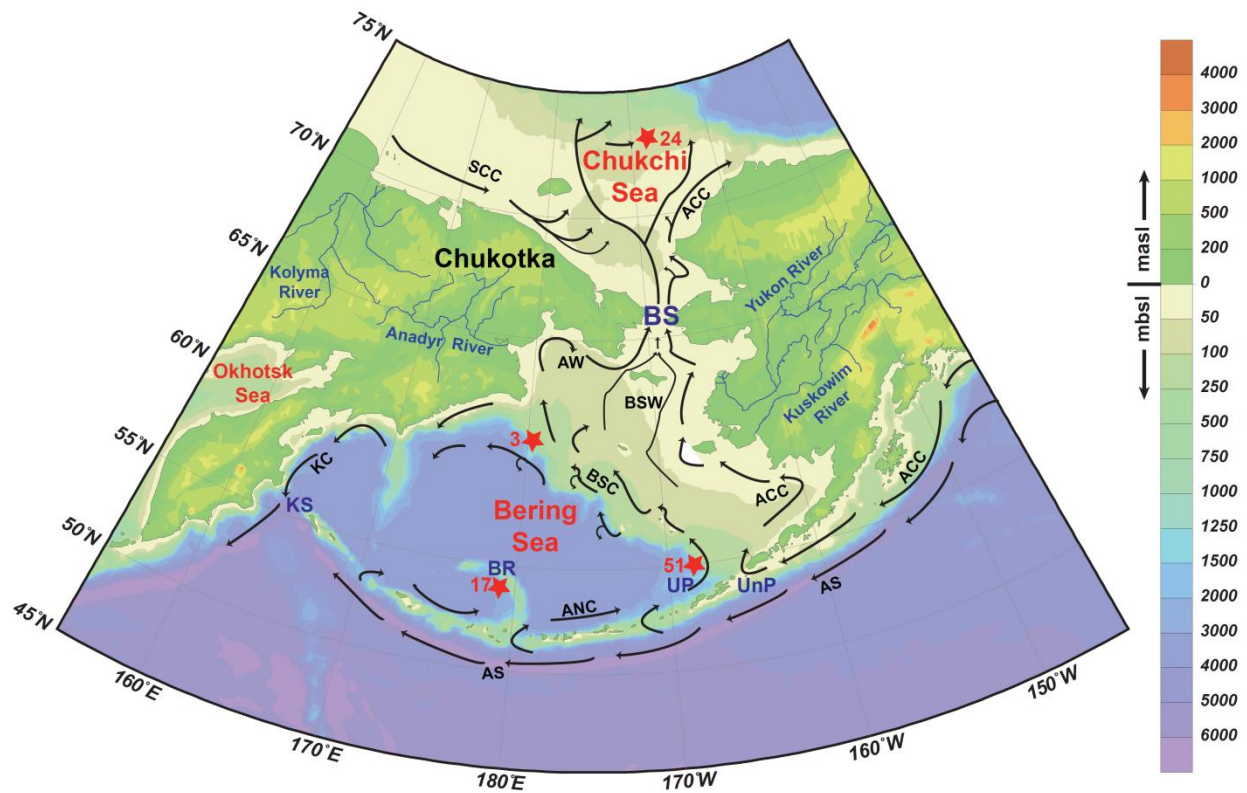


Figure 2.1. Bathymetric and topographic map of Beringia, the North Pacific, and the Bering and Chukchi Seas with locations of cores (numbered red stars, see Table 2.1). Currents denoted by black arrows and labeled in black: Alaskan Stream (AS), Aleutian North Slope Current (ANC), Alaskan Coastal Current (ACC), Bering Shelf Current (BSC), Bering Shelf Water (BSW), Anadyr Water (AW), and Siberian Coastal Current (SCC). The Bering Strait (BS), Umnak Plateau (UP), Unimak Pass (UnP), Bowers Ridge (BR), and Kamchatka Strait (KS) are labeled in blue.

are well suited to represent the Bering Sea as a whole through the climatically dynamic deglaciation period [Mix *et al.*, 1999; McManus *et al.*, 2004]. Interpretations of past productivity, terrestrial input and circulation are based on $\delta^{13}\text{C}_{\text{org}}$, %TOC, bulk $\delta^{15}\text{N}$, % N_{org} , $\text{C}_{\text{org}}/\text{N}_{\text{org}}$, elemental X-ray fluorescence (XRF) data, grain size analysis, and PCA, incorporating all of the aforementioned proxies.

Our findings describe centennial to millennial scale changes in productivity and terrestrial input that may be compared with previous paleoclimate records from the Bering Sea

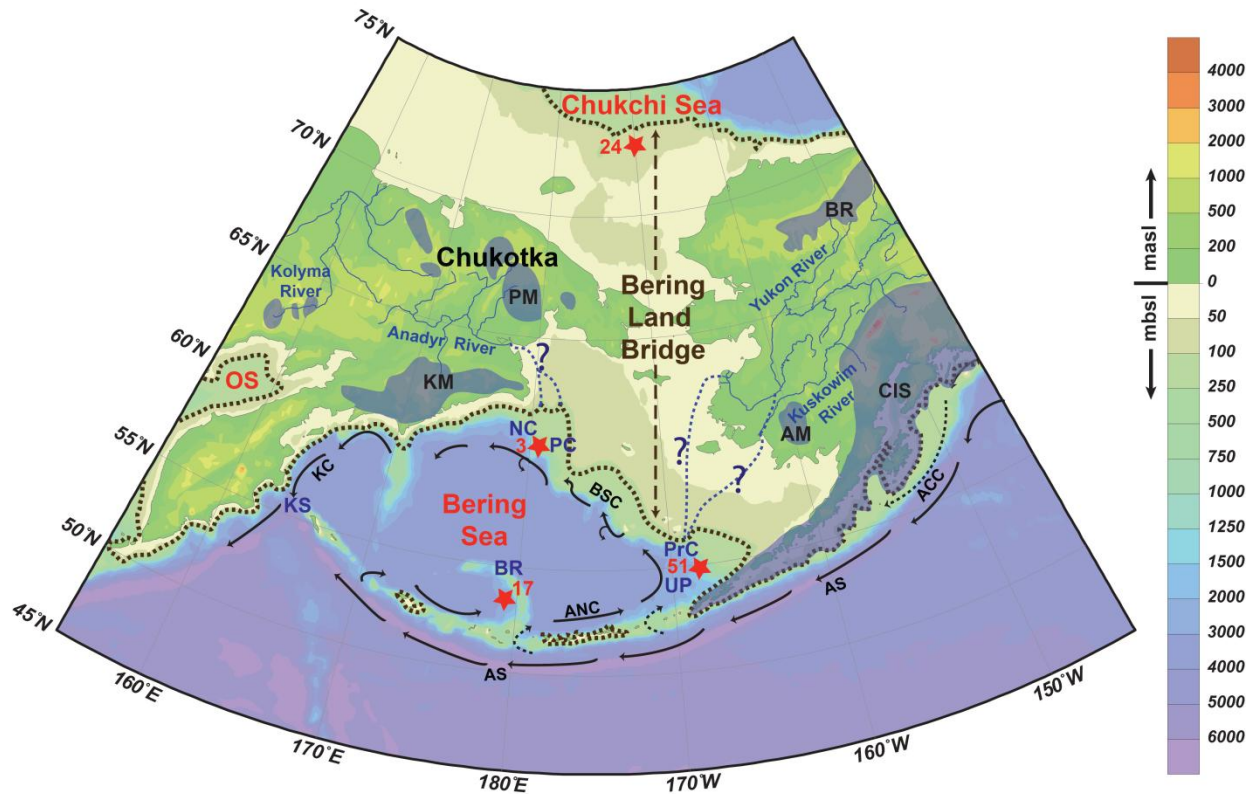


Figure 2.2. Map of the Bering Land Bridge. Brown dashed line indicates the estimated shoreline during the LGM with sea level 120-125 mbp [Peltier and Fairbanks, 2006]. Blue shaded areas on land are estimated glaciation in Alaska [Kaufman and Manley, 2004] and Chukotka [Hughes et al., 1977]: Cordilleran Ice Sheet (CIS), Ahklun Mountains (AM), Brooks Range (BR), Koryak Mountains (KM) and Pekulney Mountains (PM). Modern currents are included along with core locations (numbered red stars, as in Figure 2.1). Potential routes of drainage for the Yukon, Kuskokwim and Anadyr Rivers are seen as blue dashed lines based upon Scholl et al. [Scholl et al., 1970] and Carlson and Karl [Carlson and Karl, 1984]. The Anadyr River drains towards Navarin (N) and Pervenets (P) Canyons. The Yukon and Kuskokwim Rivers drain towards Pribilof Canyon (Pr).

[Cook et al., 2005; Brunelle et al., 2007, 2010; Caissie et al., 2010; Kim et al., 2011; Schlung et al., 2013], Gulf of Alaska [Barron et al., 2009; Davies et al., 2011; Addison et al., 2012], and North Pacific [Keigwin et al., 1992; Lam et al., 2013]. We find that marine carbon was the dominant source of OC to the Bering Sea shelf slope during the LGM and Holocene, and terrestrial carbon supply was the primary source during the deglaciation (~18-11 ka). Based on clay content, and TOC $\delta^{13}\text{C}_{\text{org}}$, we find that modern circulation through the Bering Strait was

established ~8 ka as recorded in the Chukchi Sea, following a potential reversal of flow possibly corresponding to the 8.2 ka event, ~3–4 ka after the submergence of the Bering Strait [*Elias et al.*, 1996; *Dyke and Savelle*, 2001; *Keigwin et al.*, 2006].

Table 2.1. Regional cores referred to in text with primary citations, location and relevant proxies. Cores used in this study are in bold font.

Core Name	Source	General Area	Proxy
HLY0202-51JPC	Caissie et al. [2011]	Umnak Plateau, Bering Sea	Diatom assemblages, $\delta^{13}\text{C}$, C_{37} total, $\text{U}^{\text{K}}37$, $\delta^{18}\text{O}$
HLY0202-3JPC	Cook et al. [2005]	W. Shelf Slope, Bering Sea	Diatom assemblages, $\delta^{18}\text{O}$
HLY0202-17JPC	Cook et al. [2005] and Brunelle 2007, 2010.	Bowers Ridge, Bering Sea	$\delta^{18}\text{O}$, $\delta^{15}\text{N}$, Opal, biogenic Ba
HLY0402-24JPC	Lundeen [2005]	NW Shelf, Chukchi Sea	$\delta^{13}\text{C}$, TOC, TN
IODP Sites U1341, U1343, U1344	Aiello and Ravello [2012]	Bering Slope	Grain Size, Diatom abundance
MR06-04 PC-23A	Itaki et al [2009], Khim et al. [2010], and Kim et al. [2011]	W. Shelf Slope, Bering Sea	TOC, CaCO_3 wt %, Opal, $\delta^{13}\text{C}$, $\delta^{15}\text{N}$, foram analysis
MD02-2489	Gebhardt et al. [2008]	Patton Seamount, N. Pacific	d18O, IRD, biogenic opal
RC14-121	Sancetta and Robinson [1983]	Umnak Plateau, Bering Sea	Diatom assemblages
UMK3A	Katsuki and Takahashi [2005] and Okazaki et al. [2005]	Umnak Plateau, Bering Sea	Diatom assemblages
BOW 9A	Katsuki and Takahashi [2005] and Okazaki et al. [2005]	Bowers Ridge, Bering Sea	CaCO_3 wt %
IODP Site U1340	Takahasi et al. [2011], Schlung et al. [2013] Aiello et al. [2012]	Bowers Ridge, Bering Sea	$\delta^{18}\text{O}$, $\delta^{13}\text{C}$, $\delta^{15}\text{N}$, Alkenone SST, Grain Size
EW0408–85JC	Davies et al. [2011] and Addison et al. [2012]	Gulf of Alaska, N. Pacific	$\delta^{18}\text{O}$, $\delta^{13}\text{C}$, $\delta^{15}\text{N}$, XRF, TOC, Opal
Vinogradov 19/4, GGC-37	Keigwin [1998], Galbraith et al. [2007], and Lam et al. [2013]	Detroit Seamount, N. Pacific	$\delta^{18}\text{O}$, Sr and Nd isotopes
MD01-2416	Gebhardt et al. [2008]	Detroit Seamount, N. Pacific	IRD, biogenic opal
RAMA 44PC	Keigwin [1992]	Meiji Seamount, N. Pacific	$\delta^{18}\text{O}$
5 GC 936	Gorbarenko et al. [2004]	Sea of Okhotsk	CaCO_3 weight percent, d18O
6 Nesmeyanov 25, GGC-15	Keigwin [1998]	Sea of Okhotsk	$\delta^{18}\text{O}$, C_{37} total, $\text{U}^{\text{K}}37$, phytol

2.2. Background

In order to interpret past changes in sedimentological, geochemical and isotopic data, it is necessary to understand the circulation regime and physical setting that were in place from the

LGM to the Holocene. The climatic intervals referred to in this paper are color coded as background shading in the XRF, isotopic and grain size plots, and by colored points in the principal component analysis (PCA) biplots. The climatic intervals are as follows: LGM: 27–18 ka, grey/black, Early Deglacial (ED) 18–15 ka, green, Bølling-Allerød (BA) 14.9–13 ka, red, Younger Dryas (YD) 12.9–11.7 ka, blue, Pre-boreal (PB) 11.7–10.5 ka, pink, and the Holocene 10.5–2.5 ka, cyan. This color scheme is used in all applicable figures.

2.2.1. Bering Sea

The Bering Sea has a broad continental shelf (50–150 m deep), and a deep basin (<4000 m) bracketed by Chukotka and Kamchatka to the northwest, Alaska to the northeast, and the Aleutian Islands to the south (Figure 2.1). It has relatively low salinity but is nutrient rich [*Cook et al.*, 2005], particularly across the shelf and slope region where high nutrient waters of North Pacific origin are upwelled [*Walsh et al.*, 1989], making the Bering Sea one of the most productive marine systems in the world [*Sambrotto et al.*, 1984].

Surface circulation over the basin is roughly defined by a cyclonic gyre, whose western boundary current is the southward flowing Kamchatka Current (Figure 2.1). In the west, within the Gulf of Anadyr, deeper Pacific water is upwelled onto the shelf, with relatively high salinity, nutrient-rich Anadyr Water (AW) [*Clement et al.*, 2005]. The Bering Slope Current (BSC) flows in the upper 300 m along the continental shelf break and defines the eastern edge of the gyre [*Schumacher and Reed*, 1992], originating near 51JPC and flowing over 3JPC (Figure 2.1). On the shelf, the principal surface flow is northward through the Bering Strait, which is about 85 km wide and averages 50 m water depth [*Schumacher and Stabeno*, 1998; *Stabeno et al.*, 1999]. Bering Shelf Water (BSW), a nutrient-rich and less saline water mass, occupies the central region of the northern Bering Sea, while a strong gradient defines the warmer (in summer),

nutrient-poor, Alaska Coastal Water (ACW) to the east [Coachman, 1986; Grebmeier *et al.*, 1988]. The ACW originates from the Alaskan Stream (AS), which flows northward through gaps in the Aleutian Islands up onto the shelf [Stabeno *et al.*, 1999] near 51JPC, where it enters the Alaska Coastal Current (ACC).

The BSC is known for high productivity and has been referred to as the Green Belt [Springer *et al.*, 1996], a band with high chlorophyll and primary production throughout the summer [Springer *et al.*, 1996; Hurst *et al.*, 2010]. Tidal mixing and transverse circulation along the shelf break keeps stratification at a minimum, bringing nutrients up from 300 to 800 m [Springer *et al.*, 1996]. The elevated biological productivity associated with the BSC [Kinney *et al.*, 2009] is responsible for high organic carbon accumulation along the Bering shelf slope as described below in 3JPC.

To the south, the Bering Sea is connected to the North Pacific through four major straits and passes from 4400 to 430 m water depth. Physical properties of water on either side of the Aleutian Islands are different below 2000 m [Cook *et al.*, 2005], indicating relatively unimpeded exchange between the Bering Sea and North Pacific except through the deep Kamchatka Strait (4420 m). In the eastern Bering Sea, northward flow through the Unimak Pass (<80m deep) is the major ACC (ASW) conduit between the North Pacific and the shelf [Stabeno *et al.*, 1999], and has a major influence on 51JPC of the Umnak Plateau [Caissie *et al.*, 2010]. During the LGM, Unimak Pass was above sea level, but given the depth of the major straits, exchange through the remainder of the Aleutian Arc was probably not constrained by sea level regression.

2.2.2. Bering Strait

Bering Strait water has an average salinity of 32.5 psu [Roach *et al.*, 1995; Aagaard *et al.*, 2006], making it relatively fresh compared to the North Atlantic (34–37 psu). Today, a net

northward flow of 0.8 Sv [*Wijffels et al.*, 1992; *Aagaard et al.*, 2006] through the Strait represents a major contribution of freshwater to the Arctic Ocean (34.8 psu) [*Aagaard and Carmack*, 1989].

The first order of significance of the Bering Strait is its role in global circulation. It is the connection between the North Pacific and Atlantic oceans via the Arctic Ocean, which in turn affects the freshwater component exiting the eastern Arctic gateway, which plays a major role in North Atlantic Deep Water (NADW) production in the subpolar North Atlantic [*Broecker et al.*, 1990; *Wijffels et al.*, 1992; *Aagaard and Carmack*, 1994; *Keigwin and Cook*, 2007]. NADW is a driving force behind Atlantic Meridional Overturning Circulation (AMOC) [*Broecker*, 1991], which advects warm, salty surface water from the south into the North Atlantic where it cools and sinks [*Broecker*, 1991; *Thornalley et al.*, 2011]. The net northward transport of warm water associated with AMOC pulls heat to the North Atlantic [*Ganachaud and Wunsch*, 2000] and is responsible for the mild climate of Europe [*Broecker et al.*, 1988; *Broecker*, 1991]. Modeling simulations [*Stouffer et al.*, 2006; *Hu et al.*, 2013], and paleoclimate records [*Broecker*, 1994; *Keigwin and Jones*, 1994; *Clark et al.*, 2007] indicate that a slowdown in AMOC can result in Northern Hemisphere cooling.

An open Bering Strait is thought to act as an 'exhaust valve' for the North Atlantic [*De Boer and Nof*, 2004], capable of dissipating freshwater anomalies in the North Atlantic at a rate hypothesized to be impossible with the Bering Strait closed [*Hu et al.*, 2014]. The reduced volume of land-based ice present in the Northern Hemisphere today [*Church et al.*, 2001] likely does not store enough freshwater to deliver an adequate volume to the North Atlantic to shut down AMOC, though a reduction in AMOC is possible [*Stouffer et al.*, 2006]. An open BS is potentially able to disperse freshwater anomalies that threaten AMOC, whereas a closed BS

significantly strengthens AMOC [Wadley and Bigg, 2002], but perhaps makes it less stable. The combination of smaller Northern Hemisphere ice volume and open Bering Strait connection, implies that the North Atlantic is largely protected from freshwater hosing today, but causes of rapid climatic change, like seen during the YD, are difficult to unequivocally solve [Bradley and England, 2008]. During deglaciation, AMOC experienced both extremes, from a near shutdown during Heinrich Event 1 (H1), which occurred in what is our ED, to an overshoot during the BA warm period [Timmermann and Menviel, 2009].

For the Bering Strait to help disperse a North Atlantic fresh water cap, flow must reverse through the strait. The end of the Younger Dryas (11.7 ka) [Alley *et al.*, 1997] may have been linked to flooding of the Bering Strait (11–12 ka) [Keigwin *et al.*, 2006], but the initial depth of the Bering Strait would have been quite shallow. The 8.2 ka event is thought to have featured a strong freshwater buoyancy forcing over the North Atlantic, but only lasted ~150 years, possibly because of an open Bering Strait. Our data indicate the possibility for a reversal of flow coeval with the 8.2 ka event, consistent with modeling simulations for dispersion of North Atlantic freshwater anomalies through the Bering Strait [De Boer and Nof, 2004; Hu and Meehl, 2005; Hu *et al.*, 2007, 2012a, 2012b, 2014].

2.2.3. Chukchi Sea

The Chukchi Sea lies to the north of the Bering Strait, bounded by Wrangel Island and the Siberian coast to the west, Alaska to the east, and the continental shelf break to the north. The Chukchi is unique among the Arctic shelf seas as it is dominated by Pacific Water advected through the Bering Strait [Weingartner *et al.*, 2005]. The productive Chukchi shelf is dependent upon the nutrients of the warm, fresh Pacific inflow, which affects ice formation and productivity [Walsh *et al.*, 1989; Martin and Drucker, 1997].

Based upon a sea level ~120–125 m lower than at present [Fairbanks, 1989; Peltier and Fairbanks, 2006], roughly 90% of the Chukchi Sea as defined by Jakobsson [Jakobsson, 2002], would have been subaerially exposed during the LGM (Figure 2.2). The BLB occupied most of the Chukchi Sea during the LGM, and cut off North Pacific nutrient rich, fresh water from reaching the Arctic Ocean. Chukchi Sea sedimentary records are largely limited to the Holocene [Darby *et al.*, 2009; Ortiz *et al.*, 2009] due to the exposure of the BLB, and a subsequent shallow transgressive sea with limited continuous sedimentation due to ice scouring [Hill and Driscoll, 2010] and sediment resuspension in its shallow depths [Reimnitz *et al.*, 1998].

The four major currents of the Chukchi Sea are the Siberian Coastal Current (SCC) in the far west, and the three main branches -- western, central and eastern -- that comprise the northward flowing currents across the Chukchi shelf [Weingartner *et al.*, 2005]. The western branch is relatively salty, cold AW which flows through the Hope and Herald Valleys [Coachman *et al.*, 1975; Woodgate *et al.*, 2005]. Over the north central Chukchi shelf, flow is bounded by the Herald Shoal to the west and Hanna Shoal to the east [Weingartner *et al.*, 1998, 2005]. The flow over the central Chukchi shelf averages 0.2 Sv, accounts for 25% of Bering Strait transport [Woodgate *et al.*, 2005], and has an eastern flow component around the Hanna Shoal, where flow appears to bifurcate, with the eastern branch flowing along the southern flank of the shoal, suggesting a connection between the north central shelf water and the ACC [Weingartner *et al.*, 2005]. In the east, warm and nutrient-poor ACW and BSW are coastally trapped in summer and fall, exiting the Chukchi into the Arctic Ocean via Barrow Canyon [Paquette and Bourke, 1974; Coachman *et al.*, 1975; Ahlnäs and Garrison, 1984].

2.2.4. Laminations

Two of our cores, 3JPC and 51JPC, feature laminae that correspond to widespread North

Pacific deposition of laminations in sediments from BA and PB warm periods bracketing bioturbated sediment deposited during the YD. These laminae are found along the northwest coast of Mexico [*Ganeshram and Pedersen, 1998*], the Gulf of California [*Sancetta, 1995; Keigwin, 2002; Barron et al., 2005*], the Santa Barbara Basin [*Kennett and Ingram, 1995; Hendy and Kennett, 2003*], the California margin [*Gardner et al., 1997; Mix et al., 1999*] to the northwestern Pacific [*Keigwin et al., 1992; Shibahara et al., 2007; Brunelle et al., 2010*], the Okhotsk Sea, and into the Bering Sea [*Cook et al., 2005; Brunelle et al., 2007; Itaki et al., 2009; Caissie et al., 2010; Okazaki et al., 2010; Khim et al., 2011; Kim et al., 2011; Schlung et al., 2013*].

Laminated sediments are deposited under dysaerobic to anoxic conditions [*Kennett and Ingram, 1995; Behl and Kennett, 1996*] with export productivity and ventilation as the accepted primary controls on benthic oxygenation [*Hendy and Pedersen, 2005*]. Deposition of laminated intervals in cores proximal to our Bering Sea sites have been attributed to changes in oxygen content of North Pacific Intermediate Water (NPIW) and increased export production, the combination of which fostered dysaerobic conditions [*Cook et al., 2005; Caissie et al., 2010; Davies et al., 2011; Kim et al., 2011; Schlung et al., 2013*].

2.3. Methods

The cores used in this study were collected during two legs (HLY02-02 and HLY02-04) of the Arctic West Summer 2002 cruise of the USCGC Healy in the Bering and Chukchi Seas led by Julie Brigham-Grette (University of Massachusetts, Amherst), Neil Driscoll (Scripps Oceanographic Institution), and Lloyd Keigwin (Woods Hole Oceanographic Institution, WHOI). The cores were collected using a jumbo piston coring apparatus aboard the USCGC Healy. The cores were split longitudinally into a working half, from which samples can be

taken, and an archive half, on which non-destructive analyses can be performed. The samples were stored at room temperature "moist" on special racks in sealed "D-tubes" in the core repository at McLean Laboratory on WHOI's Quissett Campus. We brought the cores to UMass for subsampling and core scan measurements, and stored them in a cold room at 4°C in the sealed "D-tubes".

2.3.1. Age Models

3JPC, 17JPC, and the section of 51JPC chosen for our study have six, six, and four ¹⁴C ages respectively (Table 2.2), obtained previously using *Neogloboquadrina pachyderma* (sinistral), a planktic foraminifera, [Cook *et al.*, 2005; Cook, 2006]. 24JPC has seven radiocarbon dates on paired (3) and single bivalve (3) shells and shell fragments (1) [Lundeen *et al.*, 2005]. 51JPC has two tephra deposits that were treated as instantaneous events.

For all of the cores, a reservoir age of 800 years (ΔR 400) was chosen to be consistent with other published studies of these cores [Cook *et al.*, 2005; Cook, 2006; Brunelle *et al.*, 2010, 2010; Caissie *et al.*, 2010], and other proximal cores [Itaki *et al.*, 2009; Kim *et al.*, 2011; Schlung *et al.*, 2013; Kuehn *et al.*, 2014], as well as the marine calibration dataset (<http://calib.qub.ac.uk/marine/>) using data from McNeely *et al.* [McNeely *et al.*, 2006]. However, this reservoir correction is relatively poorly constrained with estimates in the Bering Sea and northeast and northwest Pacific ranging from 460 to 1100 yrs for total modern reservoir corrections [Kuzmin *et al.*, 2001; Dumond and Griffin, 2002; Kovanen and Easterbrook, 2002; Gorbarenko *et al.*, 2005]. Both the YD [Keigwin *et al.*, 1991; McManus *et al.*, 2004] and the termination of the last glacial stage had pronounced impacts on thermohaline circulation ages. Additionally, the reservoir age in the region may have experienced considerable variation during deglaciation, particularly around 18 ka (personal correspondence, Mea Cook).

Table 2.2. Uncorrected AMS ^{14}C ages, and corrected, calibrated ages measured on *N. pachyderma* (s.) in 3, 17, and 51JPC [Cook *et al.*, 2005], and shells in 24JPC [Lundeen *et al.*, 2005]. Calibrations were performed with Clam 2.2 [Blaauw, 2010] using $\Delta R = 400$ yr, corresponding to a ~800-yr reservoir correction.

Core	Depth (cm)	^{14}C Age $\pm 1\sigma$	Cal yrs BP	Material Dated
3JPC	140.5-142.5	10050 \pm 60	10537	<i>N. pachyderma</i>
3JPC	352.5-353.5	10850 \pm 65	11570	<i>N. pachyderma</i>
3JPC	600.5-601.5	12400 \pm 65	13444	<i>N. pachyderma</i>
3JPC	839.5-840.5	13300 \pm 70	14607	<i>N. pachyderma</i>
3JPC	906.5-909.5	13350 \pm 80	14880	<i>N. pachyderma</i>
3JPC	1427.5-1428.5	18100 \pm 130	20871	<i>N. pachyderma</i>
51JPC	134.5-135.5	10600 \pm 60	11194	<i>N. pachyderma</i>
51JPC	177.5-178.5	12500 \pm 60	13551	<i>N. pachyderma</i>
51JPC	214.5-242.5	14050 \pm 85	15922	<i>N. pachyderma</i>
51JPC	479.5-480.5	18200 \pm 110	19766	<i>N. pachyderma</i>
17JPC	155.5-156.5	10000 \pm 60	10471	<i>N. pachyderma</i>
17JPC	185.5-186.5	12550 \pm 65	13599	<i>N. pachyderma</i>
17JPC	215.5-216.5	13400 \pm 60	14922	<i>N. pachyderma</i>
17JPC	383.5-384.5	25200 \pm 130	27303	<i>N. pachyderma</i>
24JPC	79	4540 \pm 40	4206	Mollusk Shell
24JPC	173	6450 \pm 40	6471	Complete Shell (<i>Natica</i>)
24JPC	271	7670 \pm 45	7732	Shell Fragments
24JPC	493	8720 \pm 55	8848	Bivalve Shell (<i>Portlandia</i>)
24JPC	576	8810 \pm 55	9020	Paired bivalve (<i>Astarte</i>)
24JPC	601	8950 \pm 60	9196	Paired bivalve
24JPC	692	11050 \pm 65	12006	Bivalve Shell (<i>Hiatella</i>)

[Keigwin *et al.*, 1991; Weaver, 2003; McManus *et al.*, 2004], which would affect global reservoir

We also applied a reservoir age of 800 years in the Chukchi Sea cores consistent with reservoir corrections from the region [Andrews *et al.*, 1993; Polyak *et al.*, 2004; Kuehn *et al.*, 2014]. However, some Arctic studies completely omit a reservoir correction [Polyak *et al.*, 2007; Kaufman *et al.*, 2008] due to high uncertainty in marine Arctic waters, especially during deglaciation [Björck *et al.*, 2003; Eiríksson *et al.*, 2004]. We have the least confidence in the oldest portion of 24JPC as Chukchi Sea sedimentary records are largely limited to the Holocene

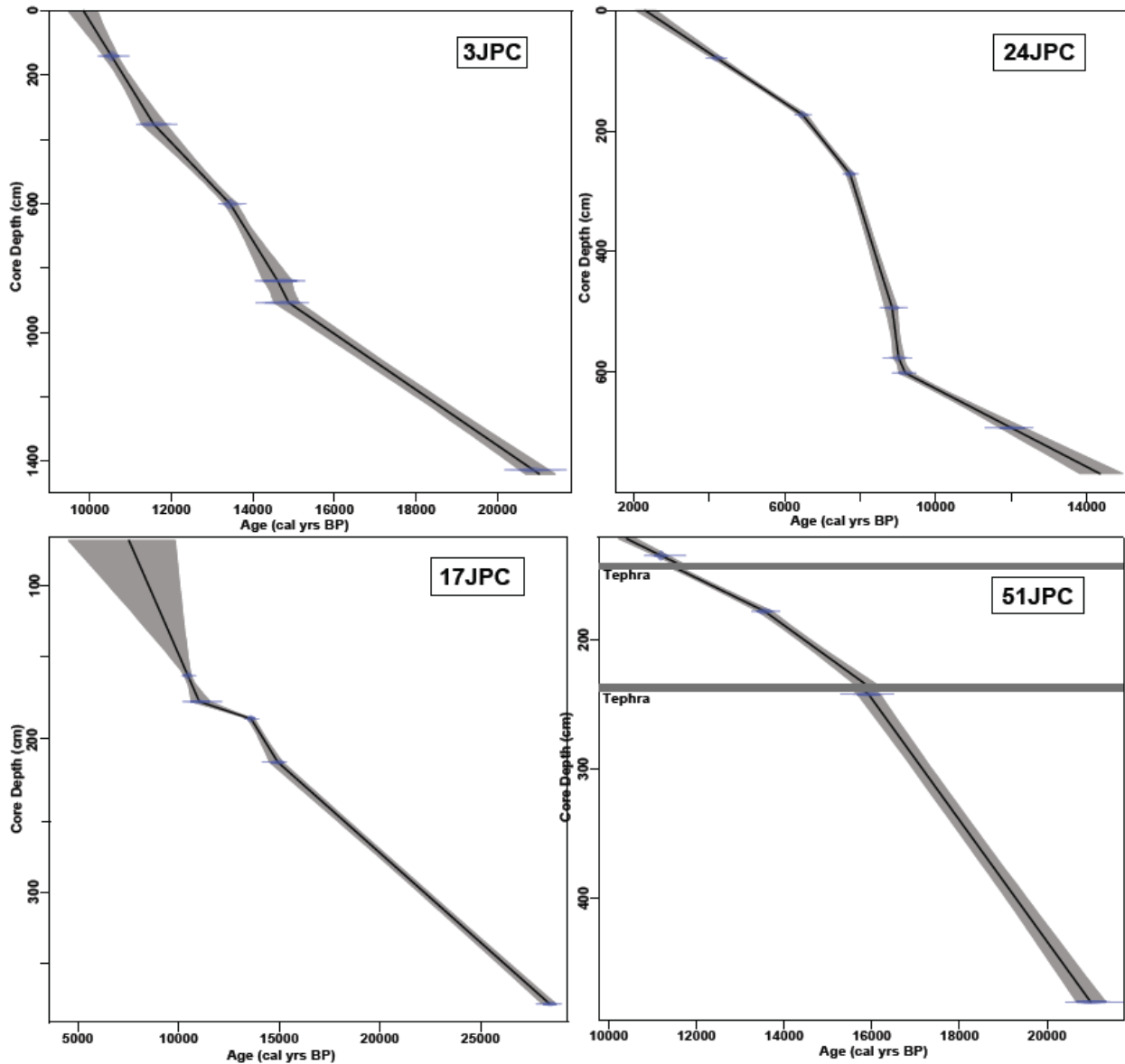


Figure 2.3. Age depth models for 3JPC (a), 24JPC (b), 17JPC (c), and 51JPC (d). Blue dots are ^{14}C ages, with 1σ error plotted. Grey shaded area is the 1σ range, which is largest when extrapolating to the core top or bottom. Tephra were treated as instantaneous events in 51JPC, and are indicated by grey bars.

[Darby *et al.*, 2009; Ortiz *et al.*, 2009] considering the exposure of the BLB, and a subsequent shallow transgressive sea in which sediment preservation would have been difficult due to ice scouring [Hill and Driscoll, 2010] and sediment resuspension in its shallow depths [Reimnitz *et*

al., 1998]. The youngest portion of 17JPC has the highest uncertainty as seen in Figure 2.3, as it lacks a date in the uppermost 150 cm.

The ^{14}C ages were calibrated using Clam version 2.2 [Blaauw, 2010] operated in the free open-source statistical software R (version 3.0.2; R Development Core Team, 2013) using the Marine13 calibration curve [Reimer *et al.*, 2013]. All age-depth models were created in Clam using linear interpolation for minimal investigator bias (Figure 2.3). While dated sedimentary units such as laminations match well with regional studies, we present our data with the caveat that reservoir age could have fluctuated by a few hundred years at certain points of the record, particularly around what we define as 18 ka.

2.3.2. Non-destructive Analysis

All archive-half sections of our cores were logged at UMass on both a Multi-Sensor Core Logger (MSCL, GEOTEK), and an high-resolution continuous micro fluorescence-X (XRF) core scanner (ITRAX, COX Analytical Systems).

2.3.2.1. Elemental XRF

The ITRAX XRF core scanner provides high-resolution elemental composition and X-Radiograph images [Löwemark *et al.*, 2008]. ITRAX (uses an intense non-destructive micro X-ray beam that irradiates the sample to collect positive X-ray images, and detects the energy of fluorescent radiation in order to provide high-resolution relative concentration of elemental profiles (from Al to U). ITRAX analyses were measured on a 4 mm-wide and 0.1 mm-thick area using a molybdenum tube. The XRF output data are an intensity given in counts per second (cps) with an average value around 19 kcps for our cores. Any measurement point with fewer than 10 kcps was not considered, and any points with Validity=0 were also not considered

(Validity generally is zero when kcps was below 10k). The ITRAX validity output is defined as 1 if the sensor is in the correct position. If zero, then the X-ray detector is not in the correct position, which occurs when the surface is uneven or shows sudden variability, such as a crack in the core. Radiograph images were taken with an exposure time of 1600 ms at a voltage of 60 kV, and a 50 mA current. XRF exposure time was 10 s at a voltage of 30 kV and a 55 mA current. XRF data were analyzed at 1000 μm scale, and though data was taken at 200 μm in laminated sections, 1000 μm scale was chosen for consistent analysis and interpretation. Without quantitative mineralogy [*Viscosi-Shirley et al.*, 2003; *Eberl*, 2004], we do not interpret XRF elemental count data as quantitative or exact, merely as a general descriptor of relative changes in sediment composition. (For a detailed description of the ITRAX core scanner see Croudace et al. [2006])

2.3.2.2. MSCL Data

The MSCL obtained magnetic susceptibility (MS), gamma ray attenuation density, spectral properties, and high-resolution images. Magnetic susceptibility was measured using a point sensor (MS2E, Bartington) mounted on an arm that allows the sensor to be placed on the core surface for each measurement. The point sensor has a field of influence of about 1 cm in diameter. The bulk density for the GEOTEK is GRAPE bulk density (gamma ray attenuation porosity evaluator) obtained using a cesium-137 gamma source which emits a narrow beam of collimated gamma rays with energies at 0.662 MeV. A color spectrophotometer (CM-2600d, Konica Minolta) measured reflectance in the near UV through the visible spectrum and just into the near IR range (wavelengths 360–740 μm).

2.3.3. Destructive Analysis–Sampling

The sediment cores were sampled for biogeochemical and isotopic data, as well as grain size analysis using 1 cm diameter sediment plugs.

3JPC was sampled at 10 cm resolution in massive sections and 5 cm resolution in both laminated intervals and the top meter of the core for isotopic and grain size analyses. 24JPC was sampled at 5 cm resolution in the upper two meters of the core (1 m for grain size) and 10 cm throughout the remainder. 51JPC was sampled at 10 cm resolution for grain size, and 2 cm resolution from 124–242 cm and 4 cm from 242–420 cm, only for $\delta^{13}\text{C}_{\text{org}}$ and %TOC. 17JPC was sampled at 10 cm resolution.

2.3.3.1. Elemental Isotopic Analyses

Bulk biogeochemical properties include $\delta^{13}\text{C}_{\text{org}}$, $\delta^{15}\text{N}$, %TOC, %N_{org} and C/N ratios measured on an Isotope Ratio Mass Spectrometer (IRMS) with a Sercon GSL and Gilson gas auto-sampler prep unit (PDZ-Europa 20/20). The isotopic data were measured by the Stable Isotope Research Unit of the Department of Crop and Soil Sciences at Oregon State University, Corvallis, OR. Samples were freeze-dried and then ground to a fine powder before being treated with 1 M HCl to remove carbonate for samples used to measure $\delta^{13}\text{C}_{\text{org}}$ and %TOC [Ramnarine *et al.*, 2011]. The samples were then mixed with deionized water, centrifuged and excess water was removed by pipette. This process was repeated five or more times, until reaching a neutral pH, after which the samples were left to air dry. Samples were then heated in an oven at 50°C and placed in a container with desiccant. The samples were encapsulated in tin capsules (Elemental Microanalysis D1008 or D1010). For all four cores we used ~150µg total C (15 mg of sample) for $\delta^{13}\text{C}_{\text{org}}$, and %TOC. Replicate analyses indicated a standard deviation of 0.91 wt% for %TOC, and 0.09‰ for $\delta^{13}\text{C}_{\text{org}}$.

For $\delta^{15}\text{N}$, %N and %TC, each sample had about 75 μg total N (55 mg sample). Replicate analyses indicated a standard deviation of 0.24‰ for $\delta^{15}\text{N}$, and 0.26 wt% for %N.

2.3.3.2. Carbon Isotope Mixing Models

The $\delta^{13}\text{C}_{\text{org}}$ of marine sediments is often used to estimate the relative amounts of terrigenous and marine organic carbon in sediment organic matter (OM) using a linear mixing model of terrigenous and marine OM [Hedges and Parker, 1976; Shultz and Calder, 1976; Prahl *et al.*, 1994; Addison *et al.*, 2012; Trefry *et al.*, 2014], according to the following equation:

$$\text{OC}_{\text{terr}}(\text{fraction}) = \frac{\delta^{13}\text{C}_{\text{sample}} - \delta^{13}\text{C}_{\text{mar}}}{\delta^{13}\text{C}_{\text{terr}} - \delta^{13}\text{C}_{\text{mar}}}$$

The value obtained from this equation (OC_{terr}) is then used to calculate the %TOC_{terr}:

$$\% \text{TOC}_{\text{terr}} = \% \text{TOC}_{\text{sample}} - (\text{OC}_{\text{terr}} \times \% \text{TOC}_{\text{sample}})$$

Depleted $\delta^{13}\text{C}_{\text{org}}$ values (-26 to -28) are typical of terrigenous OM using the C_3 pathway of photosynthesis [Stein and Macdonald, 2004], as seen in the following regions: Mackenzie Beaufort terrigenous end-member: -26.5 to -27‰ [Naidu *et al.*, 2000], Russian Rivers draining taiga/tundra: -26.5‰ [Lobbes *et al.*, 2000], Yukon: -26 to -28‰ [Guo and Macdonald, 2006], Gulf of Alaska: -26‰. Marine $\delta^{13}\text{C}_{\text{org}}$ is generally assumed to be <-25‰ [Grebmeier *et al.*, 1988], with average marine phytoplankton values of -19 to -22‰ [Fontugne and Jouanneau, 1987; Meyers, 1994]. We chose -27‰ for terrigenous OC and -21‰ from marine OM based on the above cited values, and for consistency with studies from the Bering and Chukchi Seas [Walsh *et al.*, 1989; Naidu *et al.*, 1993, 2000, 2004; Trefry *et al.*, 2014], and the Gulf of Alaska [Addison *et al.*, 2012].

2.3.3.3. C/N Ratios and %N_{org}

Arctic sediments have been known to have relatively high amounts of inorganic nitrogen bound to clay minerals (N_{bou}) [Stein and Macdonald, 2004], which can bias C/N ratios which are interpreted as "C_{org}/N_{org}". To better represent source materials, we plotted %TOC (x) versus %TN (y), where the y-intercept represents N_{bou} (Figure 2.4) [Schubert and Calvert, 2001; Stein and Macdonald, 2004].

We estimated %N_{org} using the following equation:

$$\%N_{org} = \%N - \%N_{bou}$$

Where %N_{bou} is the intercept from Figure 2.4. We calculated C/N mole ratios for 3JPC 17JPC, and 24JPC using %TOC and %N_{org} values, as no nitrogen analyses were performed on 51JPC.

2.3.3.4. Grain Size Analysis

Grain Size (GS) analyses were performed at the Marine Sediments Lab of Iowa State University, using laser diffraction (Malvern Mastersizer 3000) to measure particle size from 0.01–3500 μm . Prior to running the samples, a 3M solution of sodium hexametaphosphate (SHMP) was added to the dry material to deflocculate the clay, and then the vial was agitated. Sodium carbonate (0.05 moles) was added when making the SHMP to increase the pH to 8. Samples for grain size analysis were not treated to remove carbonates, organics, or siliceous organisms [Aiello and Ravelo, 2012], and are thus representative of bulk grain size. We followed the Wentworth grain size chart [Wentworth, 1922] in defining our grain size intervals: clay <4 μm , silt 4–63 μm , and sand 63–3500 μm [Aiello and Ravelo, 2012]. Samples were each run three times, and the data presented for each sample is the average of the three measurements.

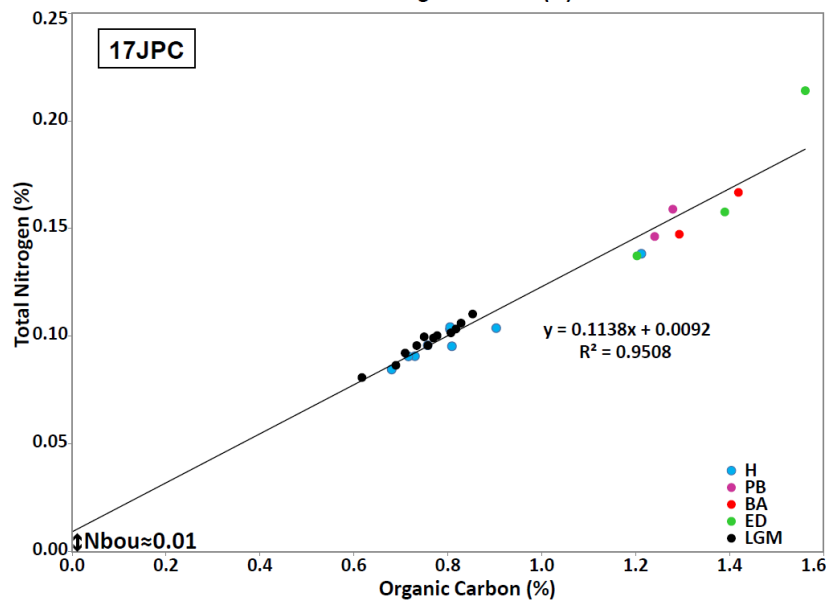
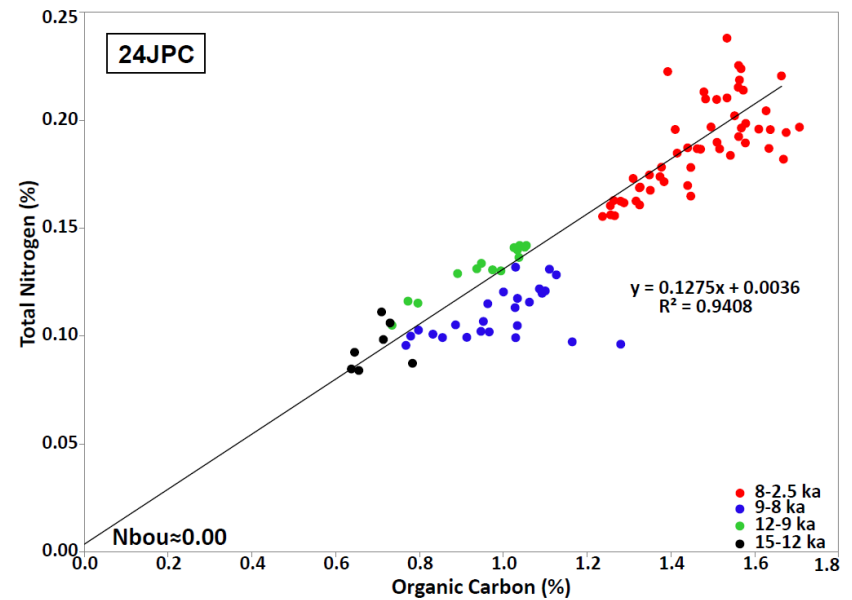
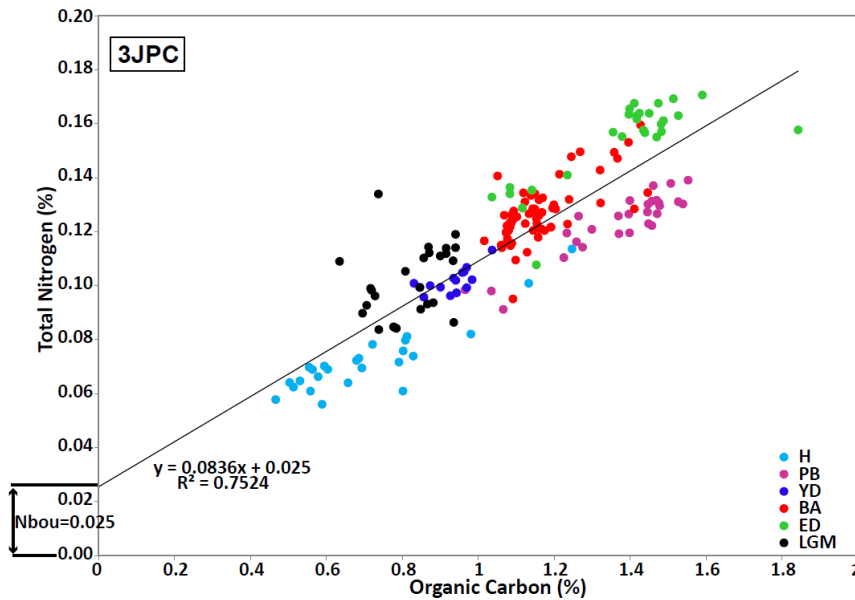


Figure 2.4. Total organic carbon versus total nitrogen correlation in 3JPC (top left), 24JPC (top right), and 17JPC (bottom left). The estimated amount of inorganic nitrogen (N_{bou}) is indicated in lower left of each figure. Note that 3JPC and 17JPC (0.01%) have a significant amount of N_{bou} , whereas 24JPC has negligible N_{bou} . See methods for further explanation.

2.3.3.5 Sediment Compositional Analysis

We took six samples from 24JPC from each of the TOC plateaus for visual analysis. Each sample was around 10 cm³ and each was washed over a 63 μm sieve. The dried residues were scanned under a microscope at x 72. We observed agglutinated forams, diatoms, woody particles, coal/charcoal, and sand. There was nothing calcareous, which is not uncommon in the Chukchi Sea; however given the age of the cores, it is possible that a minimal amount of calcareous material was present when collected, but since dissolved. All forams were agglutinated, and were very fragile. Relative abundance was estimated by Mark Leckie, UMass Amherst, from very rare to abundant.

2.3.4. Principal Component Analysis (PCA)

PCA was completed for XRF, grain size, bulk biogeochemical and isotopic data using MATLAB [MathWorks, 2014]. Data were normalized (z-score) prior to PCA. Variables were included in PCA based upon their performance within PCA, but primarily based upon Pearson correlation coefficients at a statistically significant level (0.01). Elemental XRF data were selected for PCA based upon Pearson correlation coefficients as well as the perceived value of the data. Many of the heavier elements, particularly the trace metals showed no variability and were very noisy, essentially displayed as a thick straight line, and many went undetected in sections of the cores.

In the PCA biplots, each variable is represented by a vector, and the direction and length of the vector indicate how each variable contributes to the two principal components (PC) in the plots. The PCA included further PCs, but they were not plotted as elements like Ca, S, and Mn generally loaded best onto the third PC. The elements are marked by sharp peaks with low

counts in between, and do not tell a valuable story as is. In addition to the general lack of value the third PC, the 2-d plots are far easier to visually interpret. The biplots also include a point for each observation or data point. Each data point is a sample depth from the core that is represented by all the variables (i.e. elemental XRF data, grain size data, and isotopic data). The coordinates for each observation point indicates the score of each observation for the first two principal components, where the score is the original data transformed into PC space. PCA biplots of scores for both XRF data only, and for a full suite of geochemical and sedimentologic parameters (hereafter referred to as full suite PCA), were produced in MATLAB in order to investigate differences between sediments deposited during separate climatic intervals. The samples are color coded after PCA; they are not treated differently, simply colored by age.

When a full suite of data was used for PCA, it was necessary to use the resolution of the most coarsely resolved data, the isotopes. To best represent the high resolution data, a moving, centered 11-point running average was used for the 1000 μm resolution XRF data, and a 3-point running average for 0.5 cm MSCL data, thus representing 1 cm, which is the width of the samples taken from the cores for isotopic analysis.

2.4. Results

2.4.1. Western Bering Sea Shelf Slope, 3JPC

Jumbo Piston Core 3 (HLY02-02-3JPC) was taken between Navarin and Pervenets Canyons on the Bering Sea shelf slope [Cook *et al.*, 2005], about 230 km southeast of Cape Navarin, Russia, at 1132 m water depth (Figure 2.1). At 14 m long, 3JPC (Figures 2.5, 2.6, 2.7, 2.8) contains the most expanded deglacial sequence of the cores in this study, with an average

sediment accumulation rate of 185 cm/kyr from the beginning to the end of the laminated sequences (20–10 ka). There are four visibly laminated intervals, which are composed of pairs of dark and light olive lamina ranging in thickness from <1 to 2 mm. The first three laminated intervals occur during the BA (901–763 cm, 724–602 cm, and 574–533 cm) spanning 14.7–12.9 ka (14.7–14.2, 14.0–13.45, and 13.2–12.9 ka). These intervals are recorded in excellent correspondence with NGRIP-dated BA/YD [Rasmussen *et al.*, 2006]. The final interval was deposited during the PB from 11.5–10.8 ka (342–215 cm), though there are three minor laminae groups of 2–5 cm each after 10.8 ka. Intervening massive intervals and the deepest 5.4 m of sediment are composed of homogeneous sticky dark olive–gray silty mud, with a slower sedimentation rate (87 cm/kyr).

During the LGM (21–18.1 ka), $\delta^{13}\text{C}_{\text{org}}$ averages -22.80 ± 0.2 punctuated by a precipitous drop that begins around 18 ka and bottoms out by 17 ka at -25‰ (Figure 2.5). From 17–10.7 ka, $\delta^{13}\text{C}_{\text{org}}$ averages $-24.91 \pm 0.32\text{‰}$, and at 10.7 ka there is a second rapid change as $\delta^{13}\text{C}_{\text{org}}$ values become more enriched, reaching -21.8‰ by 9.8 ka. While the trend of $\delta^{13}\text{C}_{\text{org}}$ values is one of a depletion followed by a later enrichment, the period from 17–10.7 ka does have variability, including enrichment during the BA (14.7–12.9 ka, $-24.73 \pm 0.23\text{‰}$), and a depletion during the YD (12.9–11.7 ka, $-25.08 \pm 0.23\text{‰}$).

For 3JPC, TOC begins with relatively low values (0.82%) from 21–18 ka, before rapidly rising around 18 ka to 1.46% from 17.2–14.8 ka (Figure 2.5). TOC during the LGM is predominately of marine origin given high %OC_{mar} (0.58%) and low %OC_{terr} (0.25%), before terrestrial carbon surpasses marine carbon ~17.5 ka. At the onset of the BA, TOC falls to 1.14% until the YD, where values further decrease to 0.94%, before increasing at the end of the YD around 11.6 ka. During the laminated PB interval, TOC is the highest in the record (1.41%),

before a dramatic decrease at 10.8 ka that leaves TOC around 0.5% by 9.8 ka, with OC_{mar} re-established as the largest source of TOC.

$\delta^{15}N$ averages 7.52‰ during the LGM, and decreases rapidly during the early deglaciation at ~18.15 ka (Figure 2.5). From 18–15.4 ka, $\delta^{15}N$ is relatively depleted (5.66‰) until beginning to rise preceding the BA. During the BA, $\delta^{15}N$ values increase until topping out at around 7.9‰ by 14 ka, averaging 7.07‰ from 14.7–13.7 ka, where a decrease begins that continues into the YD until around 12.5 ka. After 12.5 ka, values slowly increase until the end of the YD where the increase accelerates, bringing elevated $\delta^{15}N$ during the PB laminated interval (6.15‰) from 11.5 to 11 ka, before decreasing after 10.8 ka with an average of 5.68‰ from 10.8–9.8 ka.

During the LGM until ~18.5 ka, $\%N_{org}$ averages 0.101% (Figure 2.5). After 18.5 ka, $\%N_{org}$ begins to increase, a trend which accelerates after 18 ka with the highest $\%N_{org}$ in the record averaging 0.162% from ~17.1–14.9 ka. There is a rapid decrease in $\%N_{org}$ around the onset of the BA, and by 14.6 ka, $\%N_{org}$ is present at a relatively constant but declining 0.123% until the YD. At the onset of the YD (12.9 ka), there is a spike in $\%N_{org}$ to 0.132%, followed by a rapid decrease to 0.096% by 12.4 ka, where values remain until the end of the YD. Around 11.5 ka, $\%N_{org}$ rapidly increases coeval with the beginning of PB lamina, and remain at an average of 0.129% until ~10.8 ka after the PB laminations have ended. There is a precipitous decrease until ~10.5 ka, and from 10.5–9.8 ka average $\%N_{org}$ is the lowest in the record (0.069%).

The C/N ratio averages 15.3 from 21–20 ka, before dropping to 12.2 from 20 ka to the BA (Figure 2.5). C/N averages 13.5 during the BA, and increases during the YD, reaching 16.5

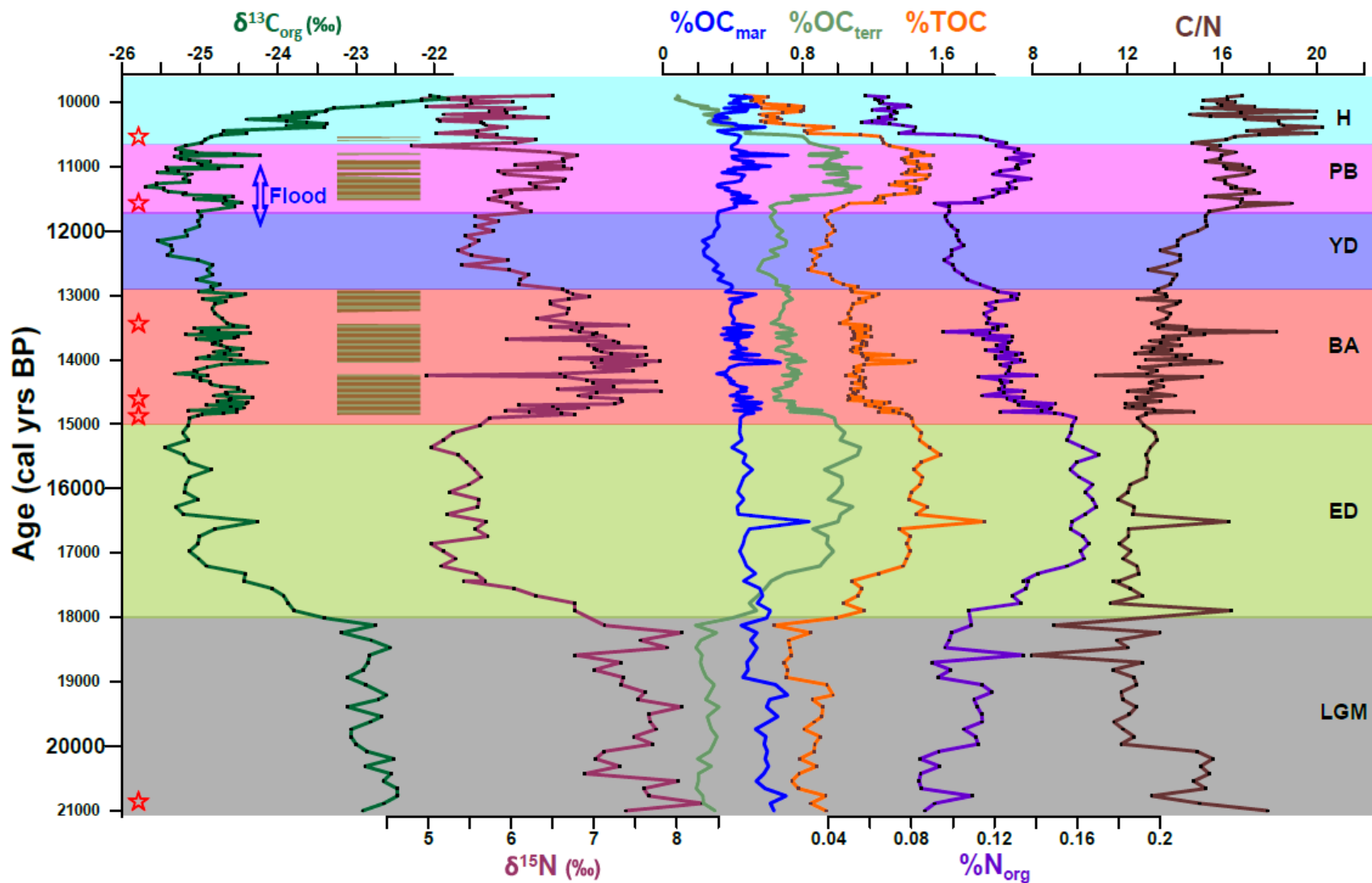


Figure 2.5. 3JPC Bulk $\delta^{13}\text{C}_{\text{org}}$ and $\delta^{15}\text{N}$, %TOC, estimated %OC_{mar} and %OC_{terr}, %N_{org}, and C/N. Laminated intervals are indicated by brown/green boxes. Six ^{14}C dates are given in calendar years, red stars [Cook *et al.*, 2005]. Blue arrow is the window of BLB flooding [Keigwin *et al.*, 2006]. Background color scheme corresponds to climatic intervals described in section 2.2, and used in all subsequent figures: H=Holocene, PB=Pre-Boreal, YD=Younger Dryas, ED=Early Deglacial, LGM=Last Glacial Maximum.

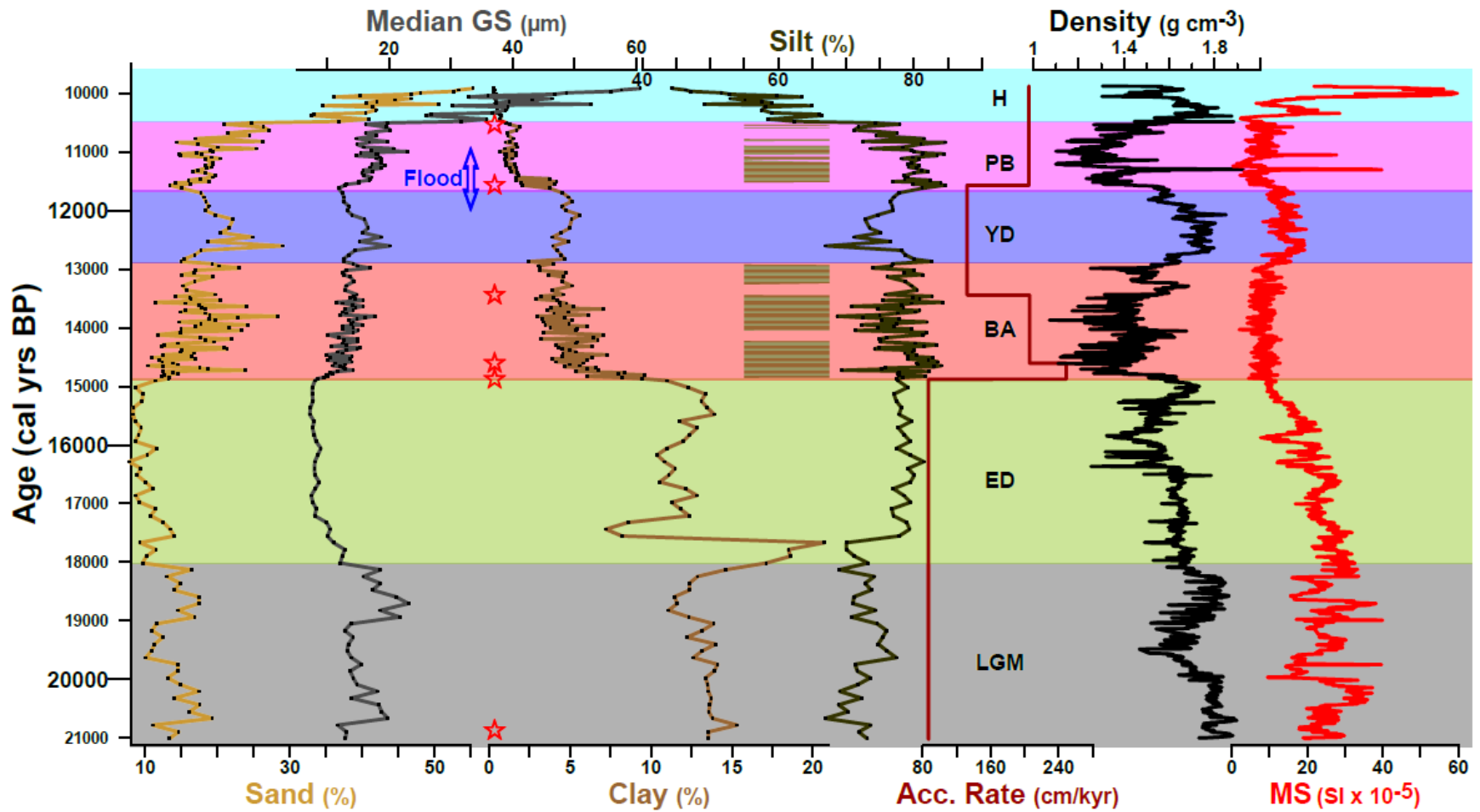


Figure 2.6. 3JPC Grain size data, accumulation rate, bulk density, and magnetic susceptibility. Laminated intervals are indicated by brown/green boxes. Six ¹⁴C dates are given in calendar years, red stars [Cook *et al.*, 2005]. Blue arrow is the window of BLB flooding [Keigwin *et al.*, 2006].

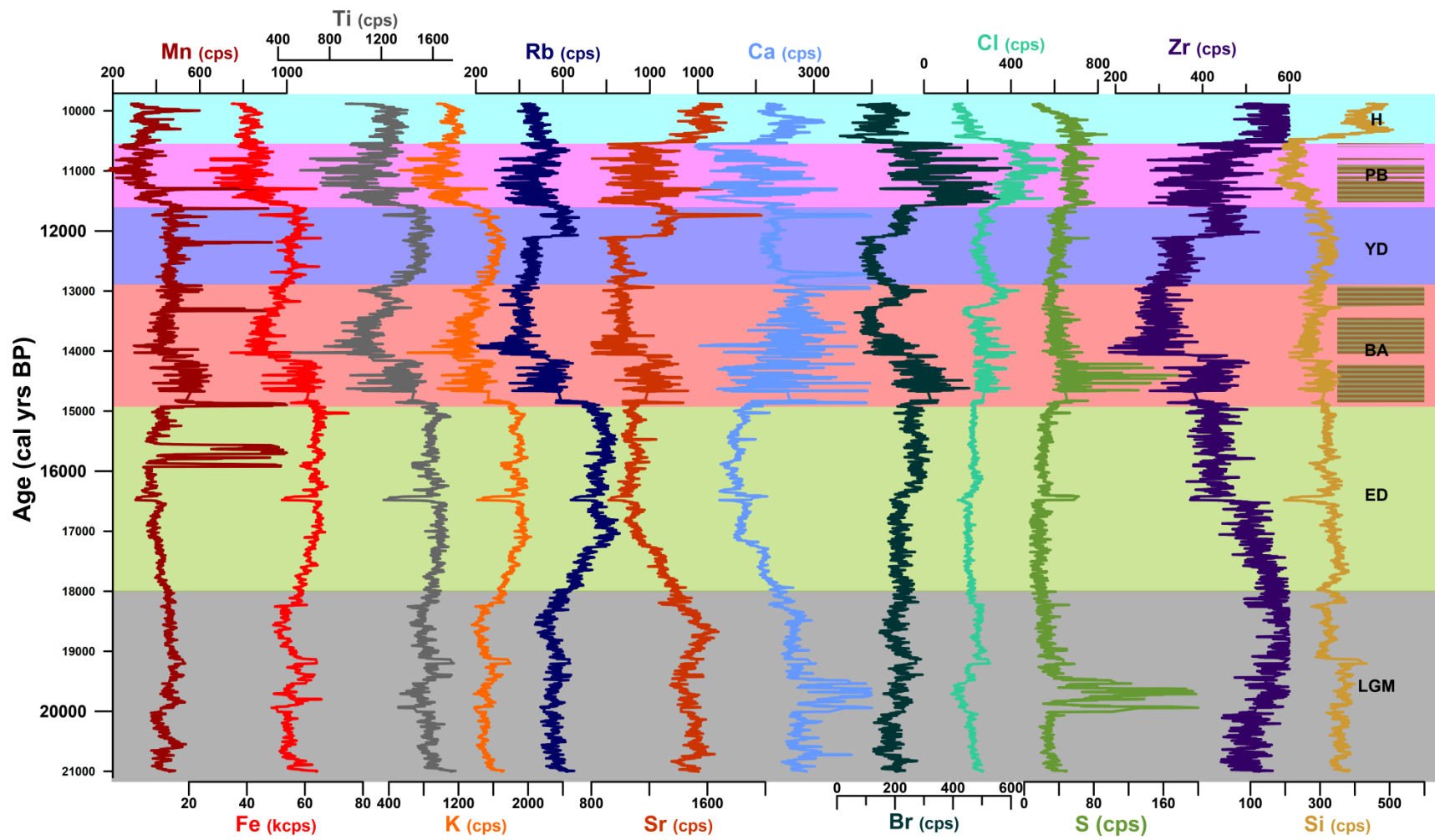


Figure 2.7. 3JPC XRF elemental intensity data in counts per second (cps). Laminated intervals indicated by brown/green bars on the right.

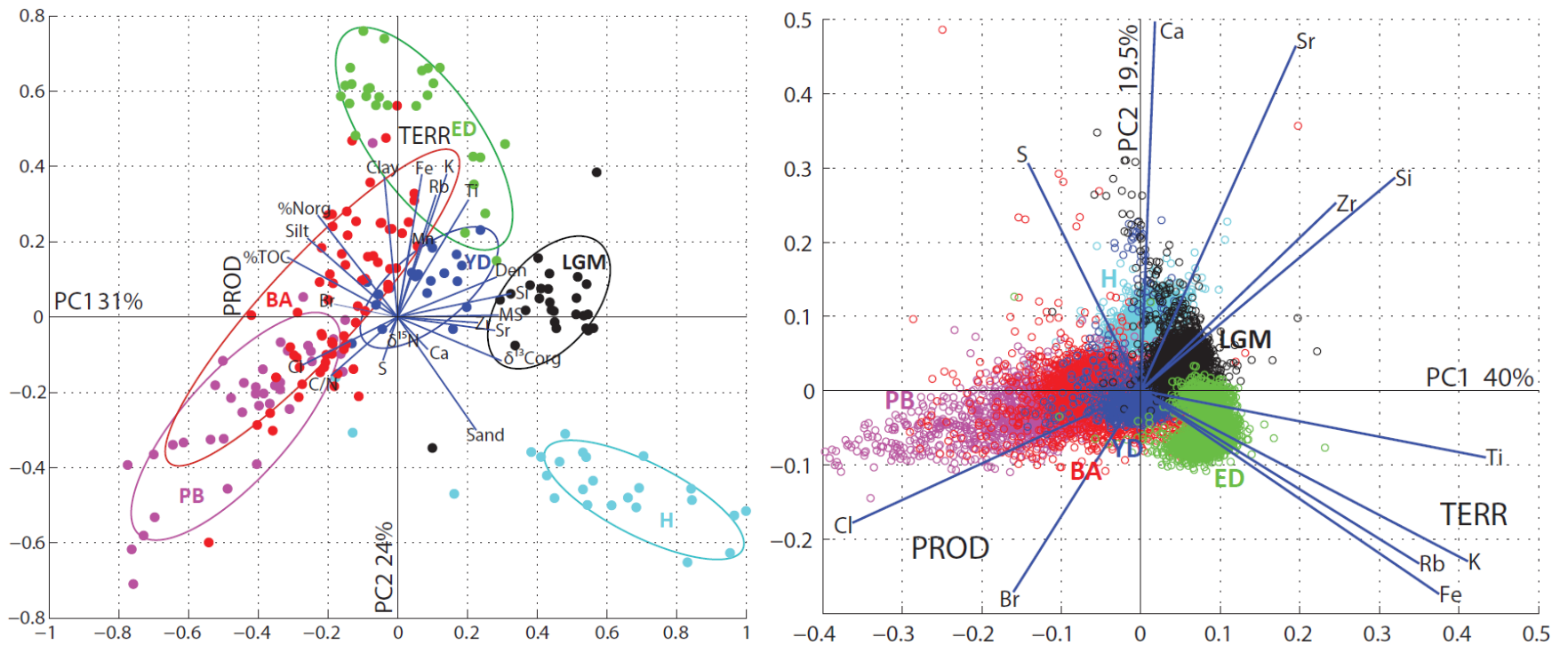


Figure 2.8. 3JPC PCA biplots. Left panel is full suite PCA. Right panel is XRF PCA. Populations are color coded by age. PC1 and PC2 are principal components one and two, and the percent label is the percent of variation in the data explained by PC1 and PC2 respectively. Blue lines PC coefficients for each variable. TERR and PROD represent the area of terrestrial and productivity end-members respectively (See Discussion 2.5.1).

during the PB before peaking at 22 during the Holocene and decreasing to 16 by the end of the record.

Median grain size averages 13.7 μm from 21–10.8 ka, before increasing to 35.1 μm from 10–9.8 ka (Figure 2.6). Laminated units have smaller median grain size (14.4 μm) than massive sections (18.2 μm). Clay in the 3JPC record began ~13% from 21–18.2 ka, followed by a sharp clay peak at the onset of the ED to ~20%. After the peak, clay is still abundant through the ED at ~12.5% until rapidly decreasing at 15 ka. Clay content plateaus at 4.8% from 14.8–11.7 ka before reaching the lowest values of the record at 1.1% in the core top from 11.5–9.8 ka. Silt is relatively stable throughout the record, averaging 77.3% from 21–10.8 ka with the only major deviation being a large increase in sand (20 to 50%) from 10.8–9.8 ka, and the corresponding drop in silt to 50%. Sand averages 14.3% through the LGM until decreasing at 18.1 ka, reaching the lowest sand content of the record (9.9%) from 18–15 ka. Though there is variability, sand averages 17.2% through the BA and YD and into the PB before the major increase at 10.8 ka.

During the laminated intervals in 3JPC, there is a decrease in Ti, Fe, K, and Rb and an increase in Cl, Br, and to a lesser extent Ca, corresponding to the BA and PB (Figure 2.7). Ti, Fe, K, and Rb are highest during the LGM, ED, and YD. Si shows little variability until increasing following the PB, in concert with an increase in sand and Sr. Rb and Sr vary together from the BA through the PB, but not before or after whereas Sr and Zr track well reasonably well together throughout the record.

In 3JPC, the ED interval tracks closest to the terrigenous end-members (Fe, Ti, K, Rb and Clay), the LGM is loaded positively onto PC1, YD centers around the origin, and the PB and BA show the greatest variability, but plot closest to %TOC, %N_{org}, silt, Cl and Br (Figure 2.8). The early Holocene is a clear anomaly and plots closest to sand.

2.4.2. Northwest Chukchi Shelf, 24JPC

24JPC (HLY04-02-24JPC) was taken from the northwest Chukchi shelf at 80 m water depth [Lundeen *et al.*, 2005], and spans much of the Holocene (14.3–2.5 ka) over 7.5 m of dark grey–green silty mud (Figures 2.9, 2.10, 2.11, 2.12). There is an interval of rapid sedimentation from 9–6 ka (223 cm/kyr), with slower, accumulation before and after this interval (30–40 cm/kyr), although the deepest portion of the core is uncertain.

$\delta^{13}\text{C}_{\text{org}}$ is relatively stable averaging $-24.69 \pm 0.16\text{‰}$ from 14–8 ka, where a steady increase begins, continuing until the end of the record with values around -22‰ by 2.5 ka (Figure 2.9). The anomalous excursion seen from $\sim 3.5\text{--}3\text{ ka}$ is likely due to sample contamination as previous results on this core suggested no such feature [Lundeen *et al.*, 2005].

$\delta^{15}\text{N}$ and $\%N_{\text{org}}$ essentially match the $\% \text{TOC}$ curve (Figure 2.9), with five intervals that could be deemed steps, and are listed with the TOC data in parentheses: ($\delta^{15}\text{N}$, N_{org}). $\%N$ is taken to be equivalent to $\%N_{\text{org}}$ because the intercept of the $\% \text{TOC}$ to $\%N$ plot ($\%N_{\text{bou}}$ Figure 2.4) is close to zero (0.0036%) [Stein and Macdonald, 2004].

$\% \text{TOC}$ shows greater variability than $\delta^{13}\text{C}_{\text{org}}$, essentially existing as five steps of like grouped data, with an overall trend towards higher TOC, with a notable excursion in the middle of the record. From 14–11.1 ka, $\% \text{TOC}$ increases slightly but averages 0.72% (5.20‰, 0.100%), until a sharp increase to average values of 1.03% (6.87‰, 0.139%) from 11–8.8 ka. The sharp excursion occurs from $\sim 8.5\text{--}8.2\text{ ka}$, with an interval of rapid sedimentation and low TOC at 0.86% (6.02‰, 0.109%) that ended as quickly as it came, with values rebounding by 8 ka to a plateau around 1.36% from 8–5.5 ka (7.92‰, 0.169%). Another increase in $\% \text{TOC}$ occurs after 5.5 ka and values reach the final step averaging 1.56% (8.63‰, 0.205%) from 5.1–2.5 ka. OC_{terr}

accounts for more than half of the TOC in 24JPC until ~7.1 ka, when OC_{mar} overtakes OC_{terr} . By the end of the record, nearly all (80%) of the TOC at 24JPC is of marine origin.

C/N ratios in 24JPC show considerable variability, averaging 8.5 from 14–8.5 ka, then increasing to 9.33 from 8.4–5.5 ka, and reaching the highest average of the record (9.68) from 5.2–3.8 ka, before falling to ~8.5 by the end of the record (Figure 2.9).

Sand is a prominent component of the bottom of 24JPC (12.4%) from 14.1–12.8 ka, before diminishing to an average of 3% by 12 ka, that is sustained throughout the remainder of the record (Figure 2.10). Following the initial peak in sand, median GS is relatively steady around 6.9 μm from 12.5–8 ka, before increasing to ~12 μm by the core top at 2.5ka. Silt is the dominant component after 8 ka, averaging 84%, compared to 68% in the earlier portion of the record, excluding the sand peak. Clay and silt both mirror TOC remarkably well. Clay is abundant early in the record, averaging 28.7%, until ~9.1 ka when clay and silt begin to decrease as TOC increases with an abrupt decrease (increase) in TOC and silt (clay) from 8.5–8.2 ka. The collapse featured clay returning to over 28%, and silt falling to 66%. After the excursion, silt rebounds dramatically, and quickly reaches the 68% average (by 7.8 ka) that is maintained to the core top while clay decreases to an average of 13% from 7.8–2.5 ka.

Elemental XRF data from 24JPC increase ~9.5 ka in S, Cl, Br, and Ca, and decrease in Ti, Fe, K and Rb (Figure 2.11). Coeval with the TOC anomaly from ~8.5–8.2 ka, there is an increase in Ti, Fe, K and Rb, with a decrease in Cl, Br, Ca, and S. Mn is prominent (870 cps) and exhibits great variability from 14.3 ka until decreasing at 8 ka (430 cps), followed by little variability.

In 24JPC, PC1 in the full suite PCA accounts for 65% of the variability, and the data loads from positive to negative along PC1 with age (Figure 2.12). The older samples plot most

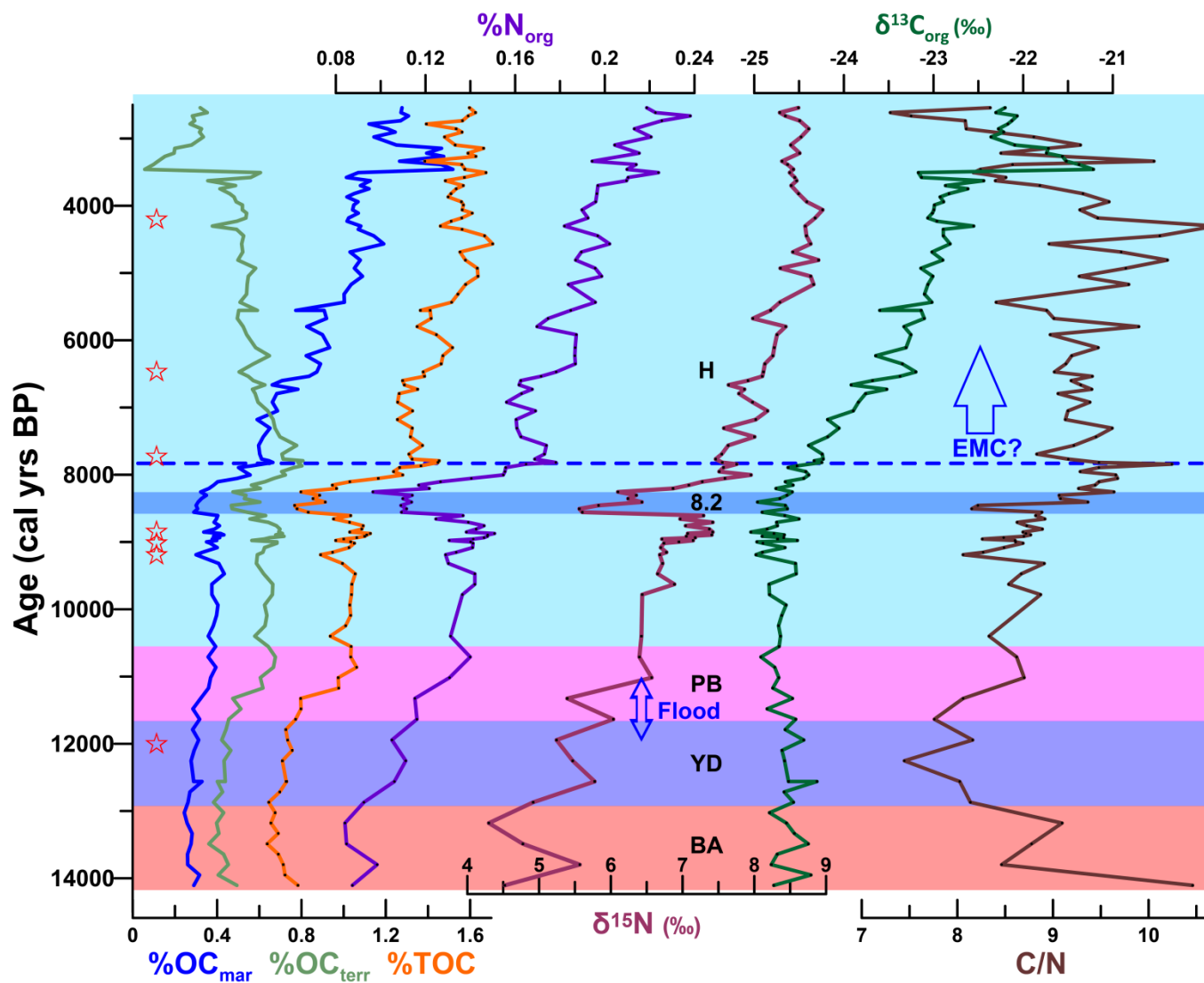


Figure 2.9. 24JPC %TOC, estimated %OC_{mar} and %OC_{terr}, %N_{org}, $\delta^{13}\text{C}_{\text{org}}$, $\delta^{15}\text{N}$, and C/N. Seven ^{14}C dates are given in calendar years, red stars [Lundeen *et al.*, 2005]. Lower blue arrow is the window of BLB flooding [Keigwin *et al.*, 2006]. Our postulated establishment of modern currents (EMC) indicated by blue dashed line and arrow. 8.2 ka event is marked by upper blue box

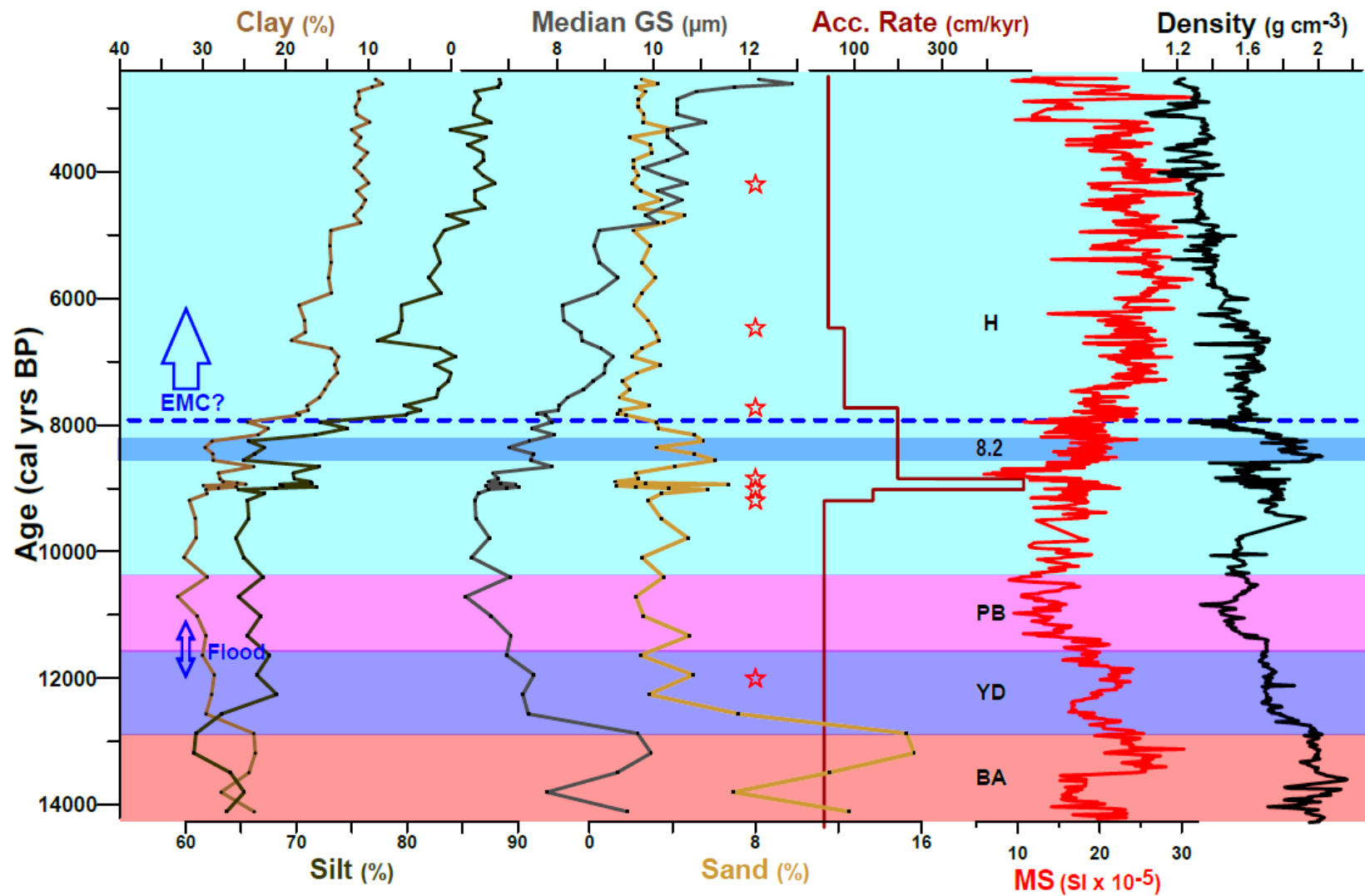


Figure 2.10. 24JPC grain size data, accumulation rate, bulk density, and magnetic susceptibility. Seven ^{14}C dates are given in calendar years, red stars [Lundeen *et al.*, 2005]. Lower blue arrow is the window of BLB flooding [Keigwin *et al.*, 2006]. Our postulated establishment of modern currents (EMC) indicated by blue line and upper arrow. Sand peak at ~ 13 ka is our transgressive-scour deposit. Final ^{14}C date may be reworked. 8.2 ka event is marked by upper blue box.

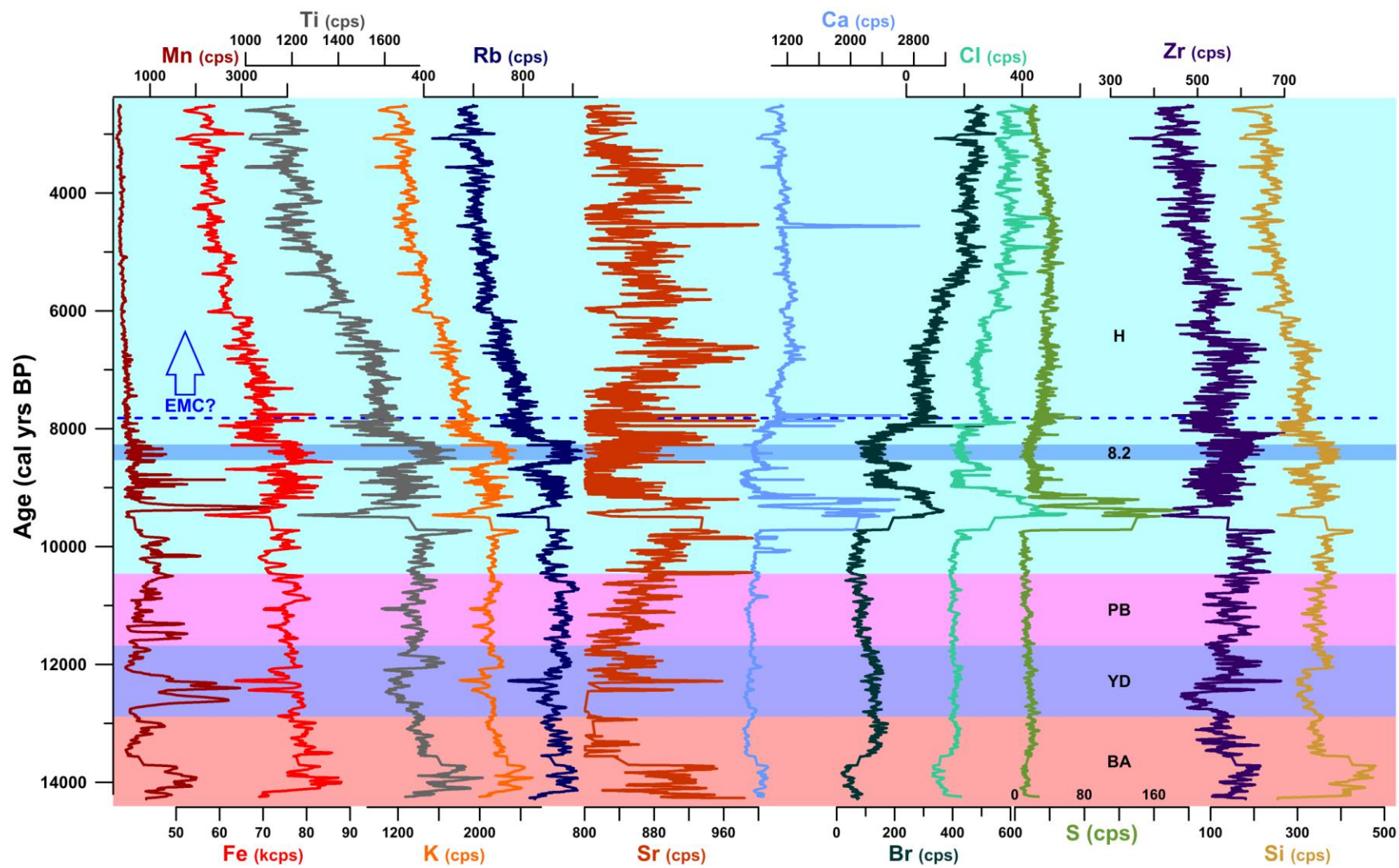


Figure 2.11. 24JPC XRF elemental intensity data in counts per second (cps). Our postulated establishment of modern currents (EMC) indicated by blue dashed line and arrow. 8.2 ka event is marked by upper blue box.

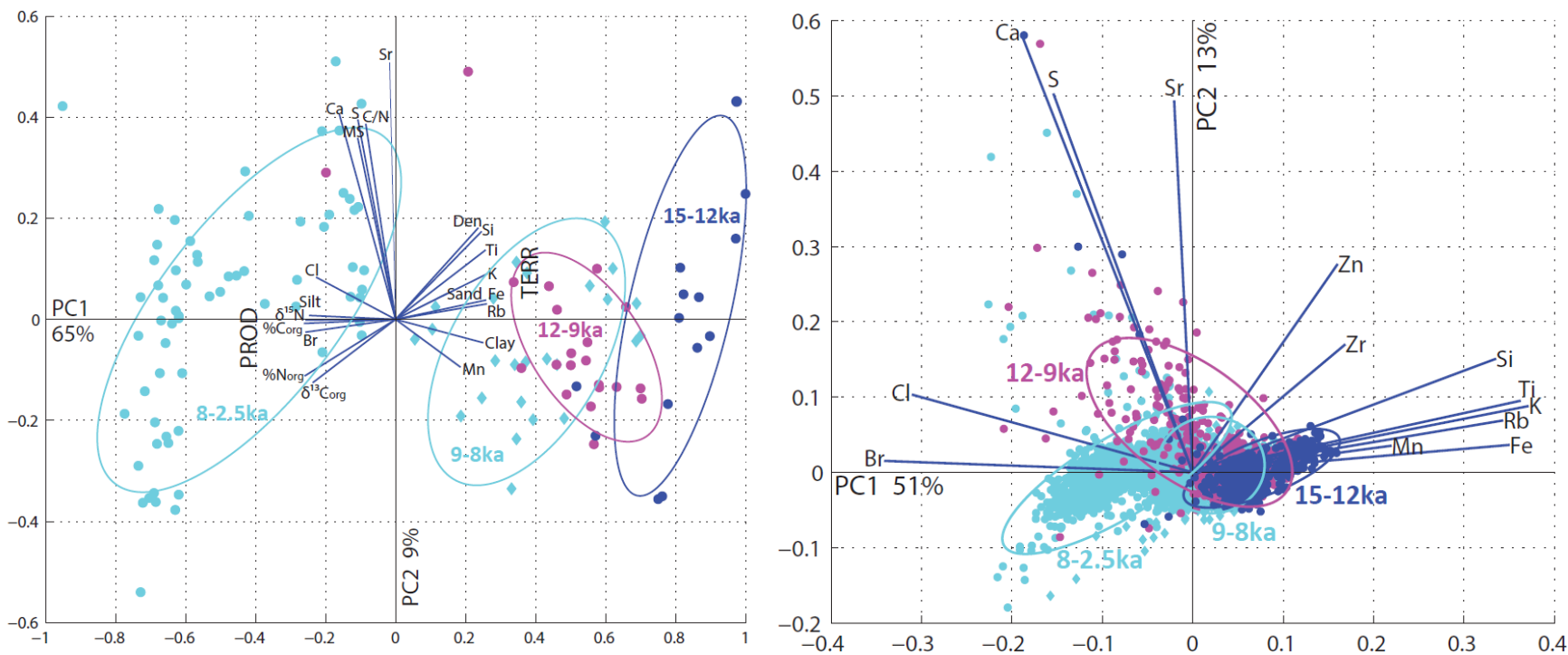


Figure 2.12. 24JPC PCA biplots. Left panel is full suite PCA. Right panel is XRF PCA. Populations are still color coded by age, but in this case are grouped not by climatic interval, but by the distinct intervals seen in %TOC (see Results). Percent variation explained is given with axes labels. Blue lines PC coefficients for each variable. TERR and PROD represent the area of terrestrial and productivity end-members respectively (see Discussion 2.5.1).

positively along PC1, loading better with the terrigenous end-members to the right (Ti, Fe, K, Rb, Clay), and younger samples plot to the left towards organic end-members (%N_{org}, %TOC, $\delta^{15}\text{N}$, silt, Br, Cl, and $\delta^{13}\text{C}_{\text{org}}$) which are negatively associated with PC1. Given that PC2 explains little of the variance (9%), PC1 best shows the change in sedimentology.

All forams found in 24JPC were agglutinated forams, which are common in the modern Arctic, and can be indicative of seasonally ice free conditions [Cronin *et al.*, 2008]. The sample from 730 cm (13.18 ka) was diluted by abundant sand, but also featured coaly and woody bits that were few to common, with very rare forams and diatoms. A sample from 620 cm (9.78 ka) featured rusty colored sediment with few forams of the *Ammo-baculoides* genus and centric diatoms, with rare coaly bits and very rare *Haplophragmoides* forams. The sample from 505 cm (8.87 ka) had few centric diatoms, rare coaly bits, and very rare pennate diatoms, *Textularia* forams, *Ammo-baculoides*, sponge spicules, and total agglutinated forams. A sample from 415 cm (8.46 ka) had common *Ammo-baculoides*, rare diatoms, and very rare *Reophax* forams, *Textularia*, and glauconite, with the biggest assemblage of agglutinated forams. The sample from 280 cm (7.78 ka) had abundant centric diatoms, few pennate diatoms and pyrite, rare *Textularia*, and very rare sponge spicules and total agglutinated forams. The sample from 86 cm (4.38 ka) had abundant centric diatoms, rare *Textularia*, very rare pyrite, *Trochammina*, *Haplophragmoides*, *Reophax*, and *Ammo-baculoides*, with the most diverse agglutinated foram assemblage, though all of them were tiny (Personal Communication, Mark Leckie).

2.4.3. Southwest Bering Sea, Bowers Ridge, 17JPC

17JPC (HLY02-02-17JPC), the southern-most and deepest core (2209 mbsl), was taken from Bowers Ridge [Cook *et al.*, 2005], 270 km north of Amchitka Island near the western end of the Aleutian Islands, and comprises the longest record of the cores in this study, from 27–8 ka,

contained in only 3 m of massive diatomaceous olive green-grey silty mud with an average sedimentation rate of 19.66 cm/kyr (Figure 2.13, 2.14, 2.15).

$\delta^{13}\text{C}_{\text{org}}$ of 17JPC averages -22.2‰ with minimal variability, likely due to the low resolution of isotopic data (Figure 2.13). During the LGM and ED, $\delta^{13}\text{C}_{\text{org}}$ averages -22.25‰ before depletion at the onset of the BA, averaging -21.87‰ through the BA, YD, and PB. The LGM/ED and Holocene portions of the record were slightly enriched (22.39‰) in comparison to the middle of the record.

TOC has three steps in the 17JPC record: low from 27–18 ka (0.75%), higher from the ED through the PB (1.55%), and lower again (0.87%) entering the Holocene (Figure 2.13). OC_{mar} comprises nearly all TOC preserved in 17JPC according to our simple mixing model. $\delta^{15}\text{N}$ averages 6.29 ± 0.68 ‰ throughout the record, but due to low resolution no trends can be confidently described (Figure 2.13). $\% \text{N}_{\text{org}}$ averages 0.126 ± 0.067 %, and is assumed to be equivalent to $\% \text{N}_{\text{org}}$ in 17JPC because $\% \text{N}_{\text{bou}}$ is close to zero (0.0092%) [Stein and Macdonald, 2004].

C/N ratios of 17JPC display the same three step pattern as TOC: low during the LGM (7.78), higher from the ED through the PB (8.38), and lower (8.15) entering the Holocene (Figure 2.13).

From 27–16 ka, median GS is 12.2 μm (Figure 2.13). After 16 ka, median GS increases to an average of 26.3 μm until the end of the record at 8 ka. The increase in median GS corresponds to an increase in sand-size particles and a reduction in silt and clay. Prior to 16 ka, average percent sand is 10.5%, before increasing to 29.3% from 16–8 ka. During these respective intervals, silt averages 74.7% and 65.6%, whereas clay decreases from 14.5% to 6.1%.

Terrigenous elements (Ti, Fe, K, and Rb) are abundant from 27–16 ka before decreasing

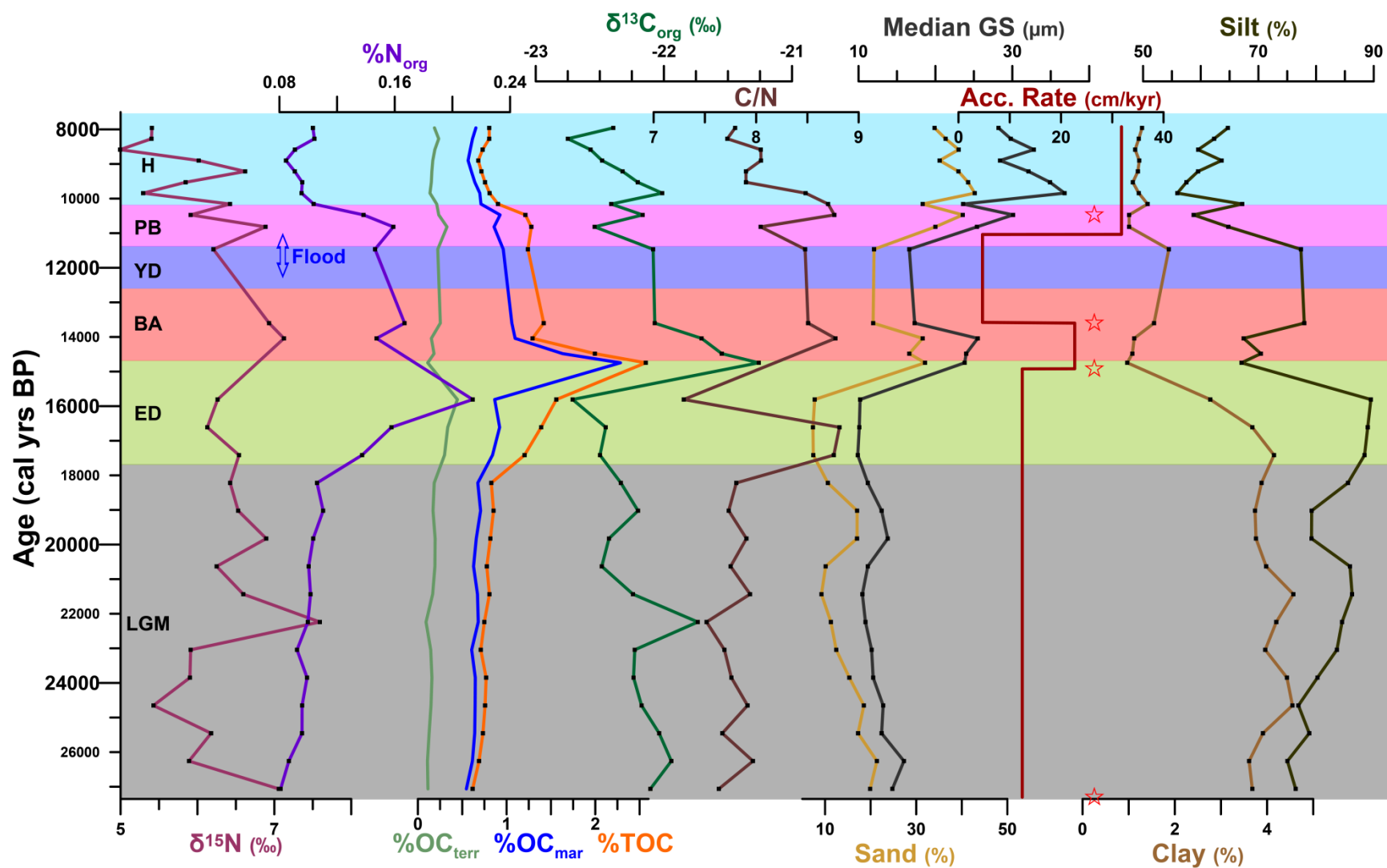


Figure 2.13. 17JPC bulk $\delta^{15}\text{N}$, $\%N_{\text{org}}$, $\% \text{TOC}$, estimated $\% \text{OC}_{\text{terr}}$ and $\% \text{OC}_{\text{mar}}$, bulk $\delta^{13}\text{C}_{\text{org}}$, C/N, grain size data, and accumulation rate. Four ^{14}C dates are given in calendar years, red stars [Cook *et al.*, 2005]. Blue arrow is the window of BLB flooding [Keigwin *et al.*, 2006].

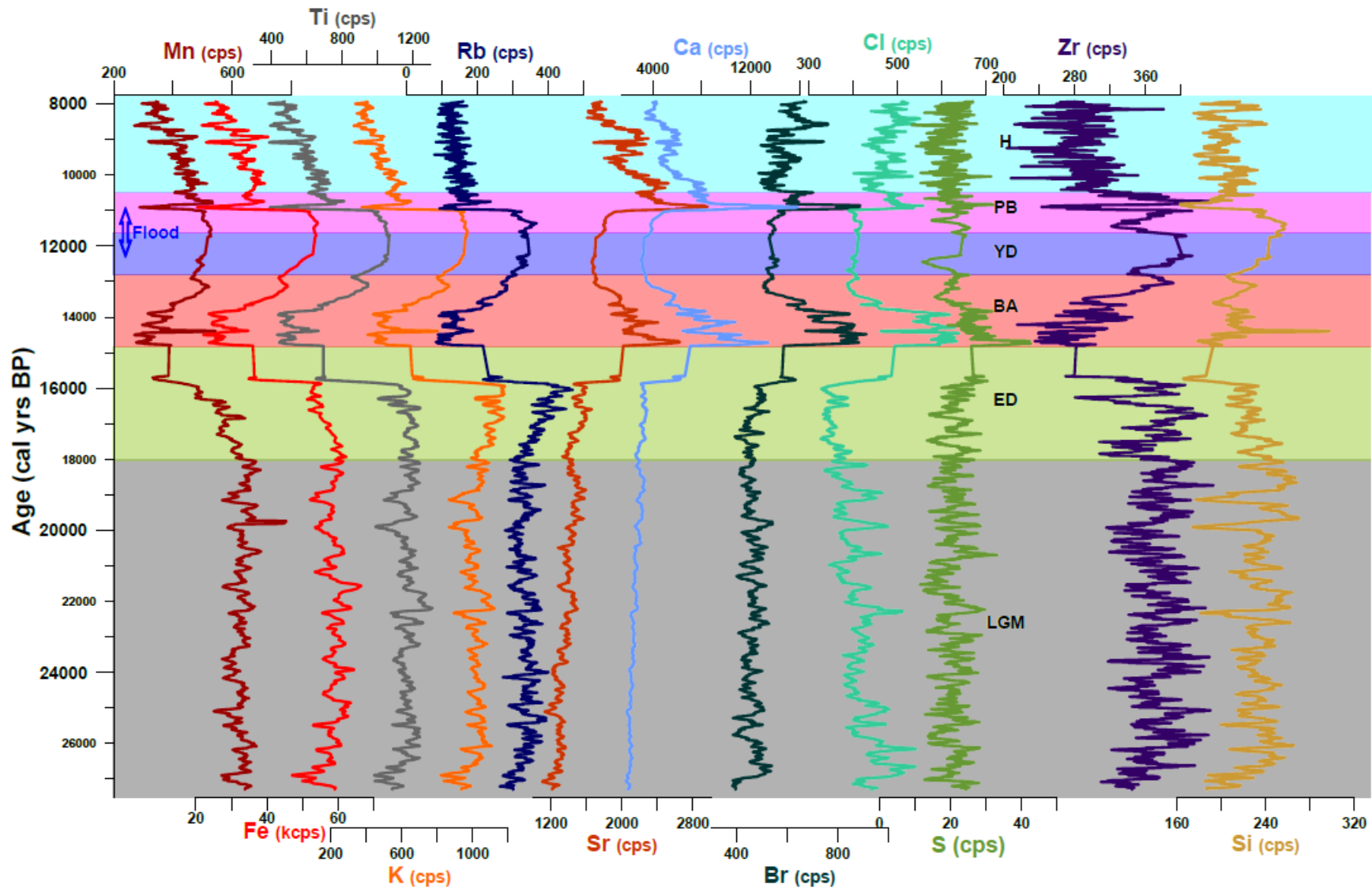


Figure 2.14. 17JPC elemental XRF intensity data in counts per second (cps). Blue arrow indicates BLB flooding window [Keigwin *et al.*, 2006].

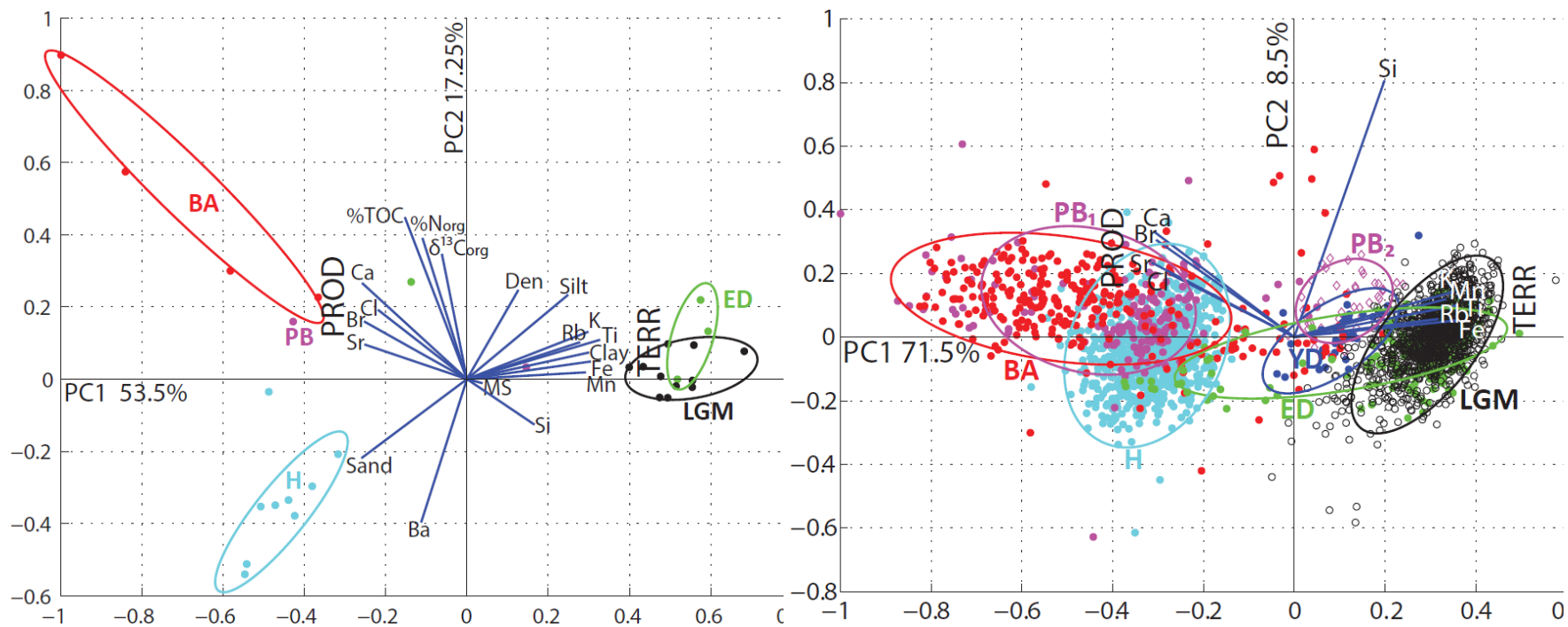


Figure 2.15. 17JPC PCA biplots. Left panel is full suite PCA. Right panel is XRF PCA. Populations are color coded by age, and percent variation explained is given with axes labels. Blue lines PC coefficients for each variable. TERR and PROD represent the area of terrestrial and productivity end-members respectively (see Discussion 2.5.1).

into the BA, where terrigenous counts are low, before increasing after 14 ka, and peaking during the YD and into the PB (Figure 2.14). Just after 11 ka, the terrigenous elements decrease sharply to counts comparable to those of the BA. When the terrigenous elements have low counts, Sr, Ca, Br, and Cl are abundant. Zr, Si, and Mn track reasonably well with the terrigenous elements listed above.

The full suite PCA (Figure 2.15) reveals that the LGM and ED plot together proximal to terrigenous end-members (Ti, Fe, K, Rb, Clay), with the Holocene associated with sand, as seen in 3JPC, and the BA plotted closer to productivity end-members including: %TOC, %N_{org}, $\delta^{13}\text{C}_{\text{org}}$, Ca, Cl, Br, and Sr. The PB only has two points in the full suite PCA so cannot be accurately represented, and the YD is completely omitted. The data are primarily influenced by PC1 (53.5%), but PC2 explains a significant portion of the variance (17.25%). The XRF PCA (Figure 2.15) captures both these intervals, with the YD plotted between the LGM/ED and the BA/PB/Holocene populations. The PB group has two distinct populations, one just above the YD, and one centered over the Holocene data. The samples plot along PC1 from right to left with age in the XRF PCA, which explains 71.5% of the variability.

2.4.4. Southeast Bering Sea, Umnak Plateau, 51JPC

51JPC (HLY02-02-51JPC) was taken from 1467 m water depth on the Umnak Plateau in the southeast Bering Sea [Cook *et al.*, 2005], about 130 km northwest of Unalaska Island. The background sediment of 51JPC is composed of relatively homogenous diatomaceous dark olive green clay and silt, which is punctuated by two tephra deposits which are each followed by a laminated interval (Figure 2.16, 2.17). The first laminated interval occurs between 218–174 cm (15–13.3 ka) and the second from 138–134 cm (11.4–11.1 ka). The laminations are composed of black to dark olive green-grey sub millimeter thick lamina. Both are underlain by thick tephra

deposits (219–240 cm and 139–148 cm). Sediment accumulation rate is 47 cm/kyr from the LGM until ~16 ka when the rate slows to an average of 23 cm/kyr into the Holocene.

$\delta^{13}\text{C}_{\text{org}}$ of 51JPC is indicative of a marine signal, averaging -22.1‰ (Figure 2.16). During the LGM and into the ED, values are relatively enriched (-22.5‰), before depletion begins ~16.5 ka, with $\delta^{13}\text{C}_{\text{org}}$ steady at -21.8‰ from ~15 ka into the Holocene.

TOC is lowest during the LGM into the ED (0.8%), and within the older tephra layer which appears to be either bioturbated and/or disturbed by coring (Figure 2.16). Around 17.5 ka TOC increases reaching 1.9% by 16.5 ka before declining to 1% leading into the older tephra unit. After the older tephra unit, TOC is relatively constant around 1.35%, until increasing at 11.5 ka to 1.43% entering the Holocene. OC_{mar} is the dominant component of TOC throughout the record, but during the ED there is an increase in OC_{terr} from ~17–16ka.

Median GS tracks the lithology, with maxima corresponding to the two tephra units around 15.5 and 11.75 ka respectively, and an overall increase in median GS when sand becomes more abundant around 16 ka (Figure 2.16). From 20–16 ka, sand was 7.6%, compared to 15.4% from 16 ka on. Clay was abundant in 51JPC during the LGM (15.1%), before increasing from 17.7 ka to 16.4 ka (20.2%), and then decreasing to an average of 8.4% from 16–10.5 ka. As the primary sediment component, silt was most prevalent in the massive units (76.2%), and least abundant in the tephra units (70%). Silt was very steady outside of the tephra units averaging 75.8%.

51JPC is difficult to interpret with respect to XRF data, because the two tephra deposits correspond with two periods of climatic significance, the end of the YD, and preceding the BA. The tephra themselves are marked by an increase in Ti, Fe, Si, and Ca, along with low Cl, K, Br, S, and Sr (Figure 2.17). Ca and Sr are high separate from the tephra activity ~13.5 ka. During

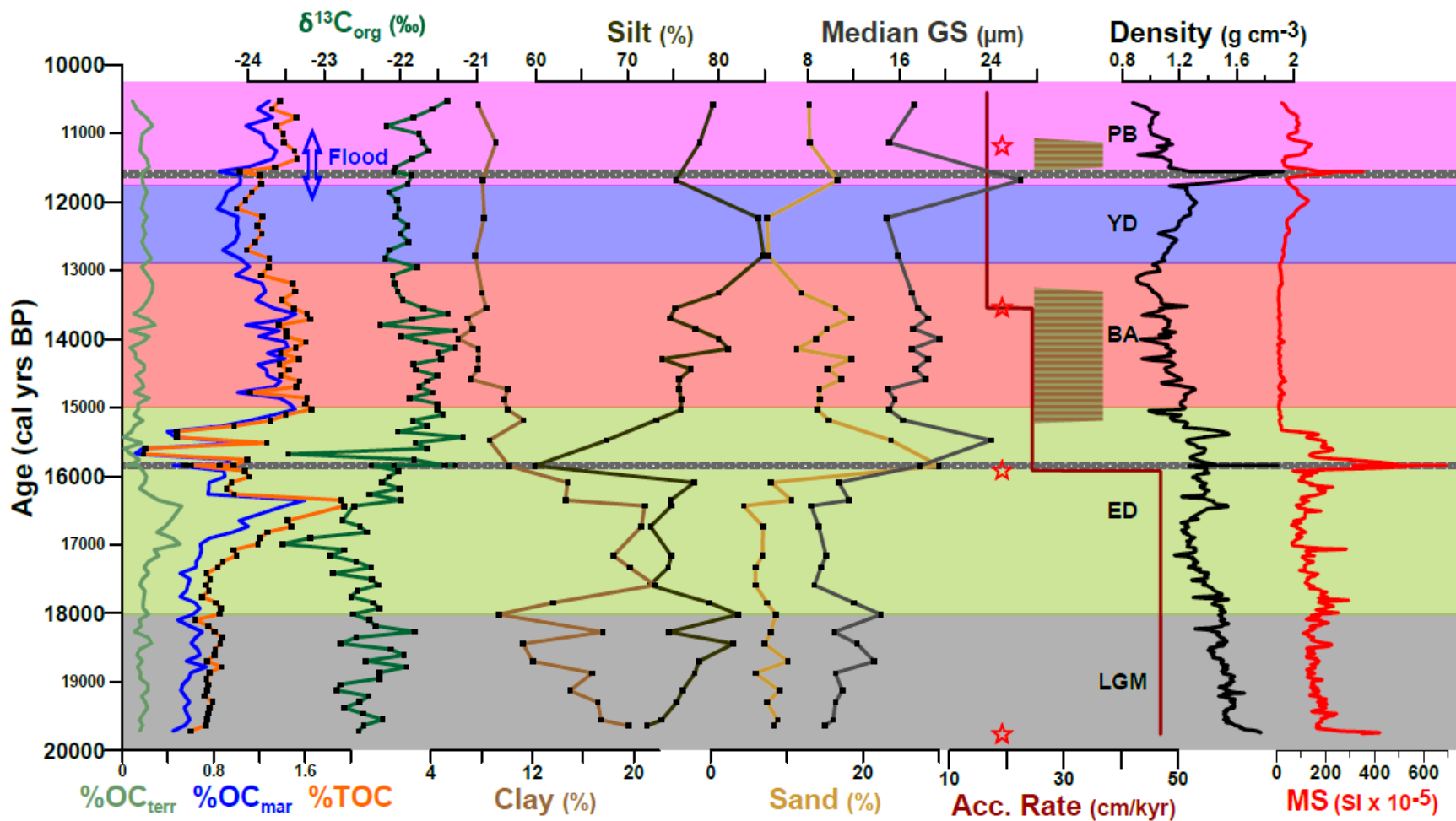


Figure 2.16. 51JPC %TOC, estimated $\% \text{OC}_{\text{mar}}$ and $\% \text{OC}_{\text{terr}}$, bulk $\delta^{13}\text{C}_{\text{org}}$, grain size data, and accumulation rate. Four ^{14}C dates are given in calendar years, red stars [Cook *et al.*, 2005]. Blue arrow is the window of BLB flooding [Keigwin *et al.*, 2006]. Laminations are indicated by brown/green striped bars, with tephra displayed as light grey boxes. Tephra were not treated as instantaneous events due to bioturbation (older unit) and disturbance during coring (younger unit is at a steep angle within the core).

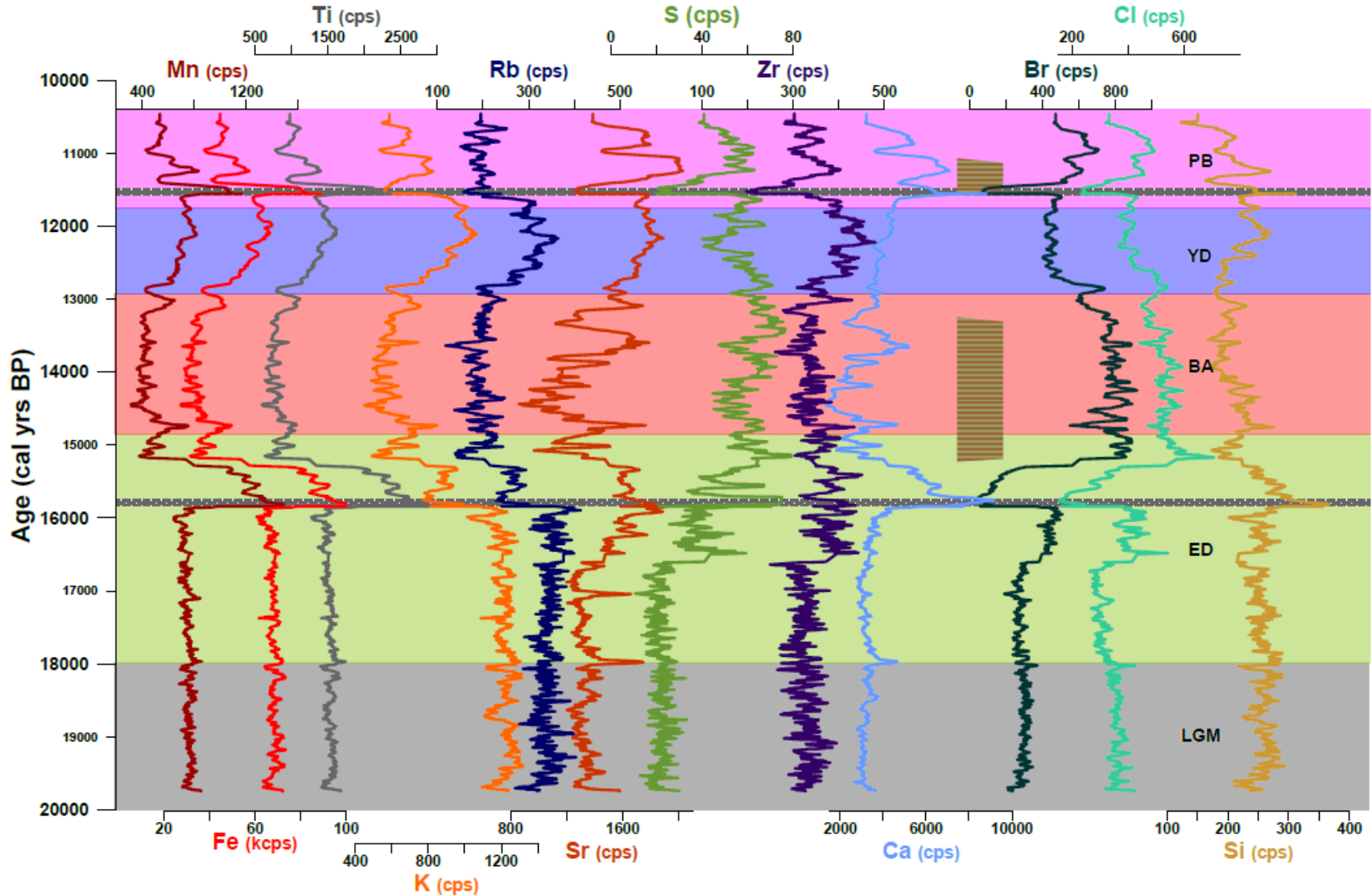


Figure 2.17. 51JPC elemental XRF intensity data in counts per second (cps). Tephra are indicated by grey stippled bars, and were treated as instantaneous. The older tephra has been dispersed through the sediment above the tephra blocks, which fall within the grey bar. The younger unit is at a steep angle within the core, clearly resulting from coring disturbance.

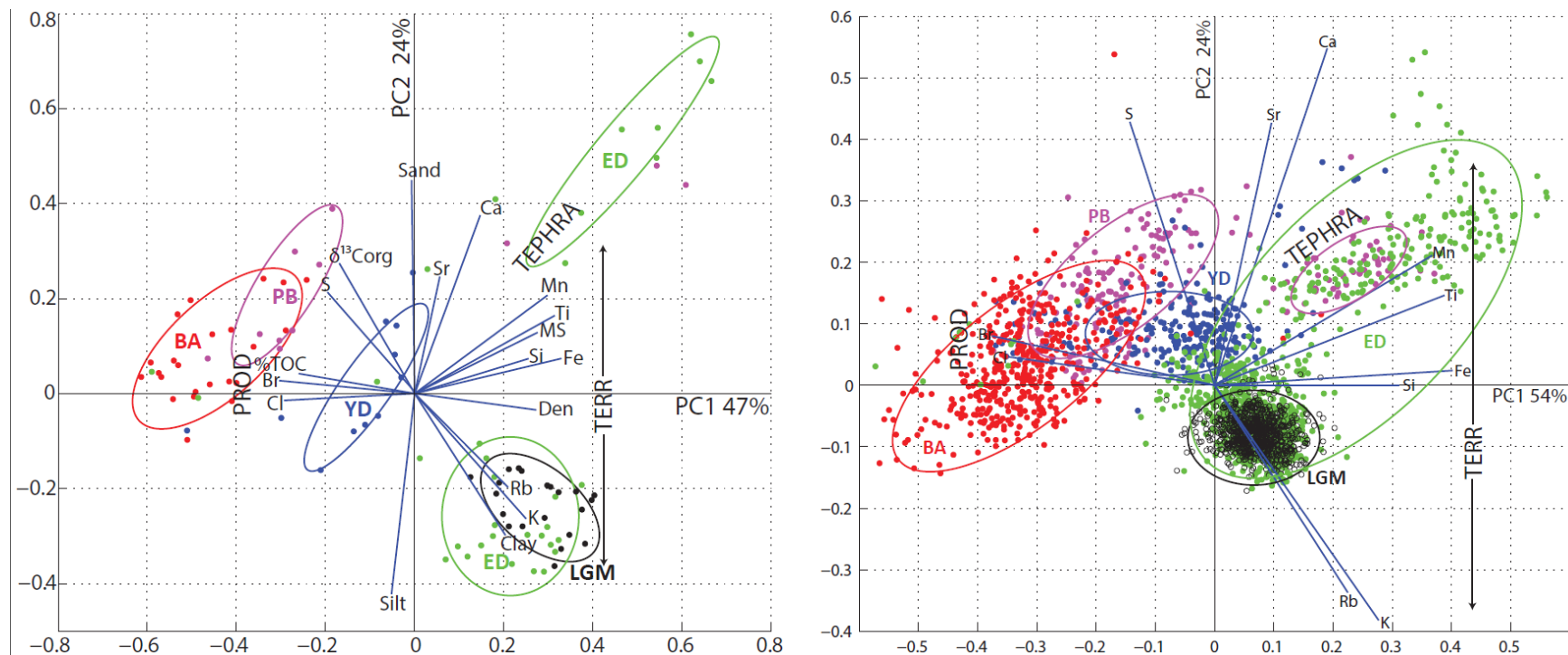


Figure 2.18. 51JPC PCA biplots. Left panel is full suite PCA. Right panel is XRF PCA with the tephra data (TEPHRA) located around the smaller PB population. Populations are color coded by age, and percent variation explained is given with axes labels. Blue lines PC coefficients for each variable. The direction and length of the vector indicate how each variable contributes to the two principal components in the plot. TERR and PROD represent the area of terrestrial and productivity end-members respectively, and TEPHRA represents the samples from the two tephra units (see Discussion 2.5.1)

the BA and PB, the terrigenous elements (Ti, Fe, K, and Rb) are low and are higher during the YD and LGM/ED outside of the tephra units. Cl, and Br are increased during the BA and PB.

Both the full suite and XRF PCA display the ED and LGM plotted together, near Rb, K and Clay (Figure 2.18). The ED shows great scatter in the XRF PCA, and two populations in the full suite PCA, with the upper population being the tephra unit, which is plotted closest to Ti, Mn, Ca and Fe, as was seen in Figure 2.17. The PB has two populations, with one population plotted with the BA with the "productivity" end-members, and the other with the XRF scatter, and is thus the other tephra unit. The YD plots in the center of both PCA plots.

2.5. Discussion

2.5.1. Principal Component Analysis End-Member Selection

We deemed Fe, Ti, K, Rb, and clay to be terrigenous end-members in this study, because all five are terrestrially derived products, they correspond with the geologic composition of Alaska and Chukotka, and plot together in our PCA biplots. For all four cores, these five variables plot together, with the samples of intervals known to have the highest terrigenous input (like the ED) plotting in close proximity (e.g. Figure 2.8). Of the four elements, only Fe can be altered by diagenesis since it is one of the few sediment seafloor electron acceptors [*Froelich et al.*, 1979]. Clay deposited in the Arctic is primarily known to be a terrestrial material [*Nürnberg et al.*, 1994; *Viscosi-Shirley et al.*, 2003] in part because concentrations of Arctic shelf sedimentary biogenic matter are generally low [*Mammone*, 1998]. Si and Mn both plot in close proximity to terrigenous end-members, but were not included as they did not plot as part of the same clear-cut group of four elements, are not strongly correlated with terrigenous elements, and have other complicating factors. Si displayed proximally to terrigenous end-members, likely due

to quartz grains, but is also a major component of diatoms and other siliceous microfossils [Sancetta, 1995], and thus is not trusted as purely a terrigenous element. Si was not well correlated with any of the four terrestrial elements, with Pearson's r-value of 0.35 to 0.58, similar to that of Mn with r-values from 0.34 to 0.54, whereas as the terrigenous elements had r-values of 0.68 to 0.88 in relation to each other (P-values all <0.01).

Mn is thought to be supplied to the Arctic Ocean via permafrost drainage down rivers during warm periods [Jakobsson *et al.*, 2000; Löwemark *et al.*, 2008], but Mn was not selected as a purely terrestrial end-member. Mn has high variability (Figure 2.11) possibly due to its known propensity for diagenetic alteration and remineralization within marine sediments [Heggie *et al.*, 1987]. The mobility of Mn within sediments [Heggie *et al.*, 1987; Van Cappellen and Wang, 1996] is the primary reason we did not include it as a terrestrial end-member. The oxides and hydroxides of Fe and Mn reductively dissolve when later buried or mixed below the aerobic surface of sediments underlying oxygenated bottom waters [Van Cappellen and Wang, 1996]. Pore waters containing Fe(II) and Mn(II) may precipitate or be transported back toward the sediment-water interface via pore water diffusion and lost from the sediment [Heggie *et al.*, 1987; Van Cappellen and Wang, 1996]. Considering that Fe tracks nearly identically with Ti, K, and Rb, we assumed in our cores that only Mn was greatly affected by diagenesis. Mn plotted along the same vector as the primary terrigenous variables (e.g. Figure 2.8), but was best loaded onto the third or fourth PC in most cases, which is why the magnitude (length) of the score vector for Mn is shorter in most plots than the other terrigenous end-members.

The geologic provinces of Chukotka are compositionally similar to those of Alaska [Deming *et al.*, 1992]. Both primarily feature sedimentary rocks, extensive unconsolidated Quaternary deposits, and volcanic rocks [Hoare, 1961; Deming *et al.*, 1992; Parfenov, 1992;

Soloviev et al., 2006]. However, Alaska has a highly variable geology, and little geologic work has been done that would allow for fingerprinting of specific sources [*VanLaningham et al.*, 2009]. *VanLaningham et al.* [2009] used bulk sediment ^{40}Ar - ^{39}Ar and Nd isotopic analysis to constrain the sediment sources of the Meiji Drift, but had to work around the lack of source rock age data from the major rivers of the region, with the exception of the Yukon [*Eberl*, 2004]. On its own, our XRF data does not seem enough to fingerprint individual sources without better quantification [*Thomson et al.*, 2006]. Nevertheless, Fe, Ti, K and Rb are widely known to be derived from the rocks and weathering products, with iron being the only element of the group subject to diagenetic alteration, which is minimal in our cores.

We have selected %TOC, %N_{org}, Br, Cl as the productivity end-members. We chose these four variables because in every PCA biplot, they all plotted closely with the sample population of the periods associated with high Bering Sea productivity (BA and PB) [*Cook et al.*, 2005; *Brunelle et al.*, 2010; *Caissie et al.*, 2010; *Schlung et al.*, 2013], and are known to be related to primary productivity and OM. TOC provides a first order estimate of paleoproductivity [*Stein*, 1986], but can be influenced by terrestrial carbon input as well as OC accumulation rates, which are influenced by oxygenation. Cl and Br are known to be concentrated in sedimentary OM [*Price and Calvert*, 1977; *Harvey*, 1980], with Br strongly bonded to OM. Cl, associated with sea salt, is elevated in OM-rich sediment in our cores, because these sections are primarily low density, leaving more room for interstitial pore fluids and thus more salt. XRF core scanning Br data has been shown to be directly related to TOC, but the relationship is weaker during intervals of high terrestrial carbon input [*Ziegler et al.*, 2008]. In certain cores, other elements appeared to be associated with productivity, like Sr and Ca in 17JPC (Figure 2.15), while not in other cores. As much as 40% of variability in silt

content of cores can be explained by diatom abundance in the Bering Sea [*Aiello and Ravelo*, 2012], but that still leaves silt content split between biogenic materials and terrigenous materials, as shown by the location of silt roughly halfway between the terrigenous and productivity end-members in the full suite PCA biplots (e.g. Figure 2.18).

Our terrigenous and productivity end-members were thus chosen to represent sediment delivery to all four cores. We do not claim that these end-members are a perfect representation and are not quantitatively applied in this study, but we have confidence that they do indeed broadly represent sediment dominated by terrigenous input as seen during the ED and LGM, and sediment dominated by biogenic components as seen during the PB and BA.

2.5.2. Last Glacial Maximum (27 to 18 ka)

Around 26 ka, the Bering and Chukchi seas were much smaller than today (Figure 2.2) due to the exposure of the continental shelves (Figure 2.1). Sea level, estimated at 120–125 m below present day [*Fairbanks*, 1989; *Peltier and Fairbanks*, 2006], closed the Bering Strait [*Hopkins*, 1959], and ended communication between the Chukchi and Bering Seas. The cold climate of the LGM permitted extensive sea ice cover over the Bering Sea [*Sancetta et al.*, 1985; *Caissie et al.*, 2010], and substantial perennial ice over what little of the Chukchi was not subaerially exposed [*Nørgaard-Pedersen*, 2003].

2.5.2.1. Western Bering Sea Shelf Slope, 3JPC

Situated between Navarin and Pervenets Canyons on the western side of the Bering Sea shelf slope, 3JPC would have been located roughly 200 km from the BLB during LGM low stand (~26 ka) [*Peltier and Fairbanks*, 2006], with a cold climate and permanent or seasonal sea ice cover [*Sancetta et al.*, 1985; *Katsuki and Takahashi*, 2005; *Caissie et al.*, 2010]. Prior to 18

ka, the environment of 3JPC would likely had relatively low biological activity, supported by limited TOC (0.8%), and the lowest sedimentation rate of the record (86 cm/kyr). Relatively enriched LGM $\delta^{13}\text{C}_{\text{org}}$ (-20.8‰) primarily represents a marine signal at the time [Walsh *et al.*, 1989; Naidu *et al.*, 1993], with low terrestrial input (low %OC_{terr}), and OC_{mar} dominating the LGM supply of TOC (Figure 2.5). PCA performed on geochemical and isotopic data of 3JPC reveals that the LGM population plots separately from other age-grouped populations, farthest from the productivity and terrigenous end-members, supporting both the low TOC and relatively enriched $\delta^{13}\text{C}_{\text{org}}$ (Figure 2.8). Restricted LGM Bering Sea and subarctic North Pacific productivity [Keigwin *et al.*, 1992; Nakatsuka *et al.*, 1995; Jaccard, 2005; Okazaki *et al.*, 2005; Tanaka and Takahashi, 2005; Caissie *et al.*, 2010; Lam *et al.*, 2013] likely corresponds to light limitation suppressing phytoplankton blooms [Tanaka and Takahashi, 2005], and minimal ventilation of nutrient rich deep water limiting the nutrient supply to the euphotic zone [Brunelle *et al.*, 2007].

2.5.2.2. Southwestern Bering Sea, Bowers Ridge, 17JPC

In contrast to 3JPC, 17JPC is purely an open marine site, with no major proximal sources of terrigenous material at any time during the record, supported by an average of -22.2‰ $\delta^{13}\text{C}_{\text{org}}$ from 27–8 ka. PCA of 17JPC XRF data indicates that the LGM had the highest terrestrial input of any time during the record, substantiated by its plotting along PC1 (Figure 2.15) where assumed terrigenous end-members are located (Fe, Ti, K, and Rb, and clay--for the full suite PCA). The highest contributions of these terrigenous end-members were observed from 27–16 ka in the XRF data. The higher input of terrestrial material at 17JPC may have resulted from increased aerial extent of the Aleutian Islands [Mann and Hamilton, 1995] with lowered sea level, increased aeolian flux [Otosaka *et al.*, 2004; Lam *et al.*, 2013], and material derived from

glacier erosion from the Aleutian Islands, Koryak Mountains, and/or Kamchatcha Peninsula [Mann and Hamilton, 1995; Gualtieri et al., 2000]. Loess deposition recorded south of 17JPC on the Detroit Seamount in GGC-37 was highest during the LGM/ED, and declined at 11 ka, coeval with the flooding of the Bering Strait, suggesting that subaerial delivery of exposed Bering Shelf sediments was the dominant contributor of loess-like material to the core [Lam et al., 2013]. Our XRF data support the Lam et al. [Lam et al., 2013] loess delivery interpretation as counts of Ti, Fe, K and Rb are high during the LGM, ED, and YD, before decreasing during the PB and Holocene once the exposed shelves would have been largely flooded. Without quantitative mineralogy [Viscosi-Shirley et al., 2003; Eberl, 2004], we do not interpret XRF elemental count data as quantitative or exact, merely as a general descriptor of relative changes in sediment composition.

2.5.2.3. Umnak Plateau, Southeastern Bering Sea, 51JPC

51JPC was also an open marine site during the LGM, as shown by $\delta^{13}\text{C}_{\text{org}}$ (-22.5‰) indicating a predominately marine signal [Naidu et al., 2000]. During the LGM, lower sea level and glaciation of the Aleutians [Mann and Hamilton, 1995; Kaufman and Manley, 2004] prevented warm ASW from arriving at 51JPC through the shallow Unimak Pass [Caissie et al., 2010]. Clay content was higher during the LGM (~12%) than during the younger portion of the record (~2%) (Figure 2.16), likely due to decreased current velocity over the site when Aleutian Island channels were blocked. Cutting off ASW injection through Aleutian Passes [Okazaki et al., 2005] would have limited the strength of the BSC [Okazaki et al., 2005], and supported sea ice growth [Overland and Pease, 1982]. In conjunction with the limitation of ASW injection, extensive sea ice cover likely limited wind forcing, weakening the strength and quantity of eddies that define the BSC [Clement et al., 2005],

PCA for 51JPC shows the LGM population plotting with terrigenous end-members, particularly K and Rb. LGM K and Rb are at their highest counts observed in the record, whereas other terrigenous elements (Ti, Fe) are higher during the YD and tephra units.

2.5.3. Early Deglaciation (18 to 15 ka)

2.5.3.1. Increased Terrestrial Influx, Bering Sea

There are four main lines of evidence supporting increased terrestrial input during the ED: $\delta^{13}\text{C}_{\text{org}}$ depletion, increased OC_{terr} , high counts of terrigenous elements, increased fine clay content ($<2\ \mu\text{m}$), and PCA plotting of ED samples with terrigenous end-members.

2.5.3.2. Organic Carbon Isotopes and Terrestrial Carbon Input

In 3JPC, the relative $\delta^{13}\text{C}_{\text{org}}$ depletion and TOC increase that begin $\sim 18\ \text{ka}$ (Figure 2.5) are likely indicators of the initiation of deglaciation, but since we lack a date in proximity to the depletion to constrain the accumulation rate (i.e., no date between ~ 20.4 and $14.7\ \text{ka}$), we do not have confidence in the timing of deglaciation as recorded by 3JPC. It is possible that the excursion is closer to $17.5\ \text{ka}$, which is the attributed date by Brunelle et al. [2010], based upon a $\delta^{15}\text{N}_{\text{db}}$ depletion corresponding to the depletion seen in our record at $18\ \text{ka}$ (Figure 2.5). The increase in TOC and $\delta^{13}\text{C}_{\text{org}}$ suggests that the low sedimentation rate applied through the period would have been higher during the TOC peak, thereby pushing the deglaciation to a later date which does not correspond with the onset of H1 (our ED). If the sedimentation rate was indeed higher in this interval, it would essentially delay the peak in TOC and $\delta^{13}\text{C}_{\text{org}}$ depletion, and extend the initial interval of low TOC and marine $\delta^{13}\text{C}_{\text{org}}$ signal seen in Figure 2.5. Oxygen isotopes of planktonic forams provide evidence for the onset of deglaciation in the region, with

$\delta^{18}\text{O}$ depletion beginning around 16.9 ka for the Gulf of Alaska [Davies *et al.*, 2011], consistent with freshening and warming of surface waters due glacial melt water and rising temperature.

By 17 ka, the $\delta^{13}\text{C}_{\text{org}}$ of 3JPC (-25‰) is dominated by terrestrial carbon, seen in OC_{terr} which overtook OC_{mar} by 17.5 ka (Figure 2.5). The increase in OC_{terr} is indicative of an influx of terrigenous material likely derived from glacial materials. The erosion of continental shelves during inundation and glacial melt [Davies *et al.*, 2011] would have also contributed, however major global sea level rise did not occur until the BA [Peltier and Fairbanks, 2006] suggesting that the OC source of the ED was most likely from further upriver on the landscape. A corresponding peak in clay content is suggestive of fine grained glacial material delivered via rivers, coastal inundation, and dust storms known to transport micronutrient-rich loess to the Gulf of Alaska [Crusius *et al.*, 2011]. This terrigenous material contribution led to the highest period of TOC in the record (1.46%) from 17.2–14.8 ka, likely fostering increased productivity seen in the Gulf of Alaska [Davies *et al.*, 2011; Addison *et al.*, 2012].

Similar to 3JPC, the most depleted $\delta^{13}\text{C}_{\text{org}}$ values of the 51JPC (-22.28‰) and 17JPC (-22.75‰) records occur during the ED. Although OC_{mar} is the dominant component throughout the 51JPC record, OC_{terr} increases during the ED, essentially matching OC_{mar} during the height of the ED (Figure 2.16). The poor resolution of isotope data in 17JPC does not lend confidence to describing the terrestrial carbon component for any one interval.

2.5.3.3. Elemental XRF data and PCA Analysis

The ED sample populations of both 3JPC and 17JPC (Figure 2.8 and Figure 2.15) plot closest to the terrigenous end-members (Fe, Ti, K, Rb and Clay). These four terrigenous elements are high in all three cores during the ED, and increase in 3JPC during the ED. The PCA plotting of ED samples with terrigenous elements and high counts during the ED supports

the interpretation of increased deglacial delivery of terrestrial material during the ED (Figure 2.5).

Interestingly, C/N ratios do not show much change during the ED in 3JPC, increasing from ~12 to 13 in 3JPC, but are nonetheless indicative of a terrestrial signal. High C/N values (>10) indicate terrestrial soil and plant material input and/or low quality, older, more refractory detrital material [Parsons *et al.*, 1977; Grebmeier *et al.*, 1988].

The ED population in 51JPC also plots closely to the terrigenous end-members, but shows great scatter in the XRF PCA, and displays two populations in the full suite PCA (Figure 2.18). The scatter in the XRF PCA that corresponds to the second population in the full suite PCA plot closely with Ti, Mn, Ca, and magnetic susceptibility, and represent the tephra units. The ED outside of the tephra units plot with the LGM population, closely associated with K and Rb. The increase in terrestrial material delivery from the LGM to the ED was likely due to glacier melt, inundation of the BLB and exposed continental shelves, and loess deposition [Lam *et al.*, 2013].

2.5.3.4. Nitrogen Isotopes of the Early Deglacial

Enriched $\delta^{15}\text{N}$ values during the LGM (7.52‰) in 3JPC decrease rapidly during the early deglaciation at ~18.15 ka, averaging 5.66‰ from 18–15.4 ka. This pattern of high LGM $\delta^{15}\text{N}$ followed by a decrease during the ED is seen across the North Pacific as documented by Brunelle *et al.* [Figure 4, 2010], in 17JPC, as well as in GGC27 of the Okhotsk Sea and PC13 of the Northern Emperor Seamounts, located in the open western subarctic Pacific. The sustained enriched $\delta^{15}\text{N}$ values of the LGM may be due to increased nutrient consumption in the Subantarctic southern ocean, lowering the nutrient content of intermediate waters traveling northwards across the Pacific [Robinson, 2005], and thus enriching the source nitrate in the

Bering Sea. At 17.5 ka, there is an interval of depleted $\delta^{15}\text{N}$ (5.5‰) in the North Pacific [Brunelle *et al.*, 2010], corresponding to our ED depleted $\delta^{15}\text{N}$ record (5.7‰). This depletion is postulated to have been driven by decreased southern ocean utilization after 18 ka [Wolff *et al.*, 2006; Winckler *et al.*, 2008], which left the source nitrate with more ^{14}N -nitrate, as well as a potential decrease in nitrate utilization in the North Pacific [Brunelle *et al.*, 2010].

2.5.3.5. Early Deglacial River Drainage Networks

The drainage network and debouchement location for the major Beringian rivers have a major impact on sediment delivery in the Bering and Chukchi Seas [McManus *et al.*, 1974; Nelson and Creager, 1977; Stein, 2000]. With a sediment discharge of ~55 million metric tons per year, the Yukon River accounts for as much as 90% of river-borne sediment entering the Bering Sea [Lisitsyn, 1966; Eberl, 2004]. The Yukon and Kuskokwim Rivers are separated by no topographic divide in their lower reaches, which has led to speculation that they may have joined in the past, perhaps even during the LGM [Scholl *et al.*, 1970] when the BLB was exposed, forcing the major regional rivers: Yukon, Kuskokwim, and Anadyr, to cross the subaerially exposed continental shelf to reach the southern Bering Sea [Kummer and Creager, 1971; Mann and Hamilton, 1995]. With the BLB submerged the rivers empty farther to the north in modern times, with Yukon and Anadyr discharge transported northward through the BS [Coachman and Aagaard, 1966; Roach *et al.*, 1995; Woodgate *et al.*, 2005].

There is not enough evidence of buried channels to tie present day rivers to submarine canyons at specific times [Carlson and Karl, 1984], but it is likely that these three rivers played an important role in excavating many of the huge submarine canyons of the Bering shelf slope [Scholl *et al.*, 1968, 1970; Hopkins, 1972; Carlson and Karl, 1984]. A probable debouchement of the Yukon and/or Kuskokwim Rivers during the LGM is Pribilof Canyon (Figure 2.2) [Scholl

et al., 1970; Hopkins, 1972; Carlson and Karl, 1984], which would have brought the Yukon closer to 3JPC, allowing the BSC to transport material to the core site from the mouth of the Yukon. Alternatively, the rivers may have drained across the BLB as sluggish, meandering streams which spread the available water over the tundra [Sancetta *et al.*, 1985]. In this scenario, the riverine materials and clay deposited over the BLB would have entered the Bering Sea during the inundation and erosion of the BLB during the ED. This material would have been ripe for transport to the Bering Sea via aeolian transport or during inundation. Whether the Yukon and Kuskokwim drained directly into the Bering Sea [Scholl *et al.*, 1970; Hopkins, 1972], or deposited most of the sediment load en route to the Bering, the ED saw an increase in the delivery of terrigenous material to the Bering Sea, as supported by an increase in OC_{terr} , PCA plotting of ED with terrigenous end-members, and high XRF counts of terrigenous elements in all three cores.

There is a rapid increase of clay before 18 ka in 3JPC from 12–20% after averaging 13% from 21–18.2 ka is coeval with an increase in OC_{terr} and N_{org} (Figure 2.5). The Yukon and Kuskokwim River watersheds are known to be rich in illite and kaolinite [Naidu and Mowatt, 1983] so an increase in clay may be from riverine transport, and this is supported by the increase in OC_{terr} and the PCA loading of the ED samples with terrigenous end-members (Figure 2.8). Interestingly there is a peak in clay <2 μm during the ED from 4% to 17%, which is seen as slightly lower clay content than during the LGM in clay <4 μm . The peak in very fine clay may be due to increased input of glacial flour. The increase in OC_{terr} indicates that the N_{org} increase was likely terrestrially-derived as well. The depleted $\delta^{13}C_{org}$ of 3JPC (-25‰) is consistent with river input, as the Yukon River (-26.5 to -28‰) [Guo and Macdonald, 2006], the Colville, Mackenzie, Anadyr, and Lena (<-26.5‰) [Naidu *et al.*, 2000], and Siberian rivers (-27.5‰),

draining both taiga and tundra [Lobbés *et al.*, 2000], are all relatively depleted.

The discovery of the "Paleo-Anadyr" [Canada. Defence Research Board. Directorate of Scientific Information Services and Kotenev, 1966] suggests that perhaps the Anadyr River played a role in excavating either the Navarin or Pervenets Canyons (Figure 2.2) during the Pleistocene [Canada. Defence Research Board. Directorate of Scientific Information Services and Kotenev, 1966; Hopkins, 1972]. If the Anadyr drained downstream of or proximal to 3JPC during the LGM, it would have been a major influence during the onset of melt during the ED, and possibly could have played a role in the increase in terrigenous elements seen in 3JPC during the ED, compared to 17JPC and 51JPC, which had high counts but saw no increase.

If the Kuskokwim River drained via the Bering Canyon, then a larger difference would be expected between the LGM/ED $\delta^{13}\text{C}_{\text{org}}$ (-22.5‰) and the remainder of the record (-21.8‰). The <1‰ change in $\delta^{13}\text{C}_{\text{org}}$ can be explained via the proximity to land, blockage of North Pacific Water (NPW) injection through the Aleutians due to extensive glaciation and lower sea level [Mann and Hamilton, 1995; Katsuki and Takahashi, 2005; Caissie *et al.*, 2010]. Increased glacier input from the portion of the Cordilleran Ice Sheet occupying the Aleutian Range [Kaufman and Manley, 2004] may account for the high clay content during the LGM and ED (16%) versus the BA through the Holocene (8%).

Identifying where these major rivers drained in the past has implications for sediment delivery at core sites of the Bering and Chukchi Seas, as their nutrients and detrital material are an important part of the ecosystem and sedimentary budget of the region [McManus *et al.*, 1974; Nelson and Creager, 1977; Stein, 2000], and would have been even more significant during the height of the deglaciation.

2.5.4. Bølling-Allerød (15 to 13 ka)

The BA warm period marked the end of the ED. An abrupt freshening and/or warming event is recorded in planktonic foraminifer $\delta^{18}\text{O}$ of the Bering shelf-slope at 14.4 ka [Cook *et al.*, 2005], and at 15 ka on the Umnak Plateau [Caissie *et al.*, 2010], as well as in the Gulf of Alaska [Davies *et al.*, 2011], corresponding with the 14.7 ka date of BA onset at NGRIP [Rasmussen *et al.*, 2006] that featured rapid Northern Hemisphere warming [Broecker, 1998; Schlung *et al.*, 2013], and Meltwater Pulse 1a (MWP 1a) [Weaver, 2003]. Meltwater pulse 1a increased eustatic sea level by 20 m in the span of ~500 years (14.4–13.8 ka) and was likely derived primarily from Laurentia [Tarasov and Peltier, 2005]. Freshening from MWP 1a may have relieved light limitation by shallowing the depth of the mixed layer [Lam *et al.*, 2013] and fostering elevated productivity as predicted by the critical depth theory [Sverdrup, 1953], which is valid in the western North Pacific [Obata *et al.*, 1996].

Over the Bering Sea, upper water column stability is thought to have increased due to fresh water input from melting ice [Keigwin *et al.*, 1992; Lam *et al.*, 2013], driving an increase in productivity in the Bering Sea as seen in our cores, that also occurred over the subarctic North Pacific [Keigwin *et al.*, 1992; Crusius *et al.*, 2004; Galbraith *et al.*, 2007; Jaccard *et al.*, 2009]. A freshwater influx could drive an increase in productivity by trapping nutrients in the euphotic zone, shallowing the mixed layer and relieving light limitation, our data do not support or dispute this hypothesis.

2.5.4.1. Bølling-Allerød Laminations

3JPC has two low-density laminated sections separated by a bioturbated interval (Figure 2.5) similar to many Bering Sea and North Pacific Cores [Behl and Kennett, 1996; Cook *et al.*,

2005; Ikehara *et al.*, 2006; Brunelle *et al.*, 2007; Ishizaki *et al.*, 2009; Khim *et al.*, 2011; Schlung *et al.*, 2013].

The BA laminated interval begins at 14.85 ka (BA: 14.7–13 ka, YD: 12.9–11.7 ka NGRIP (North Greenland Ice Core Project) [Rasmussen *et al.*, 2006]) and ends at 12.9 ka with laminations beginning again at 11.5 ka. Laminae deposition at 3JPC during the BA was coeval with lamina [Schlung *et al.*, 2013] and green layers rich in OM, CaCO₃, and biogenic opal seen on Bowers Ridge [Brunelle *et al.*, 2007]. The correspondence between 3JPC laminae deposition and the dating of the BA and YD in NGRIP [Rasmussen *et al.*, 2006], and with other regional cores with laminae [Behl and Kennett, 1996; Davies *et al.*, 2011], is evidence that our age depth model is robust during this period.

During the BA laminated section, there are two bioturbated gaps that last 200 years each, the first beginning at ~14.23 ka and the second at ~13.45 ka. These bioturbated intervals may represent the Older Dryas period, and Inter-Allerød Cold Period (IACP) [Lehman and Keigwin, 1992; Benson *et al.*, 1997; Björck *et al.*, 2003], and are perhaps driven by a decrease in productivity, which rendered oxygen utilization incomplete at depth, and/or better intermediate water ventilation [Mikolajewicz *et al.*, 1997]. This remarkable correspondence may support the hypothesis that there is a teleconnection between Greenland and the Bering Sea [Kuehn *et al.*, 2014]. At the least, the correspondence of our bioturbated gaps to NGRIP cold periods suggests that the large scale change in climate at these times was felt synchronously in Greenland and the Bering Sea.

2.5.4.2. Increased Bølling-Allerød Productivity

Increased productivity marked the BA in the Bering Sea [Cook *et al.*, 2005; Brunelle *et al.*, 2010; Caissie *et al.*, 2010; Schlung *et al.*, 2013; Kuehn *et al.*, 2014], but TOC in 3JPC

decreased by 0.32% from the ED (1.14%), whereas the BA in 51JPC featured its highest sustained TOC (1.35%). This TOC decrease during a time known for high productivity is likely due to decreased terrigenous input separate from marine productivity. OC_{mar} marginally increases during the BA, and OC_{terr} decreases following the initial peak in OC_{terr} during the ED (Figure 2.5). The decrease in 3JPC TOC is likely due to the inundation of the nearby BLB, making the terrigenous material supply more distal due to the increased distance to major river drainage outlets.

Given that MWP 1a occurred after the ED, it would seem that this would have provided an even larger influx to all Bering Sea cores sites. The increased productivity during the BA may have overprinted some of this terrestrial signal, implying that perhaps the ED featured a pulse of terrestrial material absent a spike in productivity.

The $\%N_{\text{org}}$ and $\%TOC$ curves look nearly identical for 3JPC, suggesting that they are similarly influenced by changes in marine and terrestrial inputs (Figure 2.5). Therefore, the decrease in $\%N_{\text{org}}$ appears to be due to a decrease in terrigenous-sourced N_{org} .

In 3JPC, the PB and BA show the greatest variability in PCA, but plot closest to productivity end-members: $\%TOC$, $\%N_{\text{org}}$, silt, Cl and Br. BA XRF data for 3JPC support a more productive, less terrigenous signal with a decrease in Ti, Fe, and K, and an increase in Cl, Br, and to a lesser extent Ca (Figure 2.7). The PB and BA plot together in PCA biplots in all three Bering Sea cores, in every case plotting closer to assumed productivity indicators and far from the terrigenous end-members. This clearly suggests that the PB and BA are best explained by productivity at the time, which likely overrode a terrigenous signal.

The southwestern Bering Sea recorded an increase in productivity during the BA [Brunelle *et al.*, 2007] as recorded by increased $\%silt$, XRF elemental data, and PCA biplots of

our data. The increase in grain size seen in 17JPC supports this increase in productivity, as approximately 40% of the variance in particle size in IODP cores from the Bering slope and Bowers Ridge (U1340, U1341, U1343, and U1344) can be explained by the abundance and preservation of diatom valves, a rough indicator of biogenic opal productivity [Aiello and Ravelo, 2012]. Like 17JPC, U1340 is also from the Bower's Ridge, suggesting that the increase in percent silt in 17JPC is recording an increase in diatoms and/or the size of diatoms, as SST warmed to $\sim 11^{\circ}\text{C}$ during the BA at Bowers Ridge [Schlung *et al.*, 2013].

2.5.4.3. $\delta^{13}\text{C}_{\text{org}}$ and Alaskan Stream Water

In 3JPC, $\delta^{13}\text{C}_{\text{org}}$ remained relatively depleted during the BA (-24.7‰), only slightly enriched relative to 17–10.7 ka (-24.9‰), perhaps indicative of a minor reduction in terrestrial material input, and/or an increase in marine carbon export.

The LGM and ED were relatively enriched in $\delta^{13}\text{C}_{\text{org}}$ at 51JPC (-22.5‰), before depletion ~ 16.5 ka, with $\delta^{13}\text{C}_{\text{org}}$ steady (-21.8‰) from the onset of the BA into the Holocene (Figure 2.16). The stable but enriched values of $\delta^{13}\text{C}_{\text{org}}$, as well as low OC_{terr} and high OC_{mar} at 51JPC suggest that sediment delivery to the core site was fairly constant from the BA into the Holocene. This could have resulted from any combination of the following: increased flux of NPW, increasing distance to land, local submergence of subaerially exposed shelf, reduction of local glaciation, and the decreasing proximity of the major river mouths, like the Kuskokwim and the rivers that empty into Bristol Bay.

The decline in sea ice cover during the BA [Caissie *et al.*, 2010], may have strengthened the BSC, improving nutrient transport from the subsurface to the euphotic zone [Kinder *et al.*, 1975; Johnson *et al.*, 2004; Okkonen *et al.*, 2004] supporting high primary productivity as suggested by Kim *et al.* [2011]. High productivity is supported by elevated %TOC and in PCA

biplots with the BA samples plotting with productivity end-members (Figure 2.8, Figure 2.15, and Figure 2.18).

2.5.4.4. Bølling-Allerød Nitrogen Isotopes

During the BA, $\delta^{15}\text{N}$ in 3JPC increased until peaking by 14 ka (7.9‰), averaging 7.1‰ from 14.7–13.7 ka, where a decrease began that continued into the YD until around 12.5 ka.

The $\delta^{15}\text{N}$ enrichment of 3JPC at the onset of the BA is best explained by the intensification of denitrification and increased nitrate utilization in the Bering Sea [Schlung *et al.*, 2013]. Although the BA has been documented as a high productivity interval in the region [Caissie *et al.*, 2010], associated higher nitrate utilization likely cannot fully explain the increase from 5.7 to 7.1‰. When surface nitrate is entirely utilized, accumulating particulate organic matter (POM) has the isotopic signature of the source nitrate [Sigman *et al.*, 2009], which is ~5–6‰ in the Bering Sea today [Lehmann *et al.*, 2005]. This makes it unlikely that enhanced nitrate utilization produced the elevated BA values without a concurrent change in the $\delta^{15}\text{N}$ of the nitrate source. Under well-oxygenated conditions, settling POM is consumed using oxygen as the electron acceptor. When oxygen becomes scarce, as suggested by laminae deposition during the BA, nitrogen becomes the preferred electron acceptor, and heterotrophic bacteria oxidize OM in order to gain energy via denitrification. During denitrification the bacteria preferentially use ^{15}N -depleted nitrogen, thus enriching the residual $\delta^{15}\text{N}$ values.

During the BA and PB periods, water column suboxia was prevalent, and enabled the deposition of laminae; whether due to elevated productivity, suppressed intermediate water oxygenation, or a combination of the two [Cook *et al.*, 2005; Caissie *et al.*, 2010; Davies *et al.*, 2011; Kim *et al.*, 2011; Schlung *et al.*, 2013]. Under suboxic conditions, denitrification at 3JPC during the BA was coeval with denitrification on Bowers Ridge [Brunelle *et al.*, 2007, 2010;

Schlung et al., 2013]. Our 3JPC BA data (7.9‰) are consistent with other studies that have measured bulk $\delta^{15}\text{N}$ BA peaks of 7.5‰ at 17JPC [*Brunelle et al.*, 2007] and 8.25‰ at IODP site 1340 [*Schlung et al.*, 2013]. The 3JPC record is further evidence of a widespread rise in denitrification from sites around the North Pacific [*Emmer and Thunell*, 2000; *Kienast et al.*, 2002; *Kao et al.*, 2008; *Brunelle et al.*, 2010; *Addison et al.*, 2012; *Schlung et al.*, 2013].

Recent work [*Studer et al.*, 2013] has indicated that bulk $\delta^{15}\text{N}$ in the region could be biased by sponge spicules ($\delta^{15}\text{N}$ ~-11‰), and while this may be the case for our core, the correspondence in $\delta^{15}\text{N}$ changes with climatic intervals and the Bowers Ridge records implies that the overall implications are unchanged, though the absolute magnitude could be affected.

2.5.5. Younger Dryas (12.9 to 11.7 ka)

AMOC is thought to have weakened or ceased altogether during the Younger Dryas cold period [*Broecker et al.*, 1988; *Timmermann and Menviel*, 2009]. The BLB was shrinking in extent, but was still a contiguous east-west landmass at the onset of the YD, with sea level ~65 mbp at the onset of the YD [*Fairbanks*, 1989]. Sea level rise slowed [*Bard et al.*, 2010] as alpine glaciers advanced in Alaska [*Briner et al.*, 2002], marking the YD as an abrupt change from the BA. Sea ice had declined during the BA, but rebounded during the YD [*Jim Kocis* submitted; *Cook et al.* 2005]. Such rapid climatic changes had a pronounced effect on the species assemblages of marine organisms and the overall productivity of the region [*Cook et al.*, 2005; *Gorbarenko et al.*, 2005; *Barron et al.*, 2009].

2.5.5.1. Decreased Younger Dryas Productivity

The YD marked a hiatus in laminae deposition in 3JPC, 51JPC and across the range cited in the BA section [e.g. *Cook et al.*, 2005; *Caissie et al.*, 2010]. This hiatus in laminae is

attributed to an increase in oxygenation due to changes in NPIW ventilation [Kennett and Ingram, 1995; Zheng *et al.*, 2000; Max *et al.*, 2014; Okazaki *et al.*, 2014], primary productivity [Mix *et al.*, 1999; Crusius *et al.*, 2004; Schlung *et al.*, 2013], or a combination of both [Hendy and Pedersen, 2005; Ishizaki *et al.*, 2009; Kim *et al.*, 2011; Gorbarenko *et al.*, 2014]. The massive sediment character during the YD interval is seen as a period of decreased productivity in all three of our Bering Sea cores as recorded by decreased sedimentation rate, decreased TOC and N_{org} , depletion of both $\delta^{15}N$ and $\delta^{13}C_{org}$, and its central but discrete location in the PCA biplots.

The YD is not a prominent feature in sediment cores from Bower's Ridge, where it is identified as an 11 cm thick massive interval in U1340 [Schlung *et al.*, 2013], and a 6 cm thick section in 17JPC, that coincided with a collapse in %biogenic Ba, $CaCO_3$, and opal [Brunelle *et al.*, 2007]. Low sedimentation rates were common during the YD as seen on Bower's Ridge (10 cm/kyr) [Schlung *et al.*, 2013], and 4–5 cm/kyr in 17JPC, as well as in the Gulf of Alaska (9 cm/kyr) [Davies *et al.*, 2011], consistent with fairly stable cold and/or saline surface conditions [Davies *et al.*, 2011].

$\delta^{13}C_{org}$ of 3JPC remained depleted during the YD, with a further slight decrease to -25.1‰, consistent with YD glacier re-advance [Briner *et al.*, 2002], which likely increased the export of terrigenous material through erosion and reworking of proglacial sediments.

Decreased YD productivity in the Bering Sea is recorded in 3JPC by lower TOC (0.95%), low N_{org} (0.095%), and a depletion of $\delta^{15}N$ (-5.73‰), indicative of decreased nitrate utilization and denitrification [Schlung *et al.*, 2013]. 51JPC also featured a TOC decrease (1.15%) during the YD, likely resulting from a reduction in productivity, as there is no net change in OC_{terr} .

PCA biplots for the Bering Sea cores display the YD at or near the center. This implies

that the YD was different from the other time periods, not as productive as the BA or PB, and with less terrestrial input than the ED, but not as biologically dormant as the LGM. In 17JPC this can only be seen for the XRF PCA (Figure 2.15), as the isotope data are too coarse to capture the YD. In 51JPC and 3JPC, the YD plots near the center in both the full-suite and XRF PCA biplots, marking the YD as a unique period of the last deglaciation in the Bering Sea.

The terrigenous elements (Fe, Ti, Rb, and K) in all three Bering Sea cores have high counts during the YD. All three cores increase around 13.5 ka from the low values of the BA, with the biggest increase coming at the onset of the YD. The increase leading into the YD cannot be used as evidence regarding the onset of the YD, but could potentially indicate preconditioning, or a gradual slide into the YD. After terrigenous-related elements peaked during the middle of the YD, a decline brought low counts by the early PB, comparable to values during the BA.

2.5.5.2. Northwest Chukchi Shelf, 24 JPC

Our age depth model for 24JPC indicates that the record begins around 14.3 ka, which is far older than most Chukchi Sea sedimentary records, which are limited to the Holocene [*Darby et al.*, 2009; *Ortiz et al.*, 2009]. The Chukchi Sea was not an ideal location for preservation until the Holocene because of the exposure of the BLB, and the subsequent shallow, transgressive sea in which sediment preservation would have been difficult due to ice scouring [*Hill and Driscoll*, 2010] and sediment re-suspension in its shallow depths [*Reimnitz et al.*, 1998]. There is a peak in sand (18%) from ~14–12.5 ka that we deem to be the transgressive-scour deposit (Figure 2.10). A sample from this interval (~13.18 ka) contained few to common coaly and woody bits, undoubtedly sourced from the BLB [*Flores et al.*, 2004]. Nevertheless, we interpret our record to begin around 14 ka with the caveat that the deepest portion of the record (~14.3–9.2 ka) may

not reach back into the BA or even the YD. Regardless, we have strong age control during the Holocene, the time we are most concerned with in the Chukchi Sea. All further discussion of 24JPC assumes that our age depth model (Figure 2.3) is valid.

Following the transgressive-scour deposit, clay content is high (29%), indicating that the current's velocity over the site was weak [Nelson and Creager, 1977], since the BLB was either not yet sufficiently flooded to open the BS, or just beginning to flood, keeping water exchange over the site to a minimum. If the BLB was flooded or not transporting a significant amount of water over the core site, then sluggish circulation would remain as is hypothesized for the YD [Polyak *et al.*, 2004; Bradley and England, 2008].

The coaly and woody bits found in the transgressive-scour deposit must have originated from the Alaskan side of the BLB [Flores *et al.*, 2004], supporting our analysis that this interval had a near-shore shallow water environment, dominated by input from the BLB. Depleted $\delta^{13}\text{C}_{\text{org}}$ (-24.7‰) provides additional support for the influence of BLB material in the core site, as the depleted value is nearer to the expected terrigenous value for the area (-27‰) than the expected marine value (-21‰) [Naidu *et al.*, 2004; Trefry *et al.*, 2014]. OC_{terr} accounts for over 60% of TOC during the early portion of the record until nearly 8 ka, indicative of BLB-sourced OC in the shallow water, near-shore environment of 24JPC. TOC (0.71%) and N_{org} (0.104%) are low, indicative of low productivity and minimal preservation.

2.5.5.3. Younger Dryas Summary

Our YD Bering Sea data provide additional evidence that productivity decreased during the YD, but also indicates that the YD was a unique period in our record, with lower productivity than the BA or PB, and lower terrestrial material input than the ED, yet was not as biologically quiet as the LGM. The increase in terrestrial end-members in XRF data, without a

corresponding change in $\delta^{13}\text{C}_{\text{org}}$, suggests that the flux of terrigenous material delivered during the YD was different than that of the ED. During the ED, there was considerable flooding of subaerially exposed continental shelves [Davies *et al.*, 2011; Lam *et al.*, 2013], which led to a large influx of material and micronutrients to the Bering Sea. The lack of a significant increase in OC_{terr} with the corresponding terrigenous XRF counts during the YD indicate that glacier readvance likely supplied a major portion of terrestrial material, consistent with the decreased rate of sea level rise during the YD [Bard *et al.*, 2010]. Sediment in the path of glacier readvance during the YD would have largely been limited in OC, with little time to build soil or allow for significant plant growth during the BA, as glaciers retreated. A further source of terrestrial material during the YD could be sea ice, which may have been largely absent during the BA, before rebounding during the YD [Sancetta *et al.*, 1985; Cook *et al.*, 2005]. The YD was a stark transition from the preceding BA warm period and the following PB, as glaciers advanced, sea ice spread, productivity declined, and sedimentation rates fell.

2.5.6. Pre-Boreal Warm Period (11.7 to 10.5 ka)

The pre-Boreal warm period (PB) marked the end of the YD and is the second major laminated interval seen in our Bering Sea cores, as well as the cores cited in the BA section above [e.g. Behl and Kennett, 1996; Cook *et al.*, 2005; Caissie *et al.*, 2010; Schlung *et al.*, 2013]. Accompanying these laminations was another increase in productivity [Crusius *et al.*, 2004; Davies *et al.*, 2011; Schlung *et al.*, 2013], and a second abrupt freshening and/or warming event recorded in planktonic foraminifer $\delta^{18}\text{O}$ of the Bering shelf-slope at 11.65 ka [Cook *et al.*, 2005].

Around the end of the YD and onset of the early Holocene (PB), the BLB likely ceased to exist as a contiguous landmass connecting Chukotka and Alaska [Elias *et al.*, 1996; Keigwin *et al.*, 2006], with sea level at the time ~50 m below modern [Fairbanks, 1989], equivalent to the

sill height of the BS [Coachman *et al.*, 1975]. For the first time since ~75 ka the BLB connection of Beringia was severed, and the BS began to mediate water interaction between the Bering and Chukchi Seas. The laminated interval of the PB was indicative of an ameliorating climate with elevated productivity in the Bering Sea [Khim *et al.*, 2011].

2.5.6.1. Increased Pre-Boreal Productivity

The increase in productivity is marked by a second laminated interval in 3JPC, and is recorded as increased TOC (1.4%) comparable to the ED (Figure 2.5), and to a lesser increase in 51JPC (0.9%) and 24JPC (1.4%). N_{org} was high during the PB in 3JPC (0.129%) and $\delta^{15}N$ increased to 6.15‰ along with C/N ratios (12.5). The increase in $\delta^{15}N$ was likely again due to an increase in local denitrification, driven by elevated productivity and the return of suboxic conditions, as seen during the BA [Cook *et al.*, 2005; Brunelle *et al.*, 2007; Schlung *et al.*, 2013]. The initial increase in TOC of 24JPC seen during the PB (Figure 2.9) may reflect the first incursion of nutrient rich NPW, with too small a quantity to affect many other proxies or stimulate a major TOC increase. Though both marine and terrigenous components of TOC increased at 3JPC, the increase of OC_{terr} was most dramatic, increasing from ~0.6 to 1% after the YD. The OC_{terr} peak may have been derived in part from meltwater pulse 1B (MWP-1b) [Bard *et al.*, 2010], which occurred ~11.3 ka [Fairbanks, 1989; Bard *et al.*, 1990, 1993], and could have further inundated coastal regions.

MWP-1B increased eustatic sea level by ~15 m over ~300 years (11.4–11.1 ka), and was likely primarily sourced from Antarctica [Domack *et al.*, 2005; Peltier and Fairbanks, 2006]. MWP-1B coincides with the flooding window for the BS (12–11 ka) [Elias *et al.*, 1996; Keigwin *et al.*, 2006], and certainly would have increased the rate of inundation.

The submergence of Unimak Pass leading into the PB allowed ASW to contribute to sea ice melt, increasing productivity by relieving light limitation [Caissie *et al.*, 2010]. Significant increase in ASW at 51JPC was marked by the proliferation of *Neodenticula seminae* ~12 ka, a Pacific Water indicator species [Caissie *et al.*, 2010], which supported elevated PB productivity marked by increased TOC (Figure 2.16) and PB PCA clustering (Figure 2.18).

PCA biplots show the PB and BA plotting together in all three Bering Sea cores. Like the BA, PB populations plot closest to the productivity end-members, but unlike the BA, there are two populations of PB sediment in 51JPC and 17JPC XRF data PCA. While both the PB and BA feature widely dispersed samples, there are not two distinct populations for the BA. These two populations exist only in the XRF PCA as there are too few data points in the full PCA to distinguish two populations. One possibility is that the samples represent light and dark lamina, but given the width of the lamina, <1 to 2 mm, the moving average applied to the data and resolution of XRF data (1000 μ m) should not allow for individual lamina to be represented in PCA. More likely, there was a change of conditions during the PB. In 51JPC, we have no sediment younger than 10.5 ka, but for 17JPC XRF data, the earlier PB interval (11.7–11 ka) of the two PB populations (Figure 2.15, pink diamonds) plots just above the YD data, and the younger population (11–10.5 ka) (Figure 2.15, pink dots) plots with the Holocene data, indicating that Holocene conditions at 17JPC began ~11 ka, following the flooding of the BS [Elias *et al.*, 1996; Keigwin *et al.*, 2006].

Loess deposition recorded south of 17JPC on the Detroit Seamount in GGC-37 was highest during the LGM/ED, and declined with the flooding of the Bering Strait at 11 ka, suggesting that subaerial delivery of exposed Bering Shelf sediments was the dominant contributor of loess-like material to the core [Lam *et al.*, 2013].

2.5.7. Holocene (10.5 to 2.5 ka)

By ~10 ka, the remainder of the BLB was largely inundated, with sea level at the time at about 20 m below modern [Hopkins, 1979; Fairbanks, 1989]. While the climate has varied during the Holocene, variability has generally been weaker in magnitude than during the last deglaciation [Mayewski *et al.*, 2004]. NADW production has fluctuated [Oppo *et al.*, 2003] during the Holocene, yet there hasn't been a weakening or shutdown to the extent seen during deglaciation [Keigwin *et al.*, 1991; Thornalley *et al.*, 2011]. Holocene ventilation of the North Pacific has been weak, as North Pacific ventilation is stronger in cold periods [Schlung *et al.*, 2013], whereas North Atlantic ventilation increased during the BA and Holocene (warm periods) [Robinson, 2005; Thornalley *et al.*, 2011].

2.5.7.1. Holocene Changes in the Chukchi Sea, 24JPC

TOC in 24JPC increases to ~1% from 11–8.8 ka before collapsing to 0.85% from 8.5–8.2 ka (Figure 2.9). This interval of low TOC is matched by decreases in %N_{org} (0.109%), $\delta^{15}\text{N}$ (6.02‰), and a rapid increase in clay from 23 to 29% (7 to 12% in the <2 μm clay), and features the biggest assemblage of agglutinated forams with *Ammo-Baculoides* counted as common, and centric diatoms as rare. This anomaly corresponds with a period of major Arctic oceanographic change with a potential shift in the Transpolar Drift to the east and the onset of flow through the Canadian Arctic Archipelago [Dyke *et al.*, 1997]. The 8.2 ka event lasted ~150 years as recorded in Greenland ice cores [Alley *et al.*, 1997; Thomas *et al.*, 2007, p.2]. It's thought to have resulted from the largest discharge to the North Atlantic of freshwater from Lake Agassiz and the melting of the Laurentide Ice Sheet [Wagner *et al.*, 2013]. The flux of fresh water is presumed to have weakened AMOC [LeGrande and Schmidt, 2008], and thus the advection of warm water

to the North Atlantic [Broecker, 1991]. In our case, a pulse of freshwater to the North Atlantic could have caused a weakening and/or reversal in flow through the BS, as net BS throughflow is controlled by the sea surface gradient between the North Pacific and North Atlantic [Coachman and Aagaard, 1966; Stigebrandt, 1984; Woodgate *et al.*, 2005]. The decrease in TOC, N_{org} , $\delta^{15}N$, and the increase in clay content could be explained by a weakening or reversal of BS throughflow which reduced NPW at the site. Less NPW would result in less nutrients to the Chukchi Sea [Walsh *et al.*, 1989; Martin and Drucker, 1997], and a decrease in overall current velocity, allowing for deposition of clay. However, diatoms appeared less abundant during this period, perhaps due to the large amount of forams, and the decrease in silt at this time 72 to 65% could mean that the clay increase is due to a decrease in silt-sized diatoms, independent of current velocity. The relative abundance of agglutinated forams, combined with reduced diatom abundance, could have resulted from sea ice coverage change [Cronin *et al.*, 2008], independent of, or resulting from, a weakening of BS throughflow.

This 8.5–8.3 ka anomaly in a trend of rising TOC and decreasing clay content ends abruptly and TOC rebounds by 8 ka to a plateau around 1.36% from 8–5.5 ka (7.92‰, 0.169%). With the increase in TOC came a decrease in clay content, which fell to 13% from 7.8 ka in the top of the record. The virtual disappearance (2%) of clay content $<2 \mu m$ in the core, and reduction of total clay content is likely due to an increase in cross-shelf current velocities with increased BS throughflow, considering that modern Chukchi shelf current velocities are sufficient to transport silt and clay sized particles [McManus *et al.*, 2004], which explains why median GS increases with steady silt/sand/clay contents during the last few thousand years of the record. The decrease in clay and increase in TOC and median GS roughly fits with the dramatic decrease in Chukchi sedimentation rates ~ 7 ka [Keigwin *et al.*, 2006; Hill and Driscoll, 2008].

OC_{mar} was a minor component in the early portion of the record, increasing sharply at 8 ka, and by 7 ka, OC_{mar} had surpassed OC_{terr} as the dominant component of TOC for the first time in the record (Figure 2.9).

Once TOC recovered following the anomalous interval, $\delta^{13}C_{\text{org}}$ began to become enriched, and TOC continued to increase throughout the record, as did silt, N_{org} , and OC_{mar} . The sharp increase in OC_{mar} and enrichment of $\delta^{13}C_{\text{org}}$ are indicative of a marine influence that suggests increased nutrient rich NPW advection over the site. This increase in NPW brought nutrients as recorded by increased TOC, N_{org} , and OC_{mar} , which supported increased productivity, and increased diatom abundance as seen in our visual analysis and increased %silt [Aiello and Ravelo, 2012]. The increase in $\delta^{15}N$ at this time may be due to increased nutrient utilization, but the nitrogen isotope record of 24JPC appears convoluted. Based upon the decrease in clay, and coeval increases in TOC, OC_{mar} , N_{org} , and enrichment of $\delta^{13}C_{\text{org}}$, we conclude that modern circulation was established shortly after 8 ka (Figure 2.9, EMC).

Sancetta [1979] suggested that modern physical oceanography was established in the North Pacific by 8 ka but does not elaborate further. Ortiz et al. [2009] examined Pacific inflow to the Chukchi Sea using chlorite and muscovite as Pacific Water tracers, but had poor age control older than 8 ka in JPC6. They observed an increase in NPW in the Chukchi from 6–3.6 ka. Early Holocene circulation may have been established ~11 ka at in the North Pacific (17JPC) as suggested in the PB section, but in order for true modern physical oceanography to be established in the North Pacific, and the Bering/Chukchi Region, flow through the Bering Strait must have been of a comparable magnitude and direction to modern circulation. Our Chukchi Sea data demonstrates that flow through the Bering Strait is too important to the region, in terms of circulation and water mass exchange [Hu and Meehl, 2005; Hu et al., 2014], for true modern

circulation to be established prior to 8 ka.

The full suite PCA for 24JPC (Figure 2.12) highlights the stark contrast between sediment from 9–8 ka (cyan diamonds) and sediment from 8–2.5 ka (cyan dots). Sediment older than 8 ka is most strongly associated with terrigenous end-members, whereas sediment younger than 8 ka is seen to be negatively associated with PC1, plotting with the productivity end-members.

Though change progressed after 8 ka, with continued increase of TOC, N_{org}, and OC_{mar} as well as $\delta^{13}\text{C}_{\text{org}}$ depletion, there was a clear transition recorded in 24JPC around 8 ka. We propose that this transition was the establishment of modern circulation, which possibly followed a period of weakened or reversed BS throughflow coeval with the 8.2 ka event. By 2.5 ka, 24JPC resembles a marine dominated site with depleted $\delta^{13}\text{C}_{\text{org}}$, low terrestrial elemental abundance, and PCA samples aligned with productivity end-members.

2.5.7.2. Bering Sea Sandy Core-top, 3JPC

Though there is variability, sand averages 16% through the BA and YD in 3JPC and into the PB before a major increase at 10.8 ka to >50%. The sediment in this interval in the nearby IODP site, U1345, is composed of quartz, feldspar, rock fragments and some volcanoclastic material [*Expedition 323 Scientists et al.*, 2011]. The sandy texture may be due to a decrease in sedimentation rate, and therefore a decrease in dilution by clay and marine biogenics, as both clay (0.3%), TOC (0.5%) and OC_{terr} (<0.1%) fall to the lowest values of the record. The near-cessation of terrigenous organic input is reflected in the dramatic change in $\delta^{13}\text{C}_{\text{org}}$ (-22‰) to open marine values [*Naidu et al.*, 2000], but C/N ratios increase dramatically with the onset of the sand peak. The peak in sand content is seen by a major increase in Si, Sr and Zr (Figure 2.7). The Holocene in 3JPC is a clear anomaly with the Holocene sample population plotting closest

to sand in the full suite PCA (Figure 2.8). Based on the apparent lithology and lack of OC_{terr} while OC_{mar} becomes the dominant TOC component for the first time since the LGM, it may be that the flooding of the BLB and opening of the BS is responsible for this major increase in sand.

Prior to the flooding of the BLB, it is feasible that the Yukon and/or Kuskokwim Rivers had a major impact on the Bering Sea. Given the importance of the sediment of the Yukon to the Chukchi and northern Bering Sea today [McManus *et al.*, 1974; Nelson and Creager, 1977], it is possible that if the Yukon were to discharge in part or in full to the south, a portion of its substantial sedimentary load [Lisitsyn, 1966; Eberl, 2004] could have remained in the southern Bering Sea, and would have been transported to 3JPC by the BSC. When the BS was reopened via flooding between 12–11 ka [Keigwin *et al.*, 2006], the direction of BS throughflow is unknown, but if flow were to the north as is the case today [Coachman and Aagaard, 1966], then the Yukon sediment would be transported directly north, removing Yukon material from the sedimentary budget of the Bering shelf slope and 3JPC.

Alternatively, with flow strengthened to the north over the Bering Sea, the BSC could have increased in strength with the increased northward flow velocity, which could have prevented deposition of fine grain terrestrial material, making the top of core 3JPC a contourite [Hans Nelson *et al.*, 1993].

2.6. Conclusions

Beringia and the surrounding seas experienced not only rapid climatic change during the last deglaciation, but also major physical change as the extensive Arctic continental shelves flooded and the Bering Strait was re-opened. The Bering and Chukchi Seas clearly capture local change, but also record changes seen across the North Pacific and in Greenland with remarkably consistent timing [Kuehn *et al.*, 2014].

3JPC captures a changing environment along the productive Bering shelf slope region, where a relatively biologically dormant marine LGM environment changed into a terrestrially dominated but productive site during the early deglacial through the PB. The early Holocene featured a return to marine dominated conditions, with little biogenic sedimentation, but abundant sand. Sedimentologic and geochemical data from 3JPC potentially indicate changing influence of the Yukon and other major rivers to the southern Bering Sea through the deglaciation. Previously hypothesized North Pacific denitrification during the BA and PB is supported by bulk $\delta^{15}\text{N}$ in 3JPC, further supporting the concept of large regional changes in productivity, and water column ventilation through the deglaciation [Kao *et al.*, 2008; Max *et al.*, 2014]. All three of the Bering Sea cores capture the transition from sediment dominated by terrigenous influx to marine productivity, as seen in the PCA biplots, which indicate that while some of the climatic intervals were similar, each featured a unique depositional environment. Though more in depth statistical analysis would be valuable, our study demonstrates that PCA is a valuable tool for studies with many discrete proxies.

24JPC in the Chukchi Sea captures the establishment of modern circulation through the Bering Strait ~8 ka, shortly after the hypothesized shift of the Transpolar Drift, and the onset of flow through the Canadian Arctic Archipelago. Our data suggest that the establishment of modern oceanography followed an anomaly seen in TOC, N_{org} , $\delta^{15}\text{N}$, and clay content, from 8.5-8.2 ka, that may have represented a weakening or reversal in flow direction associated with the 8.2 ka event.

CHAPTER 3

FUTURE PERSPECTIVES

This thesis presents the results of a wide variety of sedimentological, geochemical, and isotopic data from a suite of four cores collected from the Bering and Chukchi Seas. We used our results to investigate circulation, productivity, and sediment delivery conditions during the last deglaciation. This project advanced our understanding of the establishment of modern circulation through the Bering Strait, and has further distinguished the differences in sediment delivery and productivity between different climatic periods of the last deglaciation.

The primary results of the thesis were fully detailed in Chapter Two, and the remainder of Chapter Three focuses on what we envision as valuable work going forward; lines of investigation that we believe would improve upon this study and other studies of the region.

3.1 Reversal of Flow through the Bering Strait?

We were able to draw interesting conclusions from the 24JPC sedimentary record, particularly the establishment of modern circulation ~8 ka. The anomalous interval from 8.5-8.2 ka in our record is also intriguing. It features a very rapid sedimentation rate (~200 cm/kyr), with low TOC and N_{org} , along with depleted $\delta^{15}N$ and high clay content. We believe that this could be evidence for a reversal of flow through the Bering Strait occurred coeval to the 8.2 ka event. In order to better understand, and to provide corroborating evidence that this event was a widespread phenomenon, other Arctic cores that observe similar change must be found. If there was indeed a weakening of AMOC resulting from buoyancy forcing over the North Atlantic,

then it stands to reason that flow would have reversed through the BS as shown in modeling simulations [De Boer and Nof, 2004; Hu and Meehl, 2005; Hu et al., 2007, 2012a, 2012b, 2014].

The Bering Sea cores did not provide evidence for or against this reversal of flow theory, as the Holocene section of 3JPC did not have enough planktonic foraminifera to allow dating [Cook et al., 2005], and our selected sections from the three Bering Sea cores did not contain sediment younger than 8 ka. If there were a reversal of flow, even if only for a short period, it should show up in some records from the Bering Sea, but given the distance from the BS of the Bering shelf slope (no long cores exist from the Bering Shelf north of the shelf slope), the effect may have been minimal, and not easy to detect given the low sedimentation rates at the time. Nevertheless, it would be very interesting to have sedimentologic evidence that corroborates reversal of flow for periods of AMOC shutdown/weakening that are manifest in modeling simulations [Hu et al., 2014]. If the Bering Strait can indeed function like an "exhaust valve" for North Atlantic freshwater anomalies [De Boer and Nof, 2004], this has major implications for interpretation of Quaternary paleoclimate records. If the Bering Strait is capable of dispersing freshwater anomalies, then potentially the short duration of the 8.2 ka event (150 yrs) [Alley et al., 1997; Thomas et al., 2007] in comparison to the YD (~1200 yrs [Alley et al., 1997; Rasmussen et al., 2006]) is a direct result of having an open BS during the 8.2 ka event.

3.2 Reservoir Ages

The reservoir age used in a paleoclimate study is very important, and for consistency within our study and with other published research from the area, we used a single reservoir age for all four cores. However, the Chukchi Sea in particular lacks a well defined reservoir age [Polyak et al., 2007], which is not surprising given the magnitude of changes experienced by the Bering Strait and Chukchi Sea since the last deglaciation. Marine reservoir ages in Arctic waters

are poorly defined, especially for deglaciation [*Björck et al.*, 2003; *Eiríksson et al.*, 2004]. Given that most Chukchi cores only cover the Holocene [*Ortiz et al.*, 2009], a better constrained reservoir age for the Chukchi Sea over the Holocene would be extremely valuable, and fortunately is under way (personal correspondence, Leonid Polyak, Ohio State University). Ortiz et al [2009] examined Pacific inflow to the Chukchi Sea using chlorite and muscovite as Pacific Water tracers, but had poor age control older than 8 ka in JPC6. They observed an increase in NPW in the Chukchi from 6–3.6 ka.

Ideally we would use a network of well-dated cores that could be correlated by other proxies, like carbon isotopes, to obtain a best estimate of the Holocene/deglacial Chukchi reservoir age(s). This would give us better confidence in attributing the 8.5–8.2 ka anomaly to the 8.2 ka event.

The Bering Sea cores have datable planktonic material through the last deglaciation, but dating the onset of deglaciation has proven difficult. Work is ongoing (personal correspondence, Mea Cook, Williams College) to examine the changes around the deglaciation. In core 3JPC, we have no date near the onset of deglaciation but if we had a date, the peak in TOC and other proxies would likely be moved earlier, as the period should have seen an increase in sedimentation rate given the increased TOC and terrestrial input. Ongoing work by Mea Cook in core U1345 near 3JPC, shows planktonic and benthic foraminifera ^{14}C ages converging during H1 (our ED). Clearly strange things were happening to ventilation, with convection in the Northern Bering Sea eliminating the age difference between the planktonic and benthic community. Understanding what happened at this interval and resolving the reservoir effects during this time would allow us to assign a date to deglaciation as recorded in the Bering Sea. This would be a valuable comparison to oxygen isotope records from marine sediment cores

[Cook *et al.*, 2005; Caissie *et al.*, 2010; Davies *et al.*, 2011], and glacier landform dating [Gualtieri *et al.*, 2000; Briner and Kaufman, 2008].

3.3 Bering Strait Flooding and Isostatic Sea Level

There has been no local sea level reconstruction for the Beringia region. Isostatic rebound in the area is thought to have been small, but no sea level or flooding history study of the BLB has ever calculated isostatic rebound, and while thought to be small (<10 m) [Keigwin *et al.*, 2006], given the depth of the BS (50 m), the ~10 m isostatic rebound could have influenced the flooding chronology of the BLB. Dating the initial flooding of the BLB is important, but of equal value is constraining the time at which the water depth over the BLB allowed for significant volume transport, when water mass exchange could occur between the Bering and Chukchi Seas. Establishing control on isostatic rebound, and better constraining the sea level history of the Bering Strait would be valuable, especially if both the timing and magnitude of isostatic rebound could be constrained. If the land around the Bering Strait was at all depressed by ice in the region, this could have allowed for earlier flooding of the Bering Strait, as suggested by England and Furze [England and Furze, 2008]. Lev Tarasov (personal correspondence, Memorial University of Newfoundland) has conducted glacial isostatic adjustment for the Bering Strait. His calculations show an offset between Barbados [Fairbanks, 1989] and the BS of ~15 m during the LGM, but the BS matches Barbados sea level during the 13–12 ka interval proximal to BLB flooding. Though these calculations did not include rotational effects (which at most would be a few meters), but support the Fairbanks [1989] data, which supports the Keigwin *et al.* [2006] flooding window (12–11 ka), which we have used in this study.

3.4. Biogenic Silica

In our study we used TOC [Hendy and Pedersen, 2005], N_{org} , and estimated %OC_{mar} as proxies for productivity. Br and Cl proved to be related to OM-rich sediments as well. While our methods for determining productivity seem robust, the extent to which diatoms compose sediments in the Bering and Chukchi Seas [Takahashi *et al.*, 2000] make biogenic silica (opal) a valuable productivity proxy. In addition, organic carbon flux is in part derived from siliceous rather than calcareous plankton, so differences in OC flux can largely be explained by differences in opal flux [Takahashi *et al.*, 2000]. Clearly opal would be valuable as corroborating evidence in productivity reconstructions, and give a more complete representation of biogenic mass flux, irrespective of source species [Takahashi *et al.*, 2000].

Detailed diatom assemblage work as was done by Caissie *et al.* [2011] for 51JPC would greatly benefit the interpretations of this thesis, and better constrain changes in productivity and environmental conditions during the deglaciation.

In 3JPC, there was a drop in TOC from the early deglacial to the Bølling-Allerød warm period, that is generally associated with elevated Bering Sea productivity [Brunelle *et al.*, 2007]. We interpreted the TOC decrease to be a reduction in terrestrial organic carbon, but having opal flux data would allow us to better test this hypothesis.

3.5 PCA in Paleoclimate Studies

Principal component analysis is a valuable tool, good for finding strong associations and clusters within a dataset. We used PCA to better define the primary factors influencing our sediment, which for the most part were terrigenous and biogenic (productivity). At times there

were other factors that controlled the data; like sand for some of the Holocene samples (Figure 2.8) or tephra units in the Umnak Plateau core (Figure 2.18).

Our study did not feature the detailed analysis of other studies from the region that have looked at diatom assemblage change as climate/physical change indicators [Caissie *et al.*, 2010], but instead utilized a wide variety of sedimentological, geochemical, and isotopic data. PCA is a valuable tool for distinguishing controlling factors, and should be considered for paleoclimate studies that either have a number of different proxies, or can incorporate different proxies from past studies in the same, or proximal cores. For example, PCA may be able to provide further evidence for the factors that control diatom assemblages. Caissie *et al.* [2010] collected data on diatom assemblages, and reconstructed SSTs using Uk'37. Combining diatom assemblage data with SSTs and other proxies like $\delta^{18}\text{O}$, $\delta^{13}\text{C}$, and %TOC could elucidate controlling factors behind diatom assemblage change, and better constrain the paleoenvironment of the time. PCA is a valuable tool that has the potential to improve our ability to understand and interpret large datasets of discrete data.

3.6. Summary

The Bering and Chukchi Seas are productive marine environments that play a major role in both ecosystem health and fishery economics. The Bering Sea is characterized by high surface-water productivity [Grebmeier *et al.*, 1988; Springer *et al.*, 1996] and has a great potential to drawdown atmospheric CO_2 by acting as a biological pump [Kaltin and Anderson, 2005]. Arctic and subarctic regions are shaped by processes involving sea ice and continental ice, the formation of dense oxygenated deep waters, and some of the most productive ecosystems in the world; all of which are very sensitive to climate change [Comiso *et al.*, 2008; Grebmeier *et al.*, 2010]. Understanding how the Arctic has responded to major climate change in the recent

past, is possibly our best analogue to modern climate change that has already begun to reshape the Arctic physically through ice loss and sea ice decline [*Tang et al.*, 2013; *Snape and Forster*, 2014], and the in terms of the food web [*Grebmeier et al.*, 2010].

APPENDIX

AUXILIARY PRINCIPAL COMPONENT FIGURES

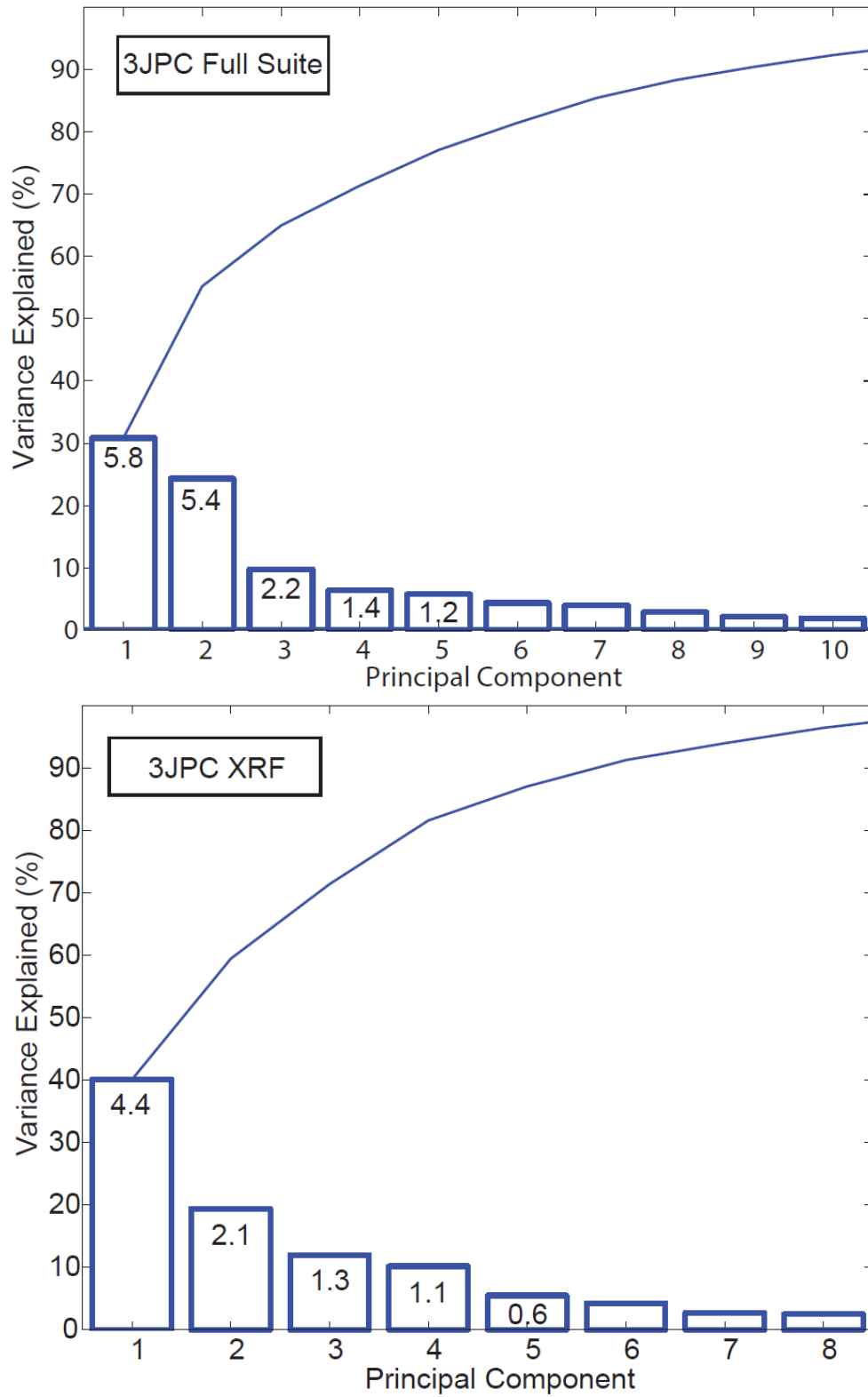


Figure A.19. 3JPC percent variance explained and eigenvalues for each principal component for both full suite and XRF PCAs. Eigenvalues are listed within each PC box.

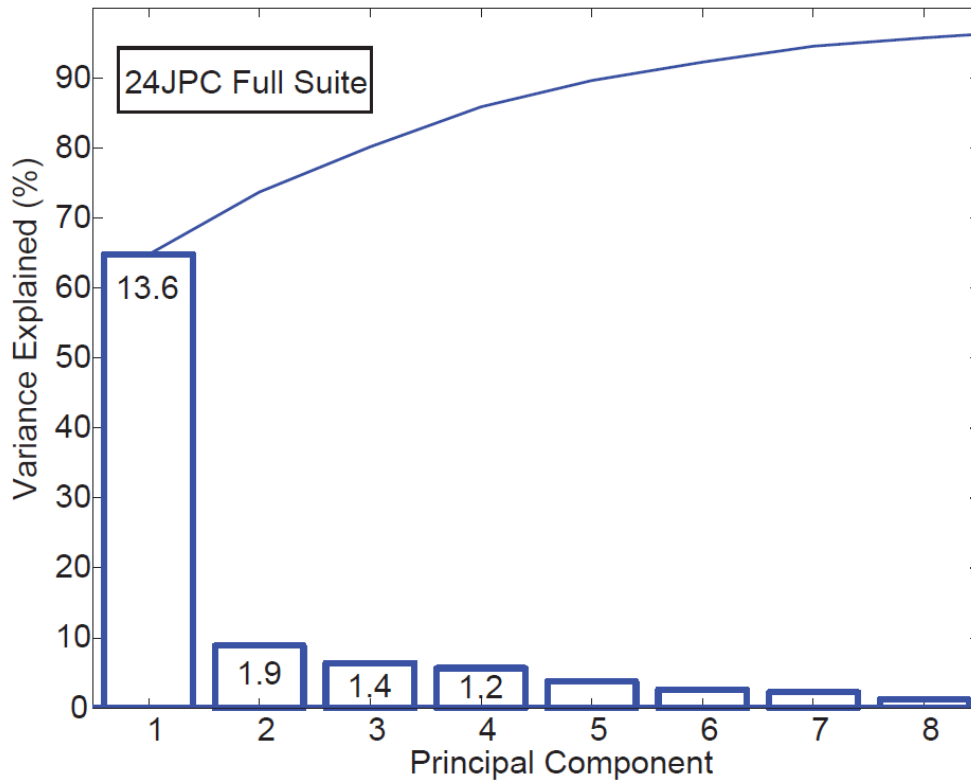
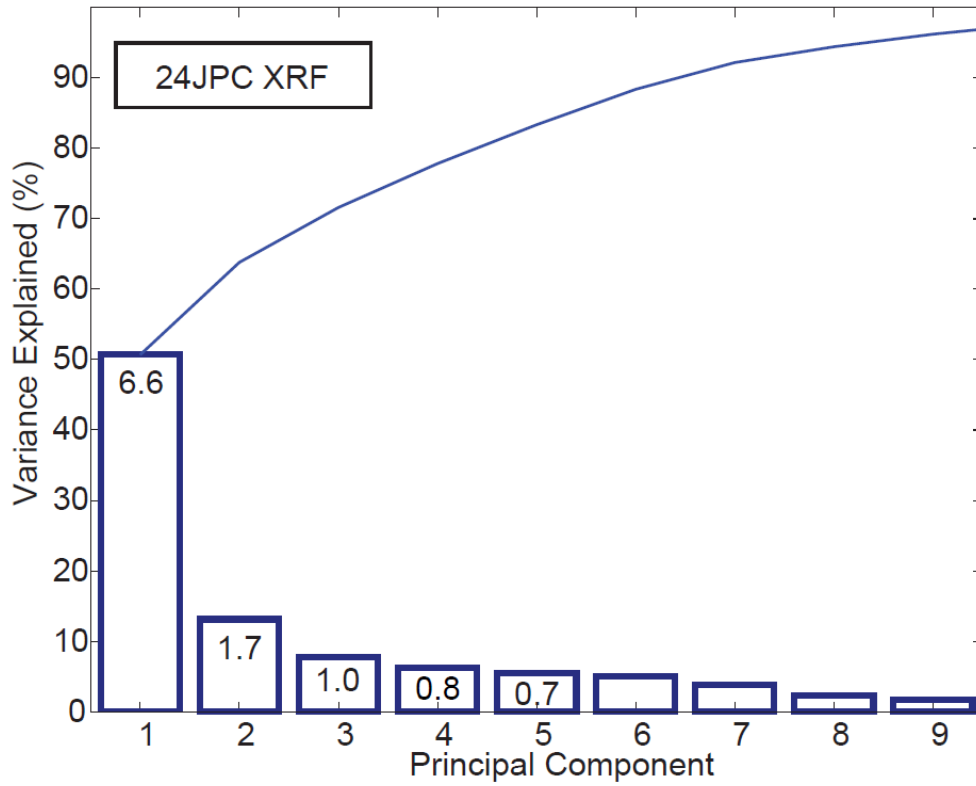


Figure A.20. 24JPC percent variance explained and eigenvalues for each principal component for both full suite and XRF PCAs. Eigenvalues are listed within each PC box.

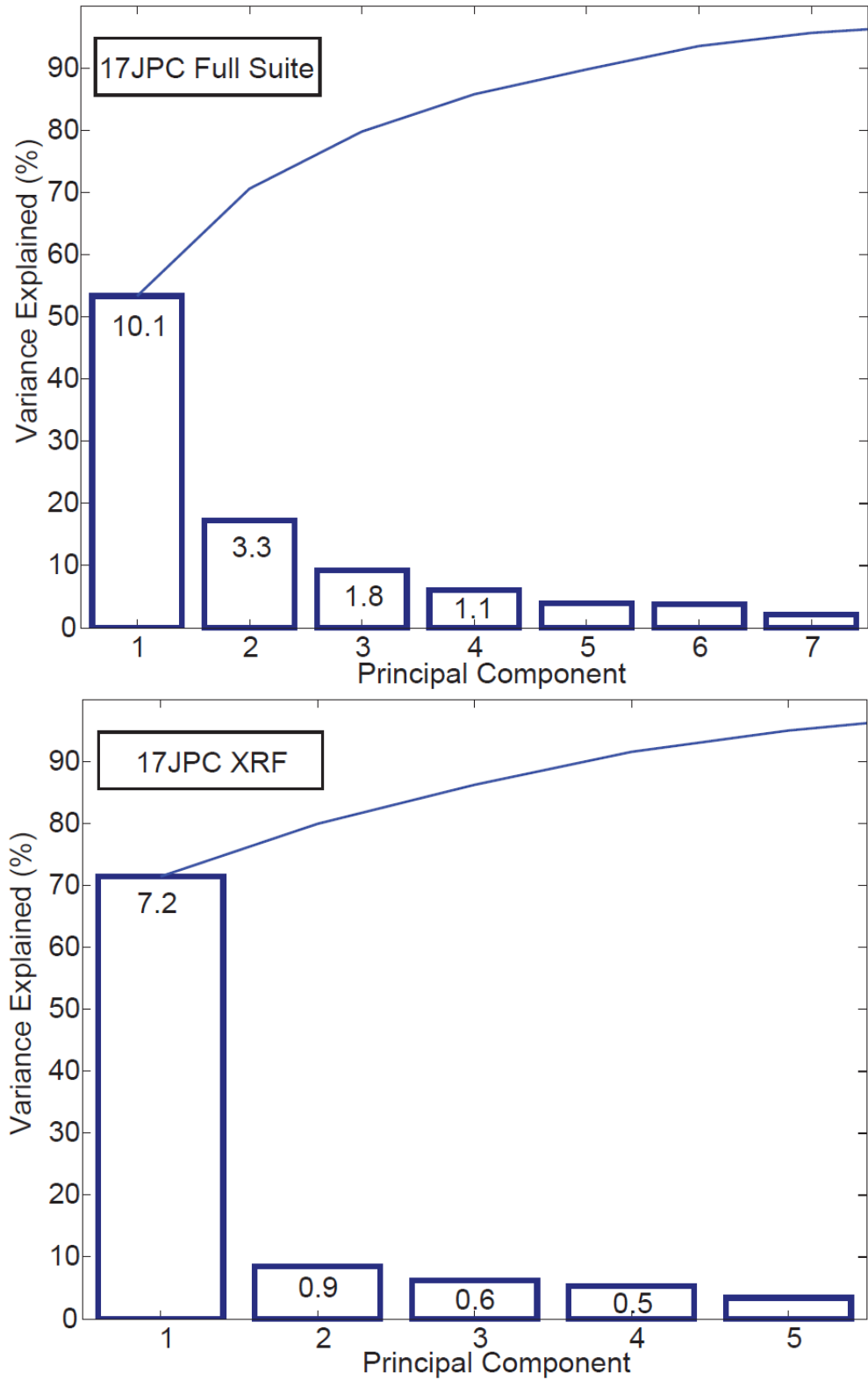


Figure A.21. 17JPC percent variance explained and eigenvalues for each principal component for both full suite and XRF PCAs. Eigenvalues are listed within each PC box.

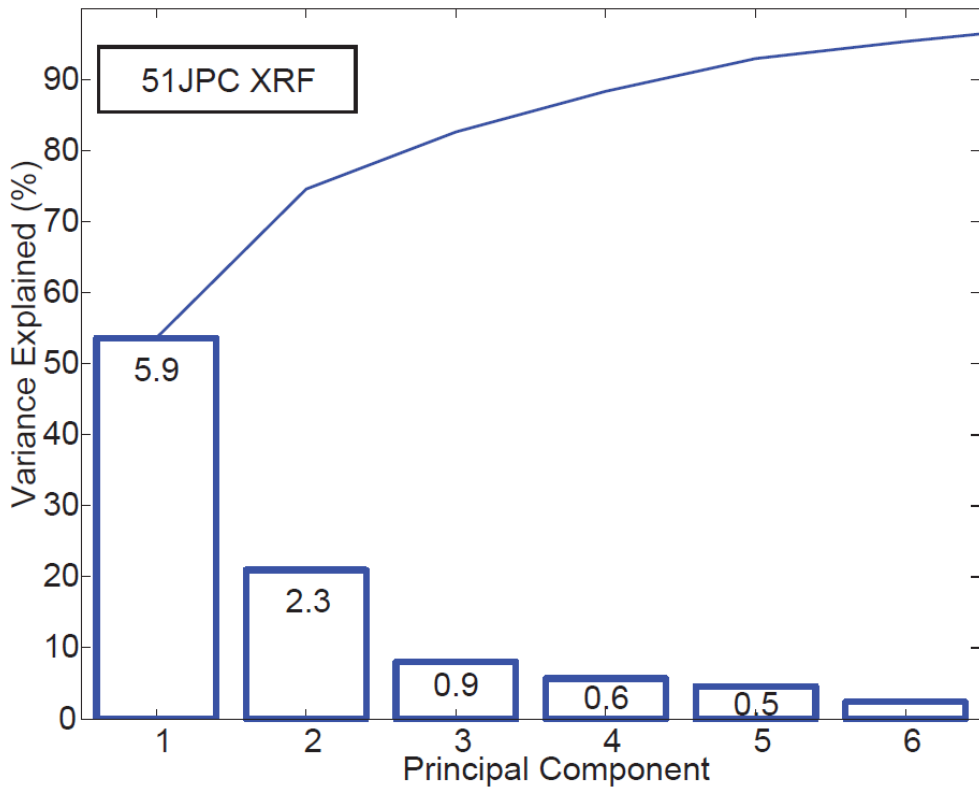
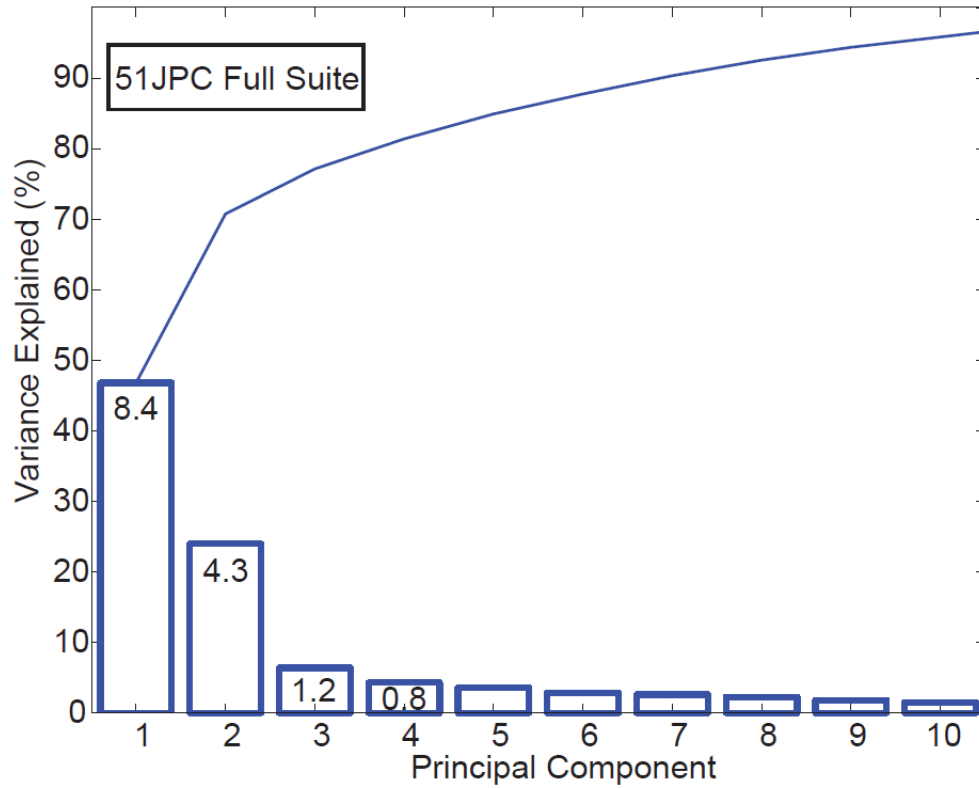


Figure A.22. 51JPC percent variance explained and eigenvalues for each principal component for both full suite and XRF PCAs. Eigenvalues are listed within each PC box.

REFERENCES

- Aagaard, K., and E. C. Carmack (1989), The role of sea ice and other fresh water in the Arctic circulation, *J. Geophys. Res. Oceans 1978–2012*, 94(C10), 14485–14498.
- Aagaard, K., and E. C. Carmack (1994), The Arctic Ocean and Climate: A Perspective, in *The Polar Oceans and Their Role in Shaping the Global Environment*, pp. 5–20, American Geophysical Union.
- Aagaard, K., T. J. Weingartner, S. L. Danielson, R. A. Woodgate, G. C. Johnson, and T. E. Whitledge (2006), Some controls on flow and salinity in Bering Strait, *Geophys. Res. Lett.*, 33(19), doi:10.1029/2006GL026612.
- Addison, J. A., B. P. Finney, W. E. Dean, M. H. Davies, A. C. Mix, J. S. Stoner, and J. M. Jaeger (2012), Productivity and sedimentary $\delta^{15}\text{N}$ variability for the last 17,000 years along the northern Gulf of Alaska continental slope: Past Gulf of Alaska Productivity, *Paleoceanography*, 27(1), doi:10.1029/2011PA002161.
- Ahlnäs, K., and G. Garrison (1984), Satellite and oceanographic observations of the warm coastal current in the Chukchi Sea, *Arctic*, 244–254.
- Aiello, I. W., and A. C. Ravelo (2012), Evolution of marine sedimentation in the Bering Sea since the Pliocene, *Geosphere*, 8(6), 1231–1253.
- Alfultis, M. A., and S. Martin (1987), Satellite passive microwave studies of the Sea of Okhotsk ice cover and its relation to oceanic processes, 1978–1982, *J. Geophys. Res. Oceans 1978–2012*, 92(C12), 13013–13028.
- Alley, R. B., P. A. Mayewski, T. Sowers, M. Stuiver, K. C. Taylor, and P. U. Clark (1997), Holocene climatic instability: A prominent, widespread event 8200 yr ago, *Geology*, 25(6), 483.
- Andrews, J. T., A. S. Dyke, K. Tedesco, and J. W. White (1993), Meltwater along the Arctic margin of the Laurentide Ice Sheet (8–12 ka) : Stable isotopic evidence and implications for past salinity anomalies, *Geology*, 21(10), 881.
- Bard, E., B. Hamelin, and R. G. Fairbanks (1990), U-Th ages obtained by mass spectrometry in corals from Barbados: sea level during the past 130,000 years, *Nature*, 346(6283), 456–458.
- Bard, E., M. Arnold, R. G. Fairbanks, and B. Hamelin (1993), ^{230}Th ^{234}U and ^{14}C Ages Obtained by Mass Spectrometry on Corals, *Radiocarbon*, 35(1), 191–199.
- Bard, E., B. Hamelin, and D. Delanghe-Sabatier (2010), Deglacial Meltwater Pulse 1B and Younger Dryas Sea Levels Revisited with Boreholes at Tahiti, *Science*, 327(5970), 1235–1237, doi:10.1126/science.1180557.

- Barron, J. A., D. Bukry, and W. E. Dean (2005), Paleooceanographic history of the Guaymas Basin, Gulf of California, during the past 15,000 years based on diatoms, silicoflagellates, and biogenic sediments, *Mar. Micropaleontol.*, 56(3-4), 81–102, doi:10.1016/j.marmicro.2005.04.001.
- Barron, J. A., D. Bukry, W. E. Dean, J. A. Addison, and B. Finney (2009), Paleooceanography of the Gulf of Alaska during the past 15,000 years: Results from diatoms, silicoflagellates, and geochemistry, *Mar. Micropaleontol.*, 72(3-4), 176–195, doi:10.1016/j.marmicro.2009.04.006.
- Behl, R. J., and J. P. Kennett (1996), Brief interstadial events in the Santa Barbara basin, NE Pacific, during the past 60 kyr, *Nature*, 379, 243–246.
- Benson, L., J. Burdett, S. Lund, M. Kashgarian, and S. Mensing (1997), Nearly synchronous climate change in the Northern Hemisphere during the last glacial termination, *Nature*, 388(6639), 263–265.
- Berger, A., and M.-F. Loutre (1991), Insolation values for the climate of the last 10 million years, *Quat. Sci. Rev.*, 10(4), 297–317.
- Björck, S., N. Koç, and G. Skog (2003), Consistently large marine reservoir ages in the Norwegian Sea during the Last Deglaciation, *Quat. Sci. Rev.*, 22(5-7), 429–435, doi:10.1016/S0277-3791(03)00002-7.
- Blaauw, M. (2010), Methods and code for “classical” age-modelling of radiocarbon sequences, *Quat. Geochronol.*, 5(5), 512–518, doi:10.1016/j.quageo.2010.01.002.
- De Boer, A. M., and D. Nof (2004), The exhaust valve of the North Atlantic, *J. Clim.*, 17(3), 417–422.
- Bradley, R. S., and J. H. England (2008), The Younger Dryas and the Sea of Ancient Ice, *Quat. Res.*, 70(1), 1 – 10, doi:10.1016/j.yqres.2008.03.002.
- Brigham-Grette, J., L. M. Gualtieri, O. Y. Glushkova, T. D. Hamilton, D. Mostoller, and A. Kotov (2003), Chlorine³⁶ 14C chronology support a limited last glacial maximum across central chukotka, northeastern Siberia, and no Beringian ice sheet, *Quat. Res.*, 59(3), 386–398.
- Briner, J. P., and D. S. Kaufman (2008), Late Pleistocene mountain glaciation in Alaska: key chronologies, *J. Quat. Sci.*, 23(6-7), 659–670, doi:10.1002/jqs.1196.
- Briner, J. P., D. S. Kaufman, A. Werner, M. Caffee, L. Levy, W. F. Manley, M. R. Kaplan, and R. C. Finkel (2002), Glacier readvance during the late glacial (Younger Dryas?) in the Ahklun Mountains, southwestern Alaska, *Geology*, 30(8), 679, doi:10.1130/0091-7613(2002)030<0679:GRDTLG>2.0.CO;2.
- Broecker, W. S. (1991), The great ocean conveyor, *Oceanography*, 4(2), 79–89.

- Broecker, W. S. (1994), Massive iceberg discharges as triggers for global climate change, *Nature*, 372, 421–424.
- Broecker, W. S. (1998), Paleocean circulation during the last deglaciation: a bipolar seesaw?, *Paleoceanography*, 13(2), 119–121.
- Broecker, W. S., M. Andree, W. Wolfli, H. Oeschger, G. Bonani, J. Kennett, and D. Peteet (1988), The chronology of the last deglaciation: Implications to the cause of the Younger Dryas event, *Paleoceanography*, 3(1), 1–19.
- Broecker, W. S., T. H. Peng, J. Jouzel, and G. Russell (1990), The magnitude of global fresh-water transports of importance to ocean circulation, *Clim. Dyn.*, 4(2), 73–79.
- Brunelle, B. G., D. M. Sigman, M. S. Cook, L. D. Keigwin, G. H. Haug, B. Plessen, G. Schettler, and S. L. Jaccard (2007), Evidence from diatom-bound nitrogen isotopes for subarctic Pacific stratification during the last ice age and a link to North Pacific denitrification changes, *Paleoceanography*, 22(1), PA1215, doi:10.1029/2005PA001205.
- Brunelle, B. G., D. M. Sigman, S. L. Jaccard, L. D. Keigwin, B. Plessen, G. Schettler, M. S. Cook, and G. H. Haug (2010), Glacial/interglacial changes in nutrient supply and stratification in the western subarctic North Pacific since the penultimate glacial maximum, *Quat. Sci. Rev.*, 29(19-20), 2579–2590, doi:10.1016/j.quascirev.2010.03.010.
- Caissie, B. E., J. Brigham-Grette, K. T. Lawrence, T. D. Herbert, and M. S. Cook (2010), Last Glacial Maximum to Holocene sea surface conditions at Umnak Plateau, Bering Sea, as inferred from diatom, alkenone, and stable isotope records, *Paleoceanography*, 25(1), PA1206, doi:10.1029/2008PA001671.
- Canada. Defence Research Board. Directorate of Scientific Information Services, and B. Kotenev (1966), *The submerged valley of the Paleo-Anadyr*.
- Van Cappellen, P., and Y. Wang (1996), Cycling of iron and manganese in surface sediments; a general theory for the coupled transport and reaction of carbon, oxygen, nitrogen, sulfur, iron, and manganese, *Am. J. Sci.*, 296(3), 197–243.
- Carlson, P. R., and H. A. Karl (1984), Discovery of two new large submarine canyons in the Bering Sea, *Mar. Geol.*, 56(1), 159–179.
- Church, J., J. Gregory, P. Huybrechts, M. Kuhn, K. Lambeck, M. Nhuan, D. Qin, and P. Woodworth (2001), Changes in sea level, *JT Houghton Ding DJ Griggs M Noguer PJ Van Linden X Dai K Maskell CA Johns. Eds Clim. Change 2001 Sci. Basis Contrib. Work. Group Third Assess. Rep. Intergov. Panel*, 639–694.
- Clague, J. J., J. M. Ryder, W. H. Matthews, O. L. Hughes, N. W. Rutter, L. E. Jackson, J. V. Matthews Jr., and G. M. MacDonald (1989), Quaternary geology of the Canadian Cordillera The geology of North America, vol. K-1, pp. 15–96, Geological Survey of Canada, Canada, Canada.

- Clark, P. U., S. W. Hostetler, N. G. Pisias, A. Schmittner, and K. J. Meissner (2007), Mechanisms for an ~7-kyr climate and sea-level oscillation during marine isotope stage 3, in *Geophysical Monograph Series*, vol. 173, edited by A. Schmittner, J. C. H. Chiang, and S. R. Hemming, pp. 209–246, American Geophysical Union, Washington, D. C.
- Clement, J. L., W. Maslowski, L. W. Cooper, J. M. Grebmeier, and W. Walczowski (2005), Ocean circulation and exchanges through the northern Bering Sea 1979–2001 model results, *Deep Sea Res. Part II Top. Stud. Oceanogr.*, 52(24-26), 3509–3540, doi:10.1016/j.dsr2.2005.09.010.
- Coachman, L. (1986), Advection and mixing on the Bering-Chukchi shelves, *Compon. Advection Mix. Coast. Water High Latit. Shelves ISHTAR*, 1–42.
- Coachman, L., and K. Aagaard (1981), Re-evaluation of water transports in the vicinity of Bering Strait, *East. Bering Sea Shelf Oceanogr. Resour.*, 1, 95–110.
- Coachman, L. K., and K. Aagaard (1966), *On the water exchange through Bering Strait*, Department of Oceanography, University of Washington.
- Coachman, L. K., K. Aagaard, and R. B. Tripp (1975), *Bering Strait: the regional physical oceanography*, Univ of Washington Press.
- Codispoti, L. A., and F. A. Richards (1968), Micronutrient Distributions in the East Siberian and Laptev Seas during Summer 1963, *Arctic*, 21(2), 67–83, doi:10.2307/40507500.
- Comiso, J. C., C. L. Parkinson, R. Gersten, and L. Stock (2008), Accelerated decline in the Arctic sea ice cover, *Geophys. Res. Lett.*, 35(1), doi:10.1029/2007GL031972.
- Cook, M. S. (2006), The paleoceanography of the Bering Sea during the last glacial cycle, Massachusetts Institute of Technology, Woods Hole Oceanographic Institute.
- Cook, M. S., L. D. Keigwin, and C. A. Sancetta (2005), The deglacial history of surface and intermediate water of the Bering Sea, *Deep Sea Res. Part II Top. Stud. Oceanogr.*, 52(16-18), 2163–2173, doi:10.1016/j.dsr2.2005.07.004.
- Cooper, L. W., T. E. Whitledge, J. M. Grebmeier, and T. Weingartner (1997), The nutrient, salinity, and stable oxygen isotope composition of Bering and Chukchi Seas waters in and near the Bering Strait, *J. Geophys. Res. Oceans*, 102(C6), 12563–12573, doi:10.1029/97JC00015.
- Creager, J. S., and D. A. McManus (1968), *Geology of the Floor of Bearing and Chukchi Seas: American Studies*, Department of Oceanography, University of Washington.
- Cronin, T. M., S. A. Smith, F. Eynaud, M. O'Regan, and J. King (2008), Quaternary paleoceanography of the central Arctic based on Integrated Ocean Drilling Program Arctic Coring Expedition 302 foraminiferal assemblages, *Paleoceanography*, 23(1), doi:10.1029/2007PA001484.

- Croudace, I. W., A. Rindby, and R. G. Rothwell (2006), ITRAX: description and evaluation of a new multi-function X-ray core scanner, *Spec. Publ.-Geol. Soc. Lond.*, 267, 51.
- Crusius, J., T. F. Pedersen, S. Kienast, L. Keigwin, and L. Labeyrie (2004), Influence of northwest Pacific productivity on North Pacific Intermediate Water oxygen concentrations during the Bølling-Ållerød interval (14.7–12.9 ka), *Geology*, 32(7), 633, doi:10.1130/G20508.1.
- Crusius, J., A. W. Schroth, S. Gassó, C. M. Moy, R. C. Levy, and M. Gatica (2011), Glacial flour dust storms in the Gulf of Alaska: Hydrologic and meteorological controls and their importance as a source of bioavailable iron, *Geophys. Res. Lett.*, 38(6), doi:10.1029/2010GL046573.
- Darby, D. A., J. Ortiz, L. Polyak, S. Lund, M. Jakobsson, and R. A. Woodgate (2009), The role of currents and sea ice in both slowly deposited central Arctic and rapidly deposited Chukchi–Alaskan margin sediments, *Glob. Planet. Change*, 68(1-2), 58–72, doi:10.1016/j.gloplacha.2009.02.007.
- Davies, M. H., A. C. Mix, J. S. Stoner, J. A. Addison, J. Jaeger, B. Finney, and J. Wiest (2011), The deglacial transition on the southeastern Alaska Margin: Meltwater input, sea level rise, marine productivity, and sedimentary anoxia, *Paleoceanography*, 26(2), doi:10.1029/2010PA002051.
- Deming, D., J. H. Sass, A. H. Lachenbruch, and R. F. de Rito (1992), Heat flow and subsurface temperature as evidence for basin-scale ground-water flow, North Slope of Alaska, *Geol. Soc. Am. Bull.*, 104(5), 528–542.
- Domack, E., D. Duran, A. Leventer, S. Ishman, S. Doane, S. McCallum, D. Amblas, J. Ring, R. Gilbert, and M. Prentice (2005), Stability of the Larsen B ice shelf on the Antarctic Peninsula during the Holocene epoch, *Nature*, 436(7051), 681–685, doi:10.1038/nature03908.
- Dumond, D. E., and D. G. Griffin (2002), Measurements of the marine reservoir effect on radiocarbon ages in the eastern Bering Sea, *Arctic*, 77–86.
- Dyke, A. S., and J. M. Savelle (2001), Holocene History of the Bering Sea Bowhead Whale (*Balaena mysticetus*) in Its Beaufort Sea Summer Grounds off Southwestern Victoria Island, Western Canadian Arctic, *Quat. Res.*, 55(3), 371–379, doi:10.1006/qres.2001.2228.
- Dyke, A. S., J. England, E. Reimnitz, and H. Jetté (1997), Changes in driftwood delivery to the Canadian Arctic Archipelago: The hypothesis of postglacial oscillations of the Transpolar Drift, *Arctic*, 50(1), 1–16.
- Dyke, A. S., J. T. Andrews, P. U. Clark, J. H. England, G. H. Miller, J. Shaw, and J. J. Veillette (2002), The Laurentide and Innuitian ice sheets during the last glacial maximum, *Quat. Sci. Rev.*, 21(1), 9–31.

- Eberl, D. (2004), Quantitative mineralogy of the Yukon River system: Changes with reach and season, and determining sediment provenance, *Am. Mineral.*, 89(11-12), 1784–1794.
- Eiríksson, J., G. Larsen, K. L. Knudsen, J. Heinemeier, and L. A. Símonarson (2004), Marine reservoir age variability and water mass distribution in the Iceland Sea, *Quat. Sci. Rev.*, 23(20-22), 2247–2268, doi:10.1016/j.quascirev.2004.08.002.
- Elias, S. A., S. K. Short, C. H. Nelson, and H. H. Birks (1996), Life and times of the Bering land bridge, *Nature*, 382(6586), 60–63.
- Emmer, E., and R. C. Thunell (2000), Nitrogen isotope variations in Santa Barbara Basin sediments: Implications for denitrification in the eastern tropical North Pacific during the last 50,000 years, *Paleoceanography*, 15(4), 377–387.
- England, J. H., and M. F. A. Furze (2008), New evidence from the western Canadian Arctic Archipelago for the resubmergence of Bering Strait, *Quat. Res.*, 70(1), 60–67, doi:10.1016/j.yqres.2008.03.001.
- Expedition 323 Scientists, K. Takahashi, A. C. Ravelo, and A. Zarikian (2011), Site U1345, , *Proc. IODP, 323: Tokyo (Integrated Ocean Drilling Program Management International, Inc.)*, doi:10.2204/iodp.proc.323.109.2011.
- Fairbanks, R. G. (1989), A 17,000-year glacio-eustatic sea level record: influence of glacial melting rates on the Younger Dryas event and deep-ocean circulation, *Nature*, 342(6250), 637–642.
- Flores, R. M., G. D. Stricker, and S. A. Kinney (2004), *Alaska coal geology, resources, and coalbed methane potential*, US Department of the Interior, US Geological Survey.
- Fontugne, M. R., and J.-M. Jouanneau (1987), Modulation of the particulate organic carbon flux to the ocean by a macrotidal estuary: evidence from measurements of carbon isotopes in organic matter from the Gironde system, *Estuar. Coast. Shelf Sci.*, 24(3), 377–387.
- Francis, J. A., W. Chan, D. J. Leathers, J. R. Miller, and D. E. Veron (2009), Winter Northern Hemisphere weather patterns remember summer Arctic sea-ice extent, *Geophys. Res. Lett.*, 36(7), doi:10.1029/2009GL037274.
- Froelich, P., G. Klinkhammer, M. al Bender, N. Luedtke, G. R. Heath, D. Cullen, P. Dauphin, D. Hammond, B. Hartman, and V. Maynard (1979), Early oxidation of organic matter in pelagic sediments of the eastern equatorial Atlantic: suboxic diagenesis, *Geochim. Cosmochim. Acta*, 43(7), 1075–1090.
- Galbraith, E. D., S. L. Jaccard, T. F. Pedersen, D. M. Sigman, G. H. Haug, M. Cook, J. R. Southon, and R. Francois (2007), Carbon dioxide release from the North Pacific abyss during the last deglaciation, *Nature*, 449(7164), 890–893, doi:10.1038/nature06227.
- Ganachaud, A., and C. Wunsch (2000), Improved estimates of global ocean circulation, heat transport and mixing from hydrographic data, *Nature*, 408(6811), 453–457.

- Ganeshram, R. S., and T. F. Pedersen (1998), Glacial-interglacial variability in upwelling and bioproductivity off NW Mexico: Implications for Quaternary paleoclimate, *Paleoceanography*, 13(6), 634–645.
- Gardner, J. V., W. E. Dean, and P. Dartnell (1997), Biogenic sedimentation beneath the California Current system for the past 30 kyr and its paleoceanographic significance, *Paleoceanography*, 12(2), 207–225.
- Glushkova, O. Y. (2001), Geomorphological correlation of Late Pleistocene glacial complexes of Western and Eastern Beringia, *Quat. Sci. Rev.*, 20(1), 405–417.
- Gorbarenko, S. A., I. A. Basov, M. P. Chekhovskaya, J. Southon, T. A. Khusid, and A. V. Artemova (2005), Orbital and millennium scale environmental changes in the southern Bering Sea during the last glacial-Holocene: Geochemical and paleontological evidence, *Deep Sea Res. Part II Top. Stud. Oceanogr.*, 52(16-18), 2174–2185, doi:10.1016/j.dsr2.2005.08.005.
- Gorbarenko, S. A., A. V. Artemova, E. L. Goldberg, and Y. P. Vasilenko (2014), The response of the Okhotsk Sea environment to the orbital-millennium global climate changes during the Last Glacial Maximum, deglaciation and Holocene, *Glob. Planet. Change*, 116, 76–90, doi:10.1016/j.gloplacha.2014.02.002.
- Grebmeier, J. M., C. P. McRoy, and H. M. Feder (1988), Pelagic-benthic coupling on the shelf of the northern Bering and Chukchi seas. I. Food supply source and benthic biomass., *Mar. Ecol. Prog. Ser. Oldendorf*, 48(1), 57–67.
- Grebmeier, J. M., S. E. Moore, J. E. Overland, K. E. Frey, and R. Gradinger (2010), Biological response to recent Pacific Arctic sea ice retreats, *Eos Trans. Am. Geophys. Union*, 91(18), 161–162.
- Gualtieri, L., O. Glushkova, and J. Brigham-Grette (2000), Evidence for restricted ice extent during the last glacial maximum in the Koryak Mountains of Chukotka, far eastern Russia, *Geol. Soc. Am. Bull.*, 112(7), 1106–1118, doi:10.1130/0016-7606(2000)112<1106:EFRIED>2.0.CO;2.
- Guilderson, T., L. Burckle, S. Hemming, and W. Peltier (2000), Late Pleistocene sea level variations derived from the Argentine Shelf, *Geochem. Geophys. Geosystems*, 1(12).
- Guo, L., and R. W. Macdonald (2006), Source and transport of terrigenous organic matter in the upper Yukon River: Evidence from isotope ($\delta^{13}\text{C}$, $\Delta^{14}\text{C}$, and $\delta^{15}\text{N}$) composition of dissolved, colloidal, and particulate phases, *Glob. Biogeochem. Cycles*, 20(2).
- Hans Nelson, C., J. Baraza, and A. Maldonado (1993), Mediterranean undercurrent sandy contourites, Gulf of Cadiz, Spain, *Sediment. Geol.*, 82(1), 103–131.
- Harvey, G. R. (1980), A study of the chemistry of iodine and bromine in marine sediments, *Mar. Chem.*, 8(4), 327–332.

- Hedges, J. I., and P. L. Parker (1976), Land-derived organic matter in surface sediments from the Gulf of Mexico, *Geochim. Cosmochim. Acta*, 40(9), 1019–1029.
- Heggie, D., G. Klinkhammer, and D. Cullen (1987), Manganese and copper fluxes from continental margin sediments, *Geochim. Cosmochim. Acta*, 51(5), 1059–1070.
- Heiser, P. A., and J. J. Roush (2001), Pleistocene glaciations in Chukotka, Russia:: moraine mapping using satellite synthetic aperture radar (SAR) imagery, *Quat. Sci. Rev.*, 20(1), 393–404.
- Hendy, I. L., and J. P. Kennett (2003), Tropical forcing of North Pacific intermediate water distribution during Late Quaternary rapid climate change?, *Quat. Sci. Rev.*, 22(5), 673–689.
- Hendy, I. L., and T. F. Pedersen (2005), Is pore water oxygen content decoupled from productivity on the California Margin? Trace element results from Ocean Drilling Program Hole 1017E, San Lucia slope, California, *Paleoceanography*, 20(4), doi:10.1029/2004PA001123.
- Hill, J. C., and N. W. Driscoll (2008), Paleodrainage on the Chukchi shelf reveals sea level history and meltwater discharge, *Mar. Geol.*, 254(3-4), 129–151, doi:10.1016/j.margeo.2008.05.018.
- Hill, J. C., and N. W. Driscoll (2010), Iceberg discharge to the Chukchi shelf during the Younger Dryas, *Quat. Res.*, 74(1), 57–62, doi:10.1016/j.yqres.2010.03.008.
- Hoare, J. M. (1961), Geology and tectonic setting of lower Kuskokwim-Bristol Bay region, Alaska, *AAPG Bull.*, 45(5), 594–611.
- Hopkins, D. M. (1959), Cenozoic History of the Bering Land Bridge The seaway between the Pacific and Arctic basins has often been a land route between Siberia and Alaska, *Science*, 129(3362), 1519–1528.
- Hopkins, D. M. (1967), *The Bering land bridge*, Stanford, Calif: Stanford University Press.
- Hopkins, D. M. (1972), The paleogeography and climatic history of Beringia during late Cenozoic time, *Inter-Nord*, 12, 121–150.
- Hopkins, D. M. (1979), Landscape and climate of Beringia during late Pleistocene and Holocene time, *First Am. Orig. Affin. Adapt.*, 15, 42.
- Hopkins, D. M. (1982), Aspects of the paleogeography of Beringia during the late Pleistocene, *Paleoecol. Beringia Acad. Press N. Y.*, 3–28.
- Hu, A., and G. A. Meehl (2005), Bering Strait throughflow and the thermohaline circulation, *Geophys. Res. Lett.*, 32(24), doi:10.1029/2005GL024424.

- Hu, A., G. A. Meehl, and W. Han (2007), Role of the Bering Strait in the thermohaline circulation and abrupt climate change, *Geophys. Res. Lett.*, *34*(5), doi:10.1029/2006GL028906.
- Hu, A., G. A. Meehl, W. Han, J. Yin, B. Wu, and M. Kimoto (2012a), Influence of Continental Ice Retreat on Future Global Climate, *J. Clim.*, *26*(10), 3087–3111, doi:10.1175/JCLI-D-12-00102.1.
- Hu, A., G. A. Meehl, W. Han, A. Timmermann, B. Otto-Bliesner, Z. Liu, W. M. Washington, W. Large, A. Abe-Ouchi, and M. Kimoto (2012b), Role of the Bering Strait on the hysteresis of the ocean conveyor belt circulation and glacial climate stability, *Proc. Natl. Acad. Sci.*, *109*(17), 6417–6422.
- Hu, A., G. A. Meehl, W. Han, J. Yin, B. Wu, and M. Kimoto (2013), Influence of Continental Ice Retreat on Future Global Climate, *J. Clim.*, *26*(10), 3087–3111, doi:10.1175/JCLI-D-12-00102.1.
- Hu, A., G. A. Meehl, W. Han, B. Otto-Bliesner, A. Abe-Ouchi, and N. Rosenbloom (2014), Effects of the Bering Strait closure on AMOC and global climate under different background climates, *Prog. Oceanogr.*, doi:10.1016/j.pocean.2014.02.004.
- Hughes, T. J., G. H. Denton, and G. Grosval'd (1977), *Was There a Late-Wurm Arctic Ice Sheet?*
- Hurst, M. P., A. M. Aguilar-Islas, and K. W. Bruland (2010), Iron in the southeastern Bering Sea: Elevated leachable particulate Fe in shelf bottom waters as an important source for surface waters, *Cont. Shelf Res.*, *30*(5), 467–480, doi:10.1016/j.csr.2010.01.001.
- Ikehara, K., K. Ohkushi, A. Shibahara, and M. Hoshiba (2006), Change of bottom water conditions at intermediate depths of the Oyashio region, NW Pacific over the past 20,000 yrs, *Glob. Planet. Change*, *53*(1-2), 78–91, doi:10.1016/j.gloplacha.2006.01.011.
- Ingólfsson, Ó., P. Miller, and H. Loken (2008), Late Quaternary marine-based Kara Sea ice sheets: a review of terrestrial stratigraphic data highlighting their formation, *Polar Res.*, *27*(2), 152–161, doi:10.1111/j.1751-8369.2008.00060.x.
- Ishizaki, Y., K. Ohkushi, T. Ito, and H. Kawahata (2009), Abrupt changes of intermediate-water oxygen in the northwestern Pacific during the last 27 kyr, *Geo-Mar. Lett.*, *29*(2), 125–131.
- Itaki, T., M. Uchida, S. Kim, H.-S. Shin, R. Tada, and B.-K. Khim (2009), Late Pleistocene stratigraphy and palaeoceanographic implications in northern Bering Sea slope sediments: evidence from the radiolarian species *Cycladophora davisiana*, *J. Quat. Sci.*, *24*(8), 856–865, doi:10.1002/jqs.1356.
- Jaccard, S. L. (2005), Glacial/Interglacial Changes in Subarctic North Pacific Stratification, *Science*, *308*(5724), 1003–1006, doi:10.1126/science.1108696.

- Jaccard, S. L., E. D. Galbraith, D. M. Sigman, G. H. Haug, R. Francois, T. F. Pedersen, P. Dulski, and H. R. Thierstein (2009), Subarctic Pacific evidence for a glacial deepening of the oceanic respired carbon pool, *Earth Planet. Sci. Lett.*, 277(1-2), 156–165, doi:10.1016/j.epsl.2008.10.017.
- Jakobsson, M. (2002), Hypsometry and volume of the Arctic Ocean and its constituent seas, *Geochem. Geophys. Geosystems*, 3(5), 1–18, doi:10.1029/2001GC000302.
- Jakobsson, M., R. Løvlie, H. Al-Hanbali, E. Arnold, J. Backman, and M. Mörth (2000), Manganese and color cycles in Arctic Ocean sediments constrain Pleistocene chronology, *Geology*, 28(1), 23, doi:10.1130/0091-7613(2000)28<23:MACCIA>2.0.CO;2.
- Johnson, G. C., P. J. Stabeno, and S. C. Riser (2004), The Bering Slope Current System Revisited., *J. Phys. Oceanogr.*, 34(2).
- Kaltin, S., and L. G. Anderson (2005), Uptake of atmospheric carbon dioxide in Arctic shelf seas: evaluation of the relative importance of processes that influence pCO₂ in water transported over the Bering–Chukchi Sea shelf, *Mar. Chem.*, 94(1-4), 67–79, doi:10.1016/j.marchem.2004.07.010.
- Kao, S., K. Liu, S. Hsu, Y. Chang, and M. Dai (2008), North Pacific-wide spreading of isotopically heavy nitrogen during the last deglaciation: Evidence from the western Pacific., *Biogeosciences*, 5(6).
- Katsuki, K., and K. Takahashi (2005), Diatoms as paleoenvironmental proxies for seasonal productivity, sea-ice and surface circulation in the Bering Sea during the late Quaternary, *Deep Sea Res. Part II Top. Stud. Oceanogr.*, 52(16-18), 2110–2130, doi:10.1016/j.dsr2.2005.07.001.
- Kaufman, D. S., and W. F. Manley (2004), Pleistocene Maximum and Late Wisconsin glacier extents across Alaska, USA, in *Quaternary Glaciations: Extent and Chronology. Part II: North America*, edited by J. Ehlers and P. L. Gibbard, pp. 9–27, Elsevier, Amsterdam.
- Kaufman, D. S., L. Polyak, R. Adler, J. E. T. Channell, and C. Xuan (2008), Dating late Quaternary planktonic foraminifer *Neogloboquadrina pachyderma* from the Arctic Ocean using amino acid racemization, *Paleoceanography*, 23(3), doi:10.1029/2008PA001618.
- Keigwin, L., G. Jones, and P. Froelich (1992), A 15,000 year paleoenvironmental record from Meiji Seamount, far northwestern Pacific, *Earth Planet. Sci. Lett.*, 111(2), 425–440.
- Keigwin, L. D. (1998), Glacial-age hydrography of the far northwest Pacific Ocean, *Paleoceanography*, 13(4), 323–339.
- Keigwin, L. D. (2002), Late Pleistocene-Holocene paleoceanography and ventilation of the Gulf of California, *J. Oceanogr.*, 58(2), 421–432.
- Keigwin, L. D., and M. S. Cook (2007), A role for North Pacific salinity in stabilizing North Atlantic climate, *Paleoceanography*, 22(3), doi:10.1029/2007PA001420.

- Keigwin, L. D., and G. A. Jones (1994), Western North Atlantic evidence for millennial-scale changes in ocean circulation and climate, *J. Geophys. Res. Oceans*, 99(C6), 12397–12410, doi:10.1029/94JC00525.
- Keigwin, L. D., G. A. Jones, S. J. Lehman, and E. A. Boyle (1991), Deglacial meltwater discharge, North Atlantic deep circulation, and abrupt climate change, *J. Geophys. Res. Oceans 1978–2012*, 96(C9), 16811–16826.
- Keigwin, L. D., J. P. Donnelly, M. S. Cook, N. W. Driscoll, and J. Brigham-Grette (2006), Rapid sea-level rise and Holocene climate in the Chukchi Sea, *Geology*, 34(10), 861, doi:10.1130/G22712.1.
- Kennett, J. P., and B. L. Ingram (1995), A 20,000-year record of ocean circulation and climate change from the Santa Barbara basin,
- Khim, B.-K., S. Kim, M. Uchida, and T. Itaki (2011), High organic carbon deposition in the northern margin of the Aleutian Basin (Bering Sea) before the last deglaciation, *Ocean Sci. J.*, 45(4), 203–211, doi:10.1007/s12601-010-0019-y.
- Kienast, S. S., S. E. Calvert, and T. F. Pedersen (2002), Nitrogen isotope and productivity variations along the northeast Pacific margin over the last 120 kyr, *Paleoceanography*, 17(4), 1–17, doi:10.1029/2001PA000650.
- Kim, S., B. K. Khim, M. Uchida, T. Itaki, and R. Tada (2011), Millennial-scale paleoceanographic events and implication for the intermediate-water ventilation in the northern slope area of the Bering Sea during the last 71kyrs, *Glob. Planet. Change*, 79(1-2), 89–98, doi:10.1016/j.gloplacha.2011.08.004.
- Kinder, T., L. Coachman, and J. Galt (1975), The Bering slope current system, *J. Phys. Oceanogr.*, 5(2), 231–244.
- Kinney, C. J., W. Maslowski, and S. Okkonen (2009), On the processes controlling shelf–basin exchange and outer shelf dynamics in the Bering Sea, *Deep Sea Res. Part II Top. Stud. Oceanogr.*, 56(17), 1351–1362, doi:10.1016/j.dsr2.2008.10.023.
- Kovanen, D. J., and D. J. Easterbrook (2002), Paleodeviations of radiocarbon marine reservoir values for the northeast Pacific, *Geology*, 30(3), 243, doi:10.1130/0091-7613(2002)030<0243:PORMRV>2.0.CO;2.
- Kuehn, H., L. Lembke-Jene, R. Gersonde, O. Esper, F. Lamry, H. Arz, and R. Tiedemann (2014), Laminated sediments in the Bering Sea reveal atmospheric teleconnections to Greenland climate on millennial to decadal timescales during the last deglaciation, *Clim. Past*, 2467–2518, doi:10.5194/cpd-10-2467-2014.
- Kummer, J. T., and J. S. Creager (1971), Marine geology and Cenozoic history of the Gulf of Anadyr, *Mar. Geol.*, 10(4), 257–280.

- Kuzmin, Y. V., G. S. Burr, and A. T. Jull (2001), Radiocarbon reservoir correction ages in the Peter the Great Gulf, Sea of Japan, and eastern coast of the Kunashir, southern Kuriles (northwestern Pacific), *Radiocarbon*, 43(2; PART A), 477–482.
- Lam, P. J., L. F. Robinson, J. Blusztajn, C. Li, M. S. Cook, J. F. McManus, and L. D. Keigwin (2013), Transient stratification as the cause of the North Pacific productivity spike during deglaciation, *Nat. Geosci.*, 6(8), 622–626, doi:10.1038/ngeo1873.
- Landvik, J. Y., S. Bondevik, A. Elverhøi, W. Fjeldskaar, J. Mangerud, O. Salvigsen, M. J. Siegert, J.-I. Svendsen, and T. O. Vorren (1998), The last glacial maximum of Svalbard and the Barents Sea area: ice sheet extent and configuration, *Quat. Sci. Rev.*, 17(1-3), 43–75.
- LeGrande, A. N., and G. A. Schmidt (2008), Ensemble, water isotope-enabled, coupled general circulation modeling insights into the 8.2 ka event, *Paleoceanography*, 23(3), doi:10.1029/2008PA001610.
- Lehman, S. I., and L. D. Keigwin (1992), Sudden changes in North Atlantic circulation during the last deglaciation, *Nature*, 356, 757.
- Lehmann, M. F., D. M. Sigman, D. C. McCorkle, B. G. Brunelle, S. Hoffmann, M. Kienast, G. Cane, and J. Clement (2005), Origin of the deep Bering Sea nitrate deficit: Constraints from the nitrogen and oxygen isotopic composition of water column nitrate and benthic nitrate fluxes, *Glob. Biogeochem. Cycles*, 19(4), doi:10.1029/2005GB002508.
- Levitan, M. A., and R. Stein (2008), History of sedimentation rates in the sea-ice sedimentation zone during the last 130 ka, *Lithol. Miner. Resour.*, 43(1), 65–75, doi:10.1134/S0024490208010069.
- Licciardi, J. M., P. U. Clark, J. W. Jenson, and D. R. Macayeay (1998), Deglaciation of a soft-bedded Laurentide Ice Sheet, *Quat. Sci. Rev.*, 17(4-5), 427–448.
- Lisitsyn, A. P. (1966), Recent sedimentation in the Bering Sea, *CFSTI Transl. NO TT 68-50315*.
- Lobbes, J. M., H. P. Fitznar, and G. Kattner (2000), Biogeochemical characteristics of dissolved and particulate organic matter in Russian rivers entering the Arctic Ocean, *Geochim. Cosmochim. Acta*, 64(17), 2973–2983.
- Löwemark, L., M. Jakobsson, M. Mrth, and J. Backman (2008), Arctic Ocean manganese contents and sediment colour cycles, *Polar Res.*, 27(2), 105–113, doi:10.1111/j.1751-8369.2008.00055.x.
- Lundeen, Z. J., J. Brigham-Grette, S. T. Petsch, and S. Burns (2005), Elemental and Isotopic Constraints on the Late Glacial-Holocene Transgression and Paleoceanography of the Chukchi Sea, M.S., University of Massachusetts Amherst.
- Mammone, K. A. (1998), Sediment provenance and transport on the Siberian Arctic shelf, Oregon State University.

- Mann, D. H., and T. D. Hamilton (1995), Late Pleistocene and Holocene paleoenvironments of the North Pacific coast, *Quat. Sci. Rev.*, *14*(5), 449–471.
- Marchitto, T. M., S. J. Lehman, J. D. Ortiz, J. Fluckiger, and A. van Geen (2007), Marine Radiocarbon Evidence for the Mechanism of Deglacial Atmospheric CO₂ Rise, *Science*, *316*(5830), 1456–1459, doi:10.1126/science.1138679.
- Martin, S., and R. Drucker (1997), The effect of possible Taylor columns on the summer ice retreat in the Chukchi Sea, *J. Geophys. Res. Oceans 1978–2012*, *102*(C5), 10473–10482.
- MathWorks (2014), *MATLAB*, Statistical Package, MathWorks.
- Max, L., L. Lembke-Jene, J.-R. Riethdorf, R. Tiedemann, D. Nürnberg, H. Kühn, and A. Mackensen (2014), Pulses of enhanced North Pacific Intermediate Water ventilation from the Okhotsk Sea and Bering Sea during the last deglaciation, *Clim. Past*, *10*(2), 591–605, doi:10.5194/cp-10-591-2014.
- Mayewski, P. A. et al. (2004), Holocene climate variability, *Quat. Res.*, *62*(3), 243–255, doi:10.1016/j.yqres.2004.07.001.
- McManus, D. A., K. Venkatarathnam, D. M. Hopkins, and C. H. Nelson (1974), Yukon River sediment on the northernmost Bering Sea shelf, *J. Sediment. Res.*, *44*(4).
- McManus, J. F., R. Francois, J.-M. Gherardi, L. D. Keigwin, and S. Brown-Leger (2004), Collapse and rapid resumption of Atlantic meridional circulation linked to deglacial climate changes, *Nature*, *428*(6985), 834–837.
- McNeely, R., A. S. Dyke, and J. R. Southon (2006), Canadian marine reservoir ages, preliminary data assessment, Open File 5049,
- Menard, H. W., and S. M. Smith (1966), Hypsometry of ocean basin provinces, *J. Geophys. Res.*, *71*(18), 4305–4325, doi:10.1029/JZ071i018p04305.
- Meyers, P. A. (1994), Preservation of elemental and isotopic source identification of sedimentary organic matter, *Chem. Geol.*, *114*(3), 289–302.
- Mikolajewicz, U., T. J. Crowley, A. Schiller, and R. Voss (1997), Modelling teleconnections between the North Atlantic and North Pacific during the Younger Dryas, *Nature*, *387*(6631), 384–387.
- Mix, A. C., D. C. Lund, N. G. Pisias, P. Bodén, L. Bornmalm, M. Lyle, and J. Pike (1999), Rapid climate oscillations in the northeast Pacific during the last deglaciation reflect Northern and Southern Hemisphere sources, *Geophys. Monogr. Ser.*, *112*, 127–148.
- Monnin, E. (2001), Atmospheric CO₂ Concentrations over the Last Glacial Termination, *Science*, *291*(5501), 112–114, doi:10.1126/science.291.5501.112.

- Naidu, A., L. Cooper, J. Grebmeier, T. Whitlege, and M. Hameedi (2004), The continental margin of the North Bering-Chukchi Sea: concentrations, sources, fluxes, accumulation and burial rates of organic carbon, *Org. Carbon Cycle Arct. Ocean Springer-Verl. Berl.*, 193–203.
- Naidu, A. S., and T. C. Mowatt (1983), Sources and dispersal patterns of clay minerals in surface sediments from the continental-shelf areas off Alaska, *Geol. Soc. Am. Bull.*, 94(7), 841, doi:10.1130/0016-7606(1983)94<841:SADPOC>2.0.CO;2.
- Naidu, A. S., R. S. Scalan, H. M. Feder, J. J. Goering, M. J. Hameedi, P. L. Parker, E. W. Behrens, M. E. Caughey, and S. C. Jewett (1993), Stable organic carbon isotopes in sediments of the north Bering-south Chukchi seas, Alaskan-Soviet Arctic Shelf, *Cont. Shelf Res.*, 13(5–6), 669 – 691, doi:10.1016/0278-4343(93)90099-J.
- Naidu, A. S., L. W. Cooper, B. P. Finney, R. W. Macdonald, C. Alexander, and I. P. Semiletov (2000), Organic carbon isotope ratios ($\delta^{13}\text{C}$) of Arctic Amerasian Continental shelf sediments, *Int. J. Earth Sci.*, 89(3), 522–532, doi:10.1007/s005310000121.
- Nakatsuka, T., K. Watanabe, N. Handa, E. Matsumoto, and E. Wada (1995), Glacial to interglacial surface nutrient variations of Bering deep basins recorded by $\delta^{13}\text{C}$ and $\delta^{15}\text{N}$ of sedimentary organic matter, *Paleoceanography*, 10(6), 1047–1061.
- Nelson, H., and J. S. Creager (1977), Displacement of Yukon-derived sediment from Bering Sea to Chukchi Sea during Holocene time, *Geology*, 5(3), 141, doi:10.1130/0091-7613(1977)5<141:DOYSFB>2.0.CO;2.
- Nørgaard-Pedersen, N. (2003), Arctic Ocean during the Last Glacial Maximum: Atlantic and polar domains of surface water mass distribution and ice cover, *Paleoceanography*, 18(3), doi:10.1029/2002PA000781.
- Nürnberg, D., I. Wollenburg, D. Dethleff, H. Eicken, H. Kassens, T. Letzig, E. Reimnitz, and J. Thiede (1994), Sediments in Arctic sea ice: Implications for entrainment, transport and release, *Mar. Geol.*, 119(3), 185–214.
- Obata, A., J. Ishizaka, and M. Endoh (1996), Global verification of critical depth theory for phytoplankton bloom with climatological in situ temperature and satellite ocean color data, *J. Geophys. Res. Oceans 1978–2012*, 101(C9), 20657–20667.
- Okazaki, Y., K. Takahashi, H. Asahi, K. Katsuki, J. Hori, H. Yasuda, Y. Sagawa, and H. Tokuyama (2005), Productivity changes in the Bering Sea during the late Quaternary, *Deep Sea Res. Part II Top. Stud. Oceanogr.*, 52(16-18), 2150–2162, doi:10.1016/j.dsr2.2005.07.003.
- Okazaki, Y., A. Timmermann, L. Menviel, N. Harada, A. Abe-Ouchi, M. O. Chikamoto, A. Mouchet, and H. Asahi (2010), Deepwater Formation in the North Pacific During the Last Glacial Termination, *Science*, 329(5988), 200–204, doi:10.1126/science.1190612.

- Okazaki, Y., K. Kimoto, H. Asahi, M. Sato, Y. Nakamura, and N. Harada (2014), Glacial to deglacial ventilation and productivity changes in the southern Okhotsk Sea, *Palaeogeogr. Palaeoclimatol. Palaeoecol.*, 395, 53–66, doi:10.1016/j.palaeo.2013.12.013.
- Okkonen, S. R., G. M. Schmidt, E. D. Cokelet, and P. J. Stabeno (2004), Satellite and hydrographic observations of the Bering Sea “Green Belt,” *Deep Sea Res. Part II Top. Stud. Oceanogr.*, 51(10-11), 1033–1051, doi:10.1016/j.dsr2.2003.08.005.
- Oppo, D. W., J. F. McManus, and J. L. Cullen (2003), Palaeo-oceanography: Deepwater variability in the Holocene epoch, *Nature*, 422(6929), 277–277.
- Ortiz, J. D., L. Polyak, J. M. Grebmeier, D. Darby, D. D. Eberl, S. Naidu, and D. Nof (2009), Provenance of Holocene sediment on the Chukchi-Alaskan margin based on combined diffuse spectral reflectance and quantitative X-Ray Diffraction analysis, *Glob. Planet. Change*, 68(1–2), 73 – 84, doi:10.1016/j.gloplacha.2009.03.020.
- Otosaka, S., M. C. Honda, and S. Noriki (2004), La/Yb and Th/Sc in settling particles: Vertical and horizontal transport of lithogenic material in the western North Pacific, *Geochem J*, 38(6), 515–525.
- Overland, J. E., and C. H. Pease (1982), Cyclone Climatology of the Bering Sea and Its Relation to Sea Ice Extent, *Mon. Weather Rev.*, 110(1), 5–13, doi:10.1175/1520-0493(1982)110<0005:CCOTBS>2.0.CO;2.
- Overland, J. E., and M. Wang (2007), Future regional Arctic sea ice declines, *Geophys. Res. Lett.*, 34(17), doi:10.1029/2007GL030808.
- Paquette, R. am, and R. Bourke (1974), Observations on the coastal current of Arctic Alaska, *J Mar Res*, 32(2), 195–207.
- Parfenov, L. (1992), Accretionary history of northeast Asia, pp. 183–188.
- Parsons, T. R., M. Takahashi, and B. Hargrave (1977), *Biological oceanographic processes*, 2nd ed., Pergamon Press.
- Peings, Y., and G. Magnúsdóttir (2014), Response of the Wintertime Northern Hemisphere Atmospheric Circulation to Current and Projected Arctic Sea Ice Decline: A Numerical Study with CAM5., *J. Clim.*, 27(1).
- Peltier, W. R., and R. G. Fairbanks (2006), Global glacial ice volume and Last Glacial Maximum duration from an extended Barbados sea level record, *Quat. Sci. Rev.*, 25(23-24), 3322–3337, doi:10.1016/j.quascirev.2006.04.010.
- Polyak, L., W. B. Curry, D. A. Darby, J. Bischof, and T. M. Cronin (2004), Contrasting glacial/interglacial regimes in the western Arctic Ocean as exemplified by a sedimentary record from the Mendeleev Ridge, *Palaeogeogr. Palaeoclimatol. Palaeoecol.*, 203(1-2), 73–93, doi:10.1016/S0031-0182(03)00661-8.

- Polyak, L., D. A. Darby, J. F. Bischof, and M. Jakobsson (2007), Stratigraphic constraints on late Pleistocene glacial erosion and deglaciation of the Chukchi margin, Arctic Ocean, *Quat. Res.*, *67*(2), 234–245, doi:10.1016/j.yqres.2006.08.001.
- Prahl, F., J. Ertel, M. Goni, M. Sparrow, and B. Eversmeyer (1994), Terrestrial organic carbon contributions to sediments on the Washington margin, *Geochim. Cosmochim. Acta*, *58*(14), 3035–3048.
- Price, N., and S. Calvert (1977), The contrasting geochemical behaviours of iodine and bromine in recent sediments from the Namibian shelf, *Geochim. Cosmochim. Acta*, *41*(12), 1769–1775.
- Ramnarine, R., R. P. Voroney, C. Wagner-Riddle, and K. E. Dunfield (2011), Carbonate removal by acid fumigation for measuring the $\delta^{13}\text{C}$ of soil organic carbon, *Can. J. Soil Sci.*, *91*(2), 247–250, doi:10.4141/cjss10066.
- Rasmussen, S. O. et al. (2006), A new Greenland ice core chronology for the last glacial termination, *J. Geophys. Res.*, *111*(D6), doi:10.1029/2005JD006079.
- Reimer, P. J., E. Bard, A. Bayliss, J. W. Beck, P. G. Blackwell, C. B. Ramsey, C. E. Buck, H. Cheng, R. L. Edwards, and M. Friedrich (2013), IntCal13 and Marine13 radiocarbon age calibration curves 0–50,000 years cal BP, *Radiocarbon*, *55*(4), 1869–1887.
- Reimnitz, E., M. McCormick, J. Bischof, and D. A. Darby (1998), Comparing sea-ice sediment load with Beaufort Sea shelf deposits: is entrainment selective?, *J. Sediment. Res.*, *68*(5).
- Roach, A. T., K. Aagaard, C. H. Pease, S. A. Salo, T. Weingartner, V. Pavlov, and M. Kulakov (1995), Direct measurements of transport and water properties through the Bering Strait, *J. Geophys. Res. Oceans*, *100*(C9), 18443–18457, doi:10.1029/95JC01673.
- Robinson, L. F. (2005), Radiocarbon Variability in the Western North Atlantic During the Last Deglaciation, *Science*, *310*(5753), 1469–1473, doi:10.1126/science.1114832.
- Rudels, B. (1989), The formation of Polar Surface Water, the ice export and the exchanges through the Fram Strait, *Prog. Oceanogr.*, *22*(3), 205–248.
- Rudels, B., E. P. Jones, L. G. Anderson, and G. Kattner (1994), On the intermediate depth waters of the Arctic Ocean, *Geophys. Monogr. Ser.*, *85*, 33–46.
- Sambrotto, R., J. Goering, and C. McRoy (1984), Large yearly production of phytoplankton in the western Bering Strait, *Science*, *225*(4667), 1147–1150.
- Sancetta, C. (1979), Oceanography of the North Pacific during the last 18,000 years: evidence from fossil diatoms, *Mar. Micropaleontol.*, *4*, 103–123.
- Sancetta, C. (1995), Diatoms in the Gulf of California: Seasonal flux patterns and the sediment record for the last 15,000 years, *Paleoceanography*, *10*(1), 67–84.

- Sancetta, C., L. Heusser, L. Labeyrie, A. S. Naidu, and S. W. Robinson (1985), Wisconsin—Holocene paleoenvironment of the Bering Sea: Evidence from diatoms, pollen, oxygen isotopes and clay minerals, *Mar. Geol.*, 62(1), 55–68.
- Schauer, U., R. D. Muench, B. Rudels, and L. Timokhov (1997), Impact of eastern Arctic shelf waters on the Nansen Basin intermediate layers, *J. Geophys. Res. Oceans*, 102(C2), 3371–3382, doi:10.1029/96JC03366.
- Schlung, S. A. et al. (2013), Millennial-scale climate change and intermediate water circulation in the Bering Sea from 90 ka: A high-resolution record from IODP Site U1340, *Paleoceanography*, 28(1), 54–67, doi:10.1029/2012PA002365.
- Scholl, D. W., E. C. Buffington, and D. M. Hopkins (1968), Geologic history of the continental margin of North America in the Bering Sea, *Mar. Geol.*, 6(4), 297–330.
- Scholl, D. W., E. C. Buffington, D. M. Hopkins, and T. R. Alpha (1970), The structure and origin of the large submarine canyons of the Bering Sea, *Mar. Geol.*, 8(3), 187–210.
- Schubert, C. J., and S. E. Calvert (2001), Nitrogen and carbon isotopic composition of marine and terrestrial organic matter in Arctic Ocean sediments: implications for nutrient utilization and organic matter composition, *Deep Sea Res. Part Oceanogr. Res. Pap.*, 48(3), 789 – 810, doi:http://dx.doi.org/10.1016/S0967-0637(00)00069-8.
- Schumacher, J., and R. Reed (1992), Characteristics of currents over the continental slope of the eastern Bering Sea, *J. Geophys. Res. Oceans 1978–2012*, 97(C6), 9423–9433.
- Schumacher, J. D., and P. J. Stabeno (1998), The continental shelf of the Bering Sea, in *The Sea: The global coastal ocean regional studies and synthesis*, vol. XI, pp. 869–909, John Wiley and Sons, New York.
- Shakun, J. D., P. U. Clark, F. He, S. A. Marcott, A. C. Mix, Z. Liu, B. Otto-Bliesner, A. Schmittner, and E. Bard (2012), Global warming preceded by increasing carbon dioxide concentrations during the last deglaciation, *Nature*, 484(7392), 49–54, doi:10.1038/nature10915.
- Shibahara, A., K. Ohkushi, J. P. Kennett, and K. Ikehara (2007), Late Quaternary changes in intermediate water oxygenation and oxygen minimum zone, northern Japan: A benthic foraminiferal perspective, *Paleoceanography*, 22(3), doi:10.1029/2005PA001234.
- Shultz, D. J., and J. A. Calder (1976), Organic carbon $^{13}\text{C}/^{12}\text{C}$ variations in estuarine sediments, *Geochim. Cosmochim. Acta*, 40(4), 381–385.
- Smith, L. C., and S. R. Stephenson (2013), New Trans-Arctic shipping routes navigable by midcentury, *Proc. Natl. Acad. Sci.*, 110(13), E1191–E1195.
- Snape, T. J., and P. M. Forster (2014), Decline of Arctic Sea Ice: Evaluation and weighting of CMIP5 projections, *J. Geophys. Res. Atmospheres*.

- Soloviev, A., J. I. Garver, and G. Ledneva (2006), Cretaceous accretionary complex related to Okhotsk-Chukotka Subduction, Omgon Range, Western Kamchatka, Russian Far East, *J. Asian Earth Sci.*, 27(4), 437–453, doi:10.1016/j.jseas.2005.04.009.
- Springer, A. M., C. P. McROY, and M. V. FLINT (1996), The Bering Sea Green Belt: shelf-edge processes and ecosystem production, *Fish. Oceanogr.*, 5(3-4), 205–223.
- Stabeno, P. J., J. D. Schumacher, and K. Ohtani (1999), The physical oceanography of the Bering Sea, *Dyn. Bering Sea*, 1–28.
- Steele, M. (2004), Circulation of summer Pacific halocline water in the Arctic Ocean, *J. Geophys. Res.*, 109(C2), doi:10.1029/2003JC002009.
- Stein, R. (1986), Organic carbon and sedimentation rate--further evidence for anoxic deep-water conditions in the Cenomanian/Turonian Atlantic Ocean, *Mar. Geol.*, 72(3), 199–209.
- Stein, R. (2000), Circum-Arctic river discharge and its geological record: an introduction, *Int. J. Earth Sci.*, 89(3), 447–449, doi:10.1007/s005310000110.
- Stein, R., and R. Macdonald (2004), Geochemical proxies used for organic carbon source identification in Arctic Ocean sediments, *Stein R Macdonald RW Eds Org. Carbon Cycle Arct. Ocean Springer-Verl. Berl.*, 24–32.
- Stigebrandt, A. (1984), The North Pacific: A global-scale estuary, *J. Phys. Oceanogr.*, 14(2), 464–470.
- Stouffer, R. J. et al. (2006), Investigating the Causes of the Response of the Thermohaline Circulation to Past and Future Climate Changes, *J. Clim.*, 19(8), 1365–1387, doi:10.1175/JCLI3689.1.
- Stroeve, J. C., M. C. Serreze, M. M. Holland, J. E. Kay, J. Malanik, and A. P. Barrett (2011), The Arctic's rapidly shrinking sea ice cover: a research synthesis, *Clim. Change*, 110(3-4), 1005–1027, doi:10.1007/s10584-011-0101-1.
- Studer, A. S., K. K. Ellis, S. Oleynik, D. M. Sigman, and G. H. Haug (2013), Size-specific opal-bound nitrogen isotope measurements in North Pacific sediments, *Geochim. Cosmochim. Acta*, 120, 179–194, doi:10.1016/j.gca.2013.06.041.
- Svendsen, J. I., H. Alexanderson, V. I. Astakhov, I. Demidov, J. A. Dowdeswell, S. Funder, V. Gataullin, M. Henriksen, C. Hjort, and M. Houmark-Nielsen (2004), Late Quaternary ice sheet history of northern Eurasia, *Quat. Sci. Rev.*, 23(11), 1229–1271.
- Sverdrup, H. (1953), On conditions for the vernal blooming of phytoplankton, *J. Cons.*, 18(3), 287–295.
- Takahashi, K. (1998), The Bering and Okhotsk Seas: modern and past paleoceanographic changes and gateway impact, *J. Asian Earth Sci.*, 16(1), 49–58.

- Takahashi, K., N. Fujitani, M. Yanada, and Y. Maita (2000), Long-term biogenic particle fluxes in the Bering Sea and the central subarctic Pacific Ocean, 1990–1995, *Deep Sea Res. Part Oceanogr. Res. Pap.*, 47(9), 1723–1759.
- Talley, L. D. (1991), An Okhotsk Sea water anomaly: Implications for ventilation in the North Pacific, *Deep Sea Res. Part Oceanogr. Res. Pap.*, 38, S171–S190.
- Tanaka, S., and K. Takahashi (2005), Late Quaternary paleoceanographic changes in the Bering Sea and the western subarctic Pacific based on radiolarian assemblages, *Deep Sea Res. Part II Top. Stud. Oceanogr.*, 52(16-18), 2131–2149, doi:10.1016/j.dsr2.2005.07.002.
- Tang, Q., X. Zhang, and J. A. Francis (2013), Extreme summer weather in northern mid-latitudes linked to a vanishing cryosphere, *Nat. Clim. Change*, 4(1), 45–50, doi:10.1038/nclimate2065.
- Tarasov, L., and W. R. Peltier (2005), Arctic freshwater forcing of the Younger Dryas cold reversal, *Nature*, 435(7042), 662–665, doi:10.1038/nature03617.
- Thomas, E. R., E. W. Wolff, R. Mulvaney, J. P. Steffensen, S. J. Johnsen, C. Arrowsmith, J. W. C. White, B. Vaughn, and T. Popp (2007), The 8.2ka event from Greenland ice cores, *Quat. Sci. Rev.*, 26(1-2), 70–81, doi:10.1016/j.quascirev.2006.07.017.
- Thomson, J., I. Croudace, and R. Rothwell (2006), A geochemical application of the ITRAX scanner to a sediment core containing eastern Mediterranean sapropel units, *Geol. Soc. Lond. Spec. Publ.*, 267(1), 65–77.
- Thornalley, D. J. R., S. Barker, W. S. Broecker, H. Elderfield, and I. N. McCave (2011), The Deglacial Evolution of North Atlantic Deep Convection, *Science*, 331(6014), 202–205, doi:10.1126/science.1196812.
- Timmermann, A., and L. Menviel (2009), What Drives Climate Flip-Flops?, *Science*, 325(5938), 273–274, doi:10.1126/science.1177159.
- Trefry, J. H., R. P. Trocine, L. W. Cooper, and K. H. Dunton (2014), Trace metals and organic carbon in sediments of the northeastern Chukchi Sea, *Deep Sea Res. Part II Top. Stud. Oceanogr.*, 102, 18–31, doi:10.1016/j.dsr2.2013.07.018.
- VanLaningham, S., N. G. Pisias, R. A. Duncan, and P. D. Clift (2009), Glacial–interglacial sediment transport to the Meiji Drift, northwest Pacific Ocean: Evidence for timing of Beringian outwashing, *Earth Planet. Sci. Lett.*, 277(1-2), 64–72, doi:10.1016/j.epsl.2008.09.033.
- Viscosi-Shirley, C., N. Pisias, and K. Mammone (2003), Sediment source strength, transport pathways and accumulation patterns on the Siberian–Arctic’s Chukchi and Laptev shelves, *Cont. Shelf Res.*, 23(11-13), 1201–1225, doi:10.1016/S0278-4343(03)00090-6.

- Wadley, M. R., and G. R. Bigg (2002), Impact of flow through the Canadian Archipelago and Bering Strait on the North Atlantic and Arctic circulation: An ocean modelling study, *Q. J. R. Meteorol. Soc.*, 128(585), 2187–2203, doi:10.1256/qj.00.35.
- Wagner, A. J., C. Morrill, B. L. Otto-Bliesner, N. Rosenbloom, and K. R. Watkins (2013), Model support for forcing of the 8.2 ka event by meltwater from the Hudson Bay ice dome, *Clim. Dyn.*, 41(11-12), 2855–2873, doi:10.1007/s00382-013-1706-z.
- Walsh, J., C. McRoy, L. Coachman, J. Goering, J. Nihoul, T. Whitledge, T. Blackburn, P. Parker, C. Wirick, and P. Shuert (1989), Carbon and nitrogen cycling within the Bering/Chukchi Seas: Source regions for organic matter effecting AOU demands of the Arctic Ocean, *Prog. Oceanogr.*, 22(4), 277–359.
- Wang, M., and J. E. Overland (2009), A sea ice free summer Arctic within 30 years?, *Geophys. Res. Lett.*, 36(7), doi:10.1029/2009GL037820.
- Weaver, A. J. (2003), Meltwater Pulse 1A from Antarctica as a Trigger of the Bolling-Allerod Warm Interval, *Science*, 299(5613), 1709–1713, doi:10.1126/science.1081002.
- Weingartner, T., K. Aagaard, R. Woodgate, S. Danielson, Y. Sasaki, and D. Cavalieri (2005), Circulation on the north central Chukchi Sea shelf, *Deep Sea Res. Part II Top. Stud. Oceanogr.*, 52(24-26), 3150–3174, doi:10.1016/j.dsr2.2005.10.015.
- Weingartner, T. J., D. J. Cavalieri, K. Aagaard, and Y. Sasaki (1998), Circulation, dense water formation, and outflow on the northeast Chukchi shelf, *J. Geophys. Res. Oceans 1978–2012*, 103(C4), 7647–7661.
- Wentworth, C. K. (1922), A scale of grade and class terms for clastic sediments, *J. Geol.*, 377–392.
- Wijffels, S. E., R. W. Schmitt, H. L. Bryden, and A. Stigebrandt (1992), Transport of freshwater by the oceans, *J. Phys. Oceanogr.*, 22(2), 155–162.
- Winckler, G., R. F. Anderson, M. Q. Fleisher, D. McGee, and N. Mahowald (2008), Covariant glacial-interglacial dust fluxes in the equatorial Pacific and Antarctica, *science*, 320(5872), 93–96.
- Wipf, S., M. Gottfried, and L. Nagy (2013), Climate change and extreme events—their impacts on alpine and arctic ecosystem structure and function, *Plant Ecol. Divers.*, 6(3-4), 303–306.
- Wolff, E. W., H. Fischer, F. Fundel, U. Ruth, B. Twarloh, G. C. Littot, R. Mulvaney, R. Röthlisberger, M. De Angelis, and C. F. Boutron (2006), Southern Ocean sea-ice extent, productivity and iron flux over the past eight glacial cycles, *Nature*, 440(7083), 491–496.
- Woodgate, R. A. (2005), Revising the Bering Strait freshwater flux into the Arctic Ocean, *Geophys. Res. Lett.*, 32(2), doi:10.1029/2004GL021747.

- Woodgate, R. A., K. Aagaard, and T. J. Weingartner (2005), A year in the physical oceanography of the Chukchi Sea: Moored measurements from autumn 1990–1991, *Deep Sea Res. Part II Top. Stud. Oceanogr.*, 52(24), 3116–3149.
- Yasuda, I. (1997), The origin of the North Pacific Intermediate water, *J. Geophys. Res. Oceans* 1978–2012, 102(C1), 893–909.
- You, Y. (2003), Implications of cabbeling on the formation and transformation mechanism of North Pacific Intermediate Water, *J. Geophys. Res. Oceans*, 108(C5), 3134, doi:10.1029/2001JC001285.
- Zheng, Y., A. Geen, R. F. Anderson, J. V. Gardner, and W. E. Dean (2000), Intensification of the Northeast Pacific oxygen minimum zone during the Bølling-Allerød Warm Period, *Paleoceanography*, 15(5), 528–536.
- Ziegler, M., T. Jilbert, G. J. de Lange, L. J. Lourens, and G.-J. Reichert (2008), Bromine counts from XRF scanning as an estimate of the marine organic carbon content of sediment cores, *Geochem. Geophys. Geosystems*, 9(5), doi:10.1029/2007GC001932.
- Zreda, M., J. England, F. Phillips, D. Elmore, and P. Sharma (1999), Unblocking of the Nares Strait by Greenland and Ellesmere ice-sheet retreat 10,000 years ago, *Nature*, 398(6723), 139–142.